

Review

Olive Mill Wastewater Valorization through Steam Reforming Using Multifunctional Reactors: Challenges of the Process Intensification

Cláudio Rocha ¹, Miguel Angel Soria ² and Luís M. Madeira ^{2,*}

- ¹ LSRE-LCM—Laboratory of Separation and Reaction Engineering—Laboratory of Catalysis and Materials, Associate Laboratory, Department of Chemical Engineering, Faculty of Engineering, University of Porto, Rua Dr. Roberto Frias s/n, 4200-465 Porto, Portugal; csrocha@fe.up.pt
- ² LEPABE—Laboratory for Process Engineering, Environment, Biotechnology and Energy, Department of Chemical Engineering, Faculty of Engineering, University of Porto, Rua Dr. Roberto Frias s/n, 4200-465 Porto, Portugal; masoria@fe.up.pt
- * Correspondence: mmadeira@fe.up.pt

Abstract: Olive oil mill wastewater (OMW) is a polluting stream derived from the production of olive oil and is a source of environmental pollution; this is relevant in many countries around the world, but particularly in all the Mediterranean region where major producers are located. In this effluent, several pollutants are present—namely, sugars, fatty acids, and polyphenols, among others. Nowadays, to reduce the pollutant load, several treatment techniques are applied, but these technologies have numerous cost and efficiency problems. For this reason, the steam reforming of the OMW (OMWSR) presents as a good alternative, because this process decreases the pollutant load of the OMW and simultaneously valorizes the waste with the production of green H₂, which is consistent with the perspective of the circular economy. Currently, the OMWSR is an innovative treatment alternative in the scientific field and with high potential. In the last few years, some groups have studied the OMWSR and used innovative reactor configurations, aiming to improve the process' effectiveness. In this review, the OMW treatment/valorization processes, the last developments on catalysis for OMWSR (or steam reforming of similar species present in the effluent), as well as the last advances on OMWSR performed in multi-functional reactors are addressed.

Keywords: olive mill wastewater valorization; steam reforming; catalyst; sorbent; H₂ perm-selective membrane



Citation: Rocha, C.; Soria, M.A.; Madeira, L.M. Olive Mill Wastewater Valorization through Steam Reforming Using Multifunctional Reactors: Challenges of the Process Intensification. *Energies* **2022**, *15*, 920. <https://doi.org/10.3390/en15030920>

Academic Editors: Antonio Zorro and Frede Blaabjerg

Received: 1 December 2021

Accepted: 13 January 2022

Published: 27 January 2022

Publisher's Note: MDPI stays neutral with regard to jurisdictional claims in published maps and institutional affiliations.



Copyright: © 2022 by the authors. Licensee MDPI, Basel, Switzerland. This article is an open access article distributed under the terms and conditions of the Creative Commons Attribution (CC BY) license (<https://creativecommons.org/licenses/by/4.0/>).

Index	
Abstract	1
1. Introduction	3
1.1. OMW Composition	7
1.2. OMW Treatment/Valorization	7
1.3. Olive Mill Wastewater Steam Reforming	10
2. Omwsr Catalysts	11
2.1. Catalysts Used for Steam Reforming of OMW	12
2.2. Catalysts Used for Steam Reforming of Model Molecules of OMW	15
2.2.1. Effect of the Active Phase	15
2.2.2. Effect of the Support	16
2.2.3. Effect of Promoters	16
2.3. Summary	17
3. Multifunctional Reactors	19
3.1. Sorption-Enhanced Reactor	19
3.1.1. CO ₂ Sorbents	20
3.1.2. Hydrotalcites	24
3.1.3. OMWSR in Sorption-Enhanced Reactors	27
3.1.4. Summary	27
3.2. Membrane Reactor	28
3.2.1. Hydrogen Perm-Selective Membranes	29
3.2.2. OMWSR in Membrane Reactors	32
3.2.3. Summary	35
3.3. Sorption-Enhanced Membrane Reactor	35
OMWSR in Sorption-Enhanced Membrane Reactors	35
4. Conclusions	36
Notation and Glossary	37
References	38

1. Introduction

The olive oil industry is very relevant in many countries around the world—particularly in the Mediterranean countries (cf. Figure 1), both economically and traditionally. Because of its excellent nutritional properties, olive oil contributes to cholesterol control and promotes cardiovascular health. This significance is explained in numbers: about 9 million hectares of olive trees have been cultivated worldwide during the 2019/2020 crop year [1]. For the 2019/2020 crop year, it was estimated that 70% of the production of olive oil around the world was performed in European Union countries, with the Iberian Peninsula (Portugal and Spain) being a leader zone (76% of the European Union’s total)—see Figure 1 [1,2]. Nevertheless, there are other countries with high levels of olive oil production: Tunisia, Morocco, Syria, and the USA. Besides that, other countries—such as Australia, Argentina and South Africa—are also employing this type of crop [3].

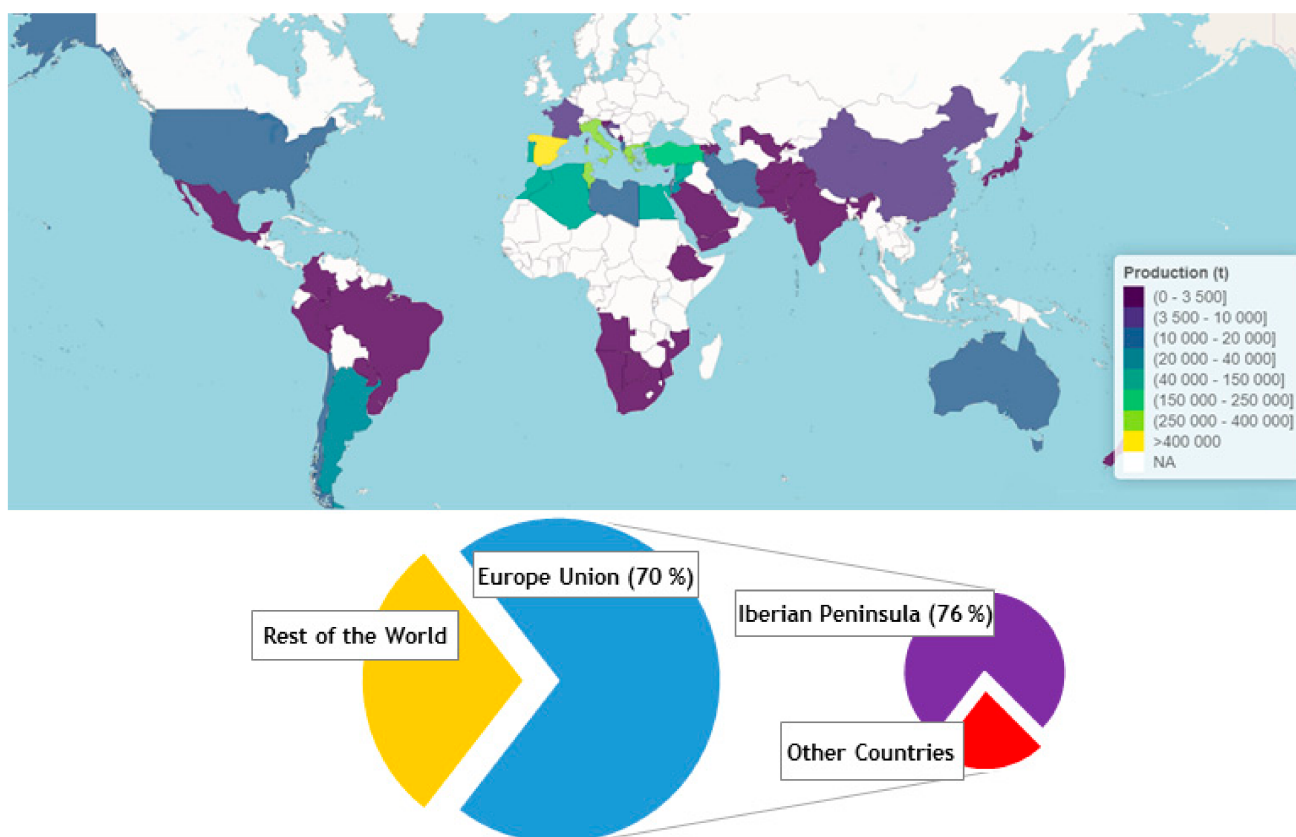


Figure 1. World and Europe Union production of olive oil for the 2019/2020 crop year—data taken from the site of International Olive Council [2]. Figure adapted from the site of International Olive Council [2].

In this way, it is observed that all these regions are significantly affected by the pollution resulting from olive oil production. The process yields massive amounts of liquid (olive oil mill wastewater—OMW) and solid waste, which have raised severe disposal difficulties for the producers. This agroindustry represents a huge environmental problem, where big quantities of effluents are produced in a small period. This environmental concern is emphasized by the large amount of world olive oil production/consumption (close to 3 million metric tons per year produced/consumed—this value has remained nearly constant in the last 10 years) [2,4,5]—see Figure 2.

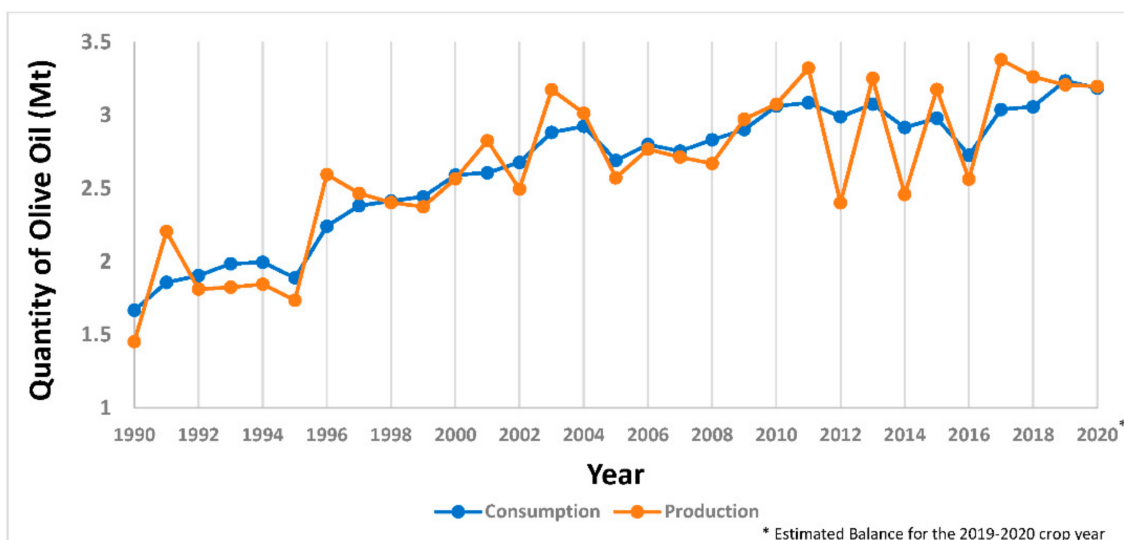


Figure 2. World consumption/production of olive oil—data taken from the site of International Olive Council [2].

The aqueous residues related to this agro-industrial activity are produced using either the traditional pressing or the centrifugation methods (three- or two-phase systems) because, in all of them, water is used to generate the olive oil from the olive [1,6]. In Figure 3, a scheme of these processes of olive oil production can be seen [7,8].

The discontinuous pressing procedure (traditional method) is the oldest and most well-known method for processing olives. In the traditional pressing (nowadays adopted only in small mills/companies), the ground olives are pressed and then the liquid mixture is rested in a sequence of decanters to separate the olive oil. To separate the oil from the other phases, a small amount of water is added. This traditional process also produces a solid fraction denominated by olive pomace (or olive cake) constituted by water, olive stone, and olive pulp. This traditional method presents several advantages such as low-priced equipment and technological simplicity. Nevertheless, it also has handicaps, such as the fact of running discontinuity and high hand-labor costs [7]. Still, because it adds water in several steps of the production process (previous to the decantation step), a large quantity of OMW (approximately 40–60 L/100 kg olives) is produced [7]. The OMW generated has a higher chemical oxygen demand (COD) compared with the OMW produced by the other methods [9]. Until 40 years ago, this was the only process used, although financial problems pushed olive mills to gradually abandon the traditional process [10,11].

In the centrifugation systems, crushed olive fruits are fed into a two-phase or three-phase decanter centrifuge and then the impure olive oil is centrifuged [12]. These processes are based on the differences in the density of the several components obtained (solids, olive oil, and water) and can produce three distinct fractions: pomace, olive oil, and OMW—see Figure 3.

Using the three-phase process (route a) in Figure 3, the olive paste is divided into three phases in the horizontal centrifugation (water added in this step): olive oil, OMW, and pomace [7,8]. Then, the liquid fraction generated (olive oil + OMW) is centrifuged (vertical centrifugation) with additional water to recover a high-quality olive oil, producing a high quantity of OMW—see Figure 3. Since the continuous three-phase centrifugation method adds water in the two centrifugation steps, a high volume of OMW is produced (about 100–120 L/100 kg olives—1.7–3 times more compared to the traditional method) [8]. Nevertheless, this three-phase system has various advantages, such as better quality of the olive oil and complete automation. Nonetheless, this system also presents several disadvantages, such as a higher level of water and energy consumption, higher volume of OMW produced (as previously mentioned), and more expensive installations [3].

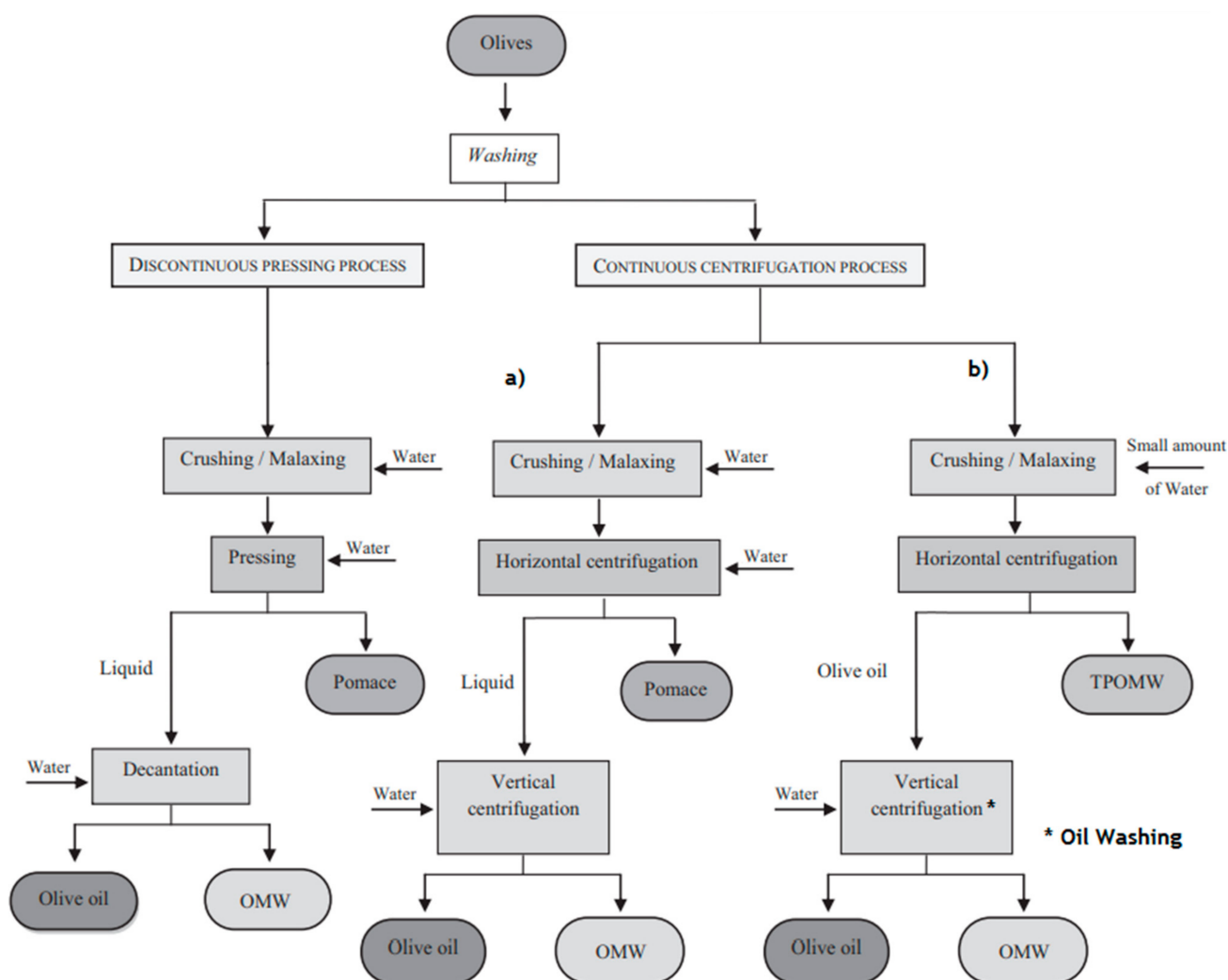


Figure 3. Main processes of olive oil production—traditional (pressing) method, (a) three-phase centrifugation method and (b) two-phase centrifugation method [7,8]. Reprinted with permission from Ref. [7]. Copyright 2021 Elsevier.

To minimize the impact of OMW, the two-phase centrifugation process (route b) in Figure 3 was developed during the 1990s [7]. Using this two-phase process, the olive paste is divided only into two phases in the horizontal centrifugation (no water added in this step): wet pomace and olive oil, the first known as two-phase olive mill waste (TPOMW), a combination of pomace and OMW—see Figure 3 [7]. Then, the olive oil generated is washed (vertical centrifugation—oil washing) with a very small amount of water, producing only a small OMW stream—see Figure 3 [8]. Despite the lower volume of OMW produced in comparison with the three-phase process, the resulting TPOMW (10 L/100 kg olives) is harder to manage and treat, because its pollutant load is more concentrated [7]. Nevertheless, some quantity of OMW is drained from the TPOMW in the storage tanks and is collected using draining valves. Besides that, it is possible to extract some oil from TPOMW through several techniques (e.g., using solvents), valorizing, in this way, this by-product [7]. In this way, the two-phase system, besides presenting the same advantages of the three-phase system, also produces a lower quantity of OMW (about 8.5–11 L/100 kg olives) and reduces water consumption; thus, this centrifugation system has been called “ecological” [3,13]. Nevertheless, like the three-phase system, the two-phase system needs expensive installations.

Figure 4 illustrates a scheme quantifying the OMW production (for all the extraction processes used in the countries of the Mediterranean area) in relation to the quantities of

olives and extractive water used, and olive oil/olive husk (pomace) produced; one can see that big ratios between generated OMW and olive oil are obtained [14]. Moreover, it is estimated that 30 Mm³ of OMW per year are produced around the world [6]. The OMW results from both the water present in the olives and the water used in the production process of the olive oil, especially with the three-phase centrifugation system and pressing method [1,6].

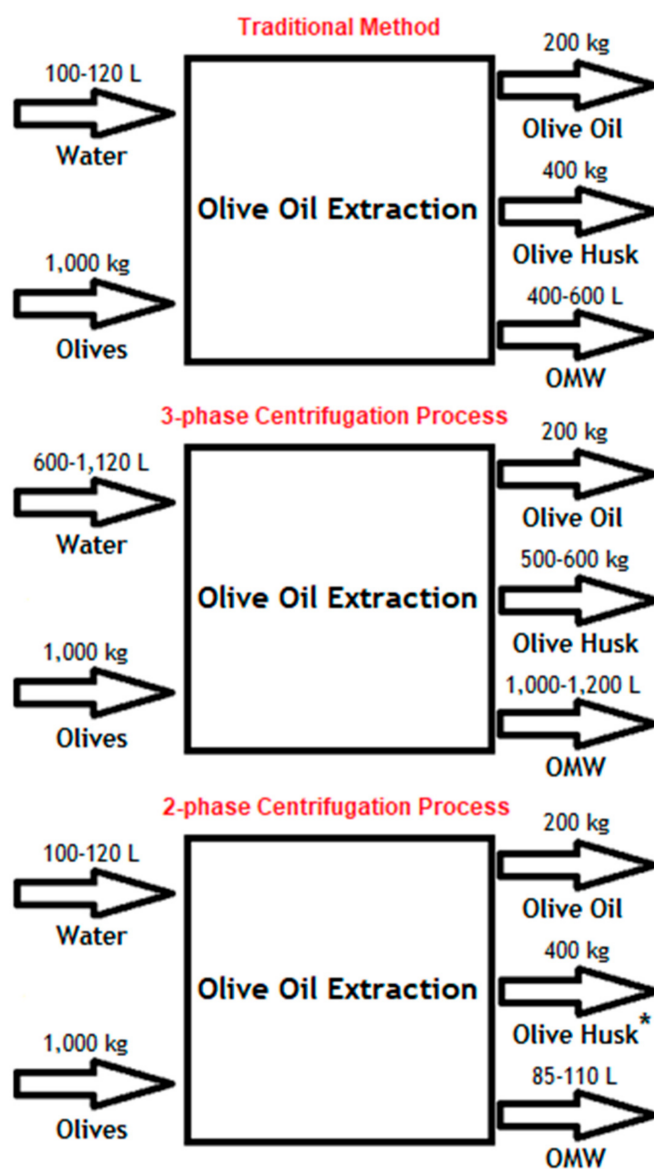


Figure 4. A quantitative relationship between the OMW production and the remaining components present in the olive oil extraction. * The olive husk mass presented in the two-phase centrifugation process does not include the mass lost in secondary drying processes. Data taken from Caputo et al. [14].

These big amounts of OMW cause large environmental problems [15–18]. It is reported that such residues have an effect on soil/air quality and on the aquatic ecosystems due to the deposition of toxic streams directly in the receiving bodies. Some of the main negative impacts are the increase of the organic charge concentration and the existence of phytotoxicity in the water systems. This happens due to the high values of COD (60–200 g·L⁻¹), total organic carbon (TOC—> 9 g·L⁻¹), and biochemical oxygen demand (BOD—14–100 g·L⁻¹) present in the OMW [6]. Pollution from OWM is expected to be 200–400 times higher than from urban wastewater [1,19,20]. The uncontrolled disposal of OMW represents economic, social, and environmental problems that must be resolved.

1.1. OMW Composition

The composition of OMW is extremely variable and suggests that minor or major compounds can be present, depending on numerous factors, which include the age of the olive tree, region of cultivation, maturation level of the olive, weather conditions that the olive was subjected to in the ripening process, treatment of the tree, and method of extracting the oil [21]. El-Abbassi et al. [22] showed that OMW resulting from the traditional method had a higher phenolic content compared to that obtained from the three-phase centrifugal system. The investigation of these effects in the OMW composition is very important, in order to develop sustainable OMW management strategies.

In general, OMW consists of solid matter and liquid, with a slightly acidic pH. The latter is composed of water, polyphenols, fatty acids, and sugars, among other organic and inorganic species [6,23]. The content of water in this stream is usually between 80–95 wt.% [6,24–26]. In Table 1, it is possible to see a typical physicochemical characterization of the OMW [23].

Table 1. Typical physicochemical characterization of the OMW. Reprinted with permission from Ref. [23]. Copyright 2022 Elsevier.

Organic Species		Inorganic Species			
Solid Waste (g·L ⁻¹)	11.5–102.5	Pb (µg·L ⁻¹)	6.7–10	Ca (g·L ⁻¹)	0.03–0.29
Organic Matter (g·L ⁻¹)	16.7–81.6	Cd (µg·L ⁻¹)	0.03–10	K (g·L ⁻¹)	0.73–6.1
Lipids (g·L ⁻¹)	1.64–9.8	Fe (mg·L ⁻¹)	0.45–20	Cl (g·L ⁻¹)	0.76–1
Polyphenols (g·L ⁻¹)	0.002–11.5	Zn (mg·L ⁻¹)	1.7–4.98	Na (g·L ⁻¹)	0.03–0.13
Sugars (g·L ⁻¹)	1.3–8.79	Cu (mg·L ⁻¹)	0.49–2.96		
Organic Acids (g·L ⁻¹)	0.78–1	Mn (mg·L ⁻¹)	0.46–20		
Total Nitrogen (g·L ⁻¹)	0.06–0.95	Mg (mg·L ⁻¹)	0.03–0.17		

The compounds most reported are the following: caffeic acid, vanillic acid, tyrosol, cinnamic acid, p-coumaric acid, D-arabinose, D-galactose, D-galacturonic acid, acetic acid, syringic acid, gallic acid, protocatechuic acid, guaiacol, phenol, phenethyl alcohol, and benzyl alcohol [1,6,7,14,21,22,26–37]. However, it is important to mention that more than 30 polyphenols and sugars have been noticed in OMW [38]. In Table 2 an example of OMW composition on a dry basis is represented [36].

Table 2. Typical composition (wt.%) on a dry basis of the OMW. Reprinted with permission from Ref. [36]. Copyright 2022 John Wiley and Sons.

Ratio of Polyphenols/Sugars	0.46
Species	
Tyrosol	16.68%
P-Coumaric acid	14.83%
D-Arabinose	22.83%
D-Galactose	22.83%
D-Galacturonic acid	22.83%

1.2. OMW Treatment/Valorization

As the substances present in OMW are very toxic, the effluent needs to be correctly treated. A great variety of treatment/valorization processes (see Figure 5) have been investigated in the past years to reduce OMW pollutant load or to allow its disposal, but research efforts turn nowadays toward other aspects. Still, those methods of OMW load reduction are not often used due to technical and economic reasons. The trivial

management of the OMW consists of the direct discharge into sewer systems and rivers, disposal in evaporation lagoons or dilution with other effluents [4,39]. In addition, the latter practice requires large areas and produces a black foul-smelling sludge that is difficult to handle, with inherent pollutant infiltration into ground water and insect proliferation. Land disposal is also a common practice considering OMW as a fertilizer, if it is well managed. Nevertheless, to avoid the contamination of the soil, land disposal must be quantitatively controlled by releasing small amounts of wastewater. Thus, nowadays, an organized and controlled release of OMW into the environment is still permitted, according to specific regulations of the different countries.

Therefore, solutions for adding value to OMW or for extracting valuable compounds from it before treatment/discharge are required. The OMW valorization/treatment methods can be organized into several general categories (see Figure 5). Among all the existing sub-categories, the following stand out:

- **Thermal Processes [4]:**
 - Distillation and Evaporation Processes: these processes concentrate the inorganic and organic contents of the OMW by water evaporation. These processes have high operation costs and the organic content must be treated afterwards;
 - Combustion: this process is very efficient but requires a large amount of energy.
- **Membrane Processes [4,26,40–42]:** these processes separate the organic and inorganic contents of the OMW by the utilization of membranes. However, the cost of the membrane and its use might be high, particularly if high pressures are required, and the process has operation problems (membrane fouling, concentration polarization, etc.). There are several types of membrane-based processes: ultrafiltration, nanofiltration, reverse osmosis, and microfiltration.
- **Physicochemical Processes [43]:** these processes consist of physical and chemical reactions involving molecules present in the OMW composition. Sometimes, they are conjugated to maximize efficiency. The following processes are included in this category:
 - Electrochemical Oxidation [44,45]; Ozonation [46,47]; Adsorption [48–50]; Ion-Exchange [51,52]; Flocculation [4,53,54]; UV Photocatalysis [45,55,56]; Wet Oxidation [57–59]; Fenton Oxidation [60–64]; Photo-Fenton [38,65]; Electro-Coagulation [66,67]; Enzymatic Catalysis [68]; Supercritical Water Gasification [69].
- **Biological Processes [70]:** these processes use microorganisms to decrease the pollutant load and, simultaneously, provide products with value (for instance, formation of CH₄ or H₂). The following are included in this category:
 - Aerobic Processes [70–73]; Anaerobic Processes [50,74–76].

Most of the methods studied aiming OMW valorization include the recovery of the polyphenols fraction owing to their interesting pharmacological properties [78–81]; besides that, OMW phenolic extracts can be used in the food industry, in order to improve the oxidative status of the products [77]. For instance, in recent years, membrane processes have been used for polyphenols recovery [26]—namely microfiltration, ultrafiltration, reverse osmosis, nanofiltration, membrane distillation, and osmotic distillation [4,40,41]. However, membrane-based processes have a range of limitations; e.g., may be limited by the OMW's high concentration of suspended solids. Adsorption processes [48,50] have been also applied to the recovery of phenolic compounds to valorize the OMW effluent.

Concerning the treatment processes, the most commonly utilized physicochemical treatments with this purpose include electrochemical oxidation [44,45], ozonation [46,47], electro-coagulation [66], adsorption [49], and advanced oxidation processes [43,82,83] (particularly Fenton oxidation [60,61]). Since the polyphenols have strong resistance to bacteria, the physicochemical methods can be extremely important, because they can reduce the organic content to make the effluent suitable for biological processes (two different techniques combined for OMW treatment/valorization).

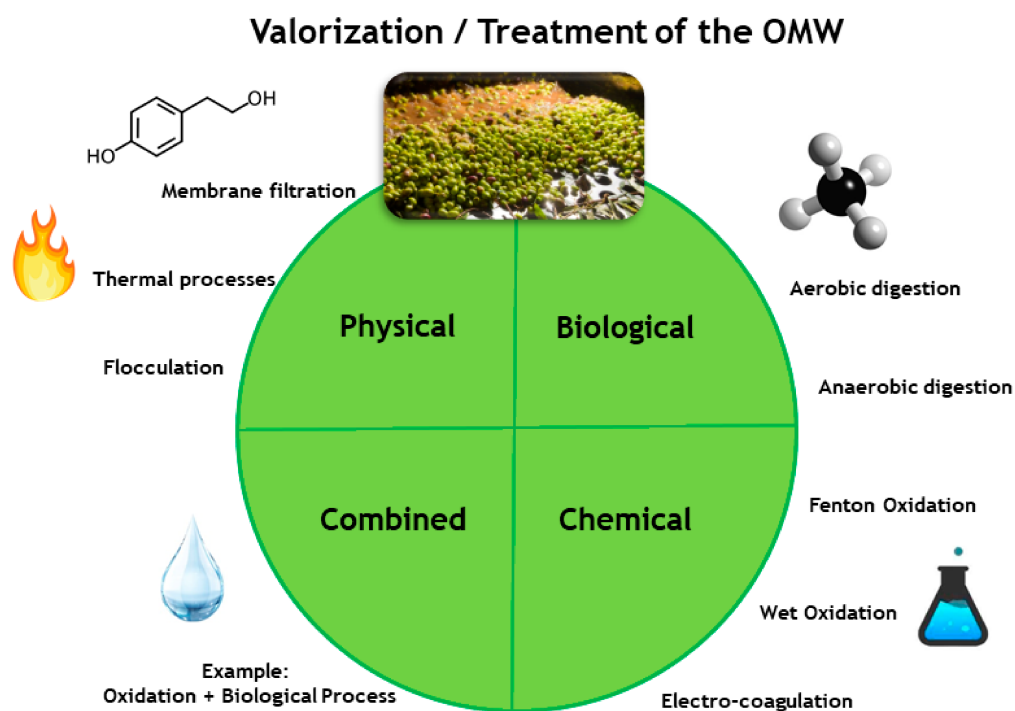


Figure 5. General scheme of different techniques applicable for OMW treatment/valorization [77].

In general terms, several conventional valorization/treatment technologies with varying degrees of success have been proposed. However, most of them require considerable financial input and show low efficiency. In addition, they frequently focus on removing the polyphenols and end up producing a secondary waste that needs additional treatment.

Therefore, it is necessary to improve the scientific and technological solutions for the treatment and valorization of these wastes to decrease the environmental impacts and to allow sustainable use of resources, in line with international waste management practices. In this perspective, the possibility of waste valorization for green energy production has been considered [84], namely through OMW steam reforming (OMWSR) [85]. This technology would permit removing the high pollutant components present in the OMW while producing H_2 , therefore providing added-value. This biofuel is environmentally attractive once it is renewable and reduces the CO_2 emission into the atmosphere [84]. Unlike fossil fuels, H_2 burns cleanly, without producing any environmental pollutants. The OMWSR would help reducing the pollution load of the effluent as well as to economically valorize a by-product of the olive oil industry without any value so far [85]. The H_2 can be applied in several technologies like in combustion engines or electrochemical cells. In this perspective, it is worth mentioning that hydrogen technologies proved extremely resilient during the COVID-19 pandemic, with their momentum staying strong in 2020 [86]. Moreover, a recent publication of the International Energy Agency reported that the global H_2 demand in the Net Zero Emission Scenario (between 2020 and 2030) will increase significantly in the next years, in order to reach international climate and sustainable energy goals—see Figure 6 [86,87]. To meet this growing demand for H_2 , the environmentally friendly production of H_2 has become an important part of the H_2 market. However, this progress falls well short of what is needed in the Net Zero Emissions Scenario.

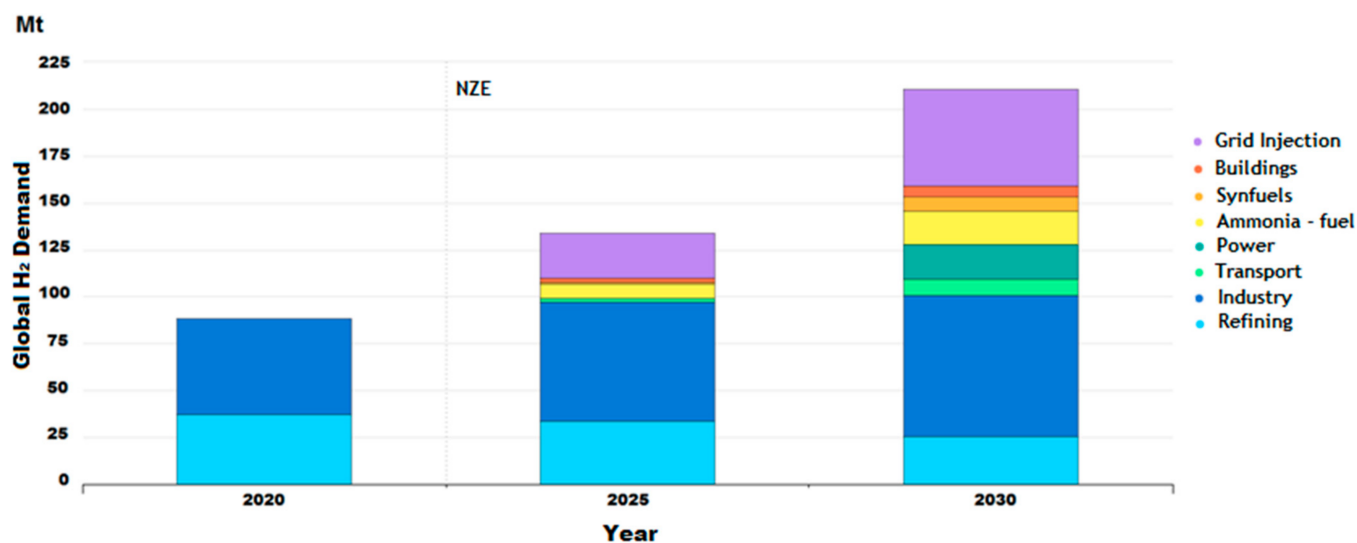
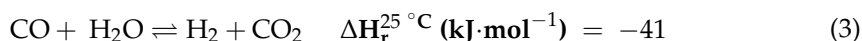
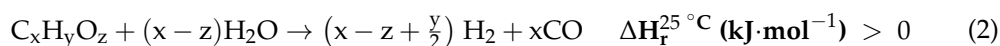
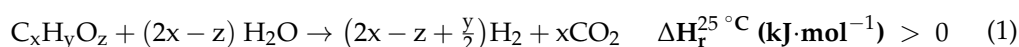


Figure 6. Global H₂ demand by sector in the Net Zero Emission Scenario, 2020–2030—data taken from the site of International Energy Agency [86,87].

1.3. Olive Mill Wastewater Steam Reforming

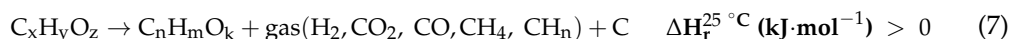
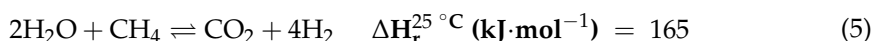
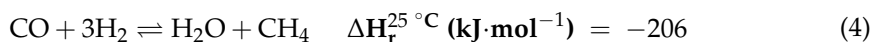
The OMWSR (Equation (1)) consists of the sum of two independent reactions: decomposition of high molecular weight molecules in the presence of steam (Equation (2)) and the water–gas shift (WGS—Equation (3)) reaction. The values of $\Delta H_r^{25\text{ }^\circ\text{C}}$ were taken from the literature [84].



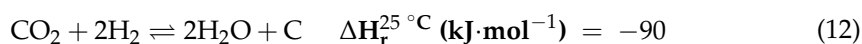
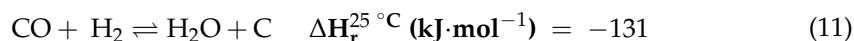
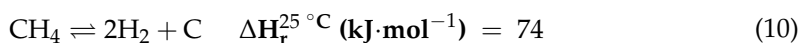
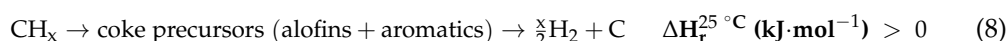
The reason why the OMWSR was chosen as a method of OMW valorization is mainly due to the fact that the steam reforming is extensively used in industry, apart from the reasons given above (i.e., environmental concern and production of green H₂). Besides that, syngas (H₂ and CO) produced can be applied as a resource for the fabrication of valuable chemicals and fuels through Fischer–Tropsch or dimethyl ether synthesis routes [88].

The OMWSR process (in a Traditional Reactor—TR—see Figure 7) has, however, some challenges that need to be overcome and optimized to be a valid approach for the OMW valorization, namely:

- The OMWSR is an endothermic reaction, thus needing high temperatures and intrinsically high operating costs; moreover, producing H₂ by this process also yields CH₄, CO₂, and CO, whose production is a target of environmental alarm and limited by legislation;
- The WGS reaction is thermodynamically limited (Equation (3));
- This process has several side reactions, which affect both the formation and purity of H₂. The main side reactions are represented by Equation (4)—methanation of carbon monoxide, Equation (5) (sum of Equation (3) and reverse of Equation (4))—steam reforming of CH₄, and Equation (6) (sum of reverse of Equation (3) and reverse of Equation (4))—dry reforming of CH₄;
- Other products apart from the previous ones—such as butane, propane, acetone, methanol, benzene, ethanol, cyclopentadiene, ethylene, butanol, and acetaldehyde—could be present in the reaction medium. These species are referred by many works as possible secondary products of some reactions (e.g., Equation (7)—cracking of oxygenates) or as intermediates of the reactions involved in this process [1,27,28];



- The formation of coke is a problem since it deactivates the catalysts (Equations (7) and (8)—cracking of hydrocarbons, Equation (9)—Boudouard reaction, Equation (10)—methane cracking, Equation (11)—carbon monoxide reduction, and Equation (12)—carbon dioxide reduction), thus affecting H₂ yield and purity and long-term operation of the process;



● Catalyst

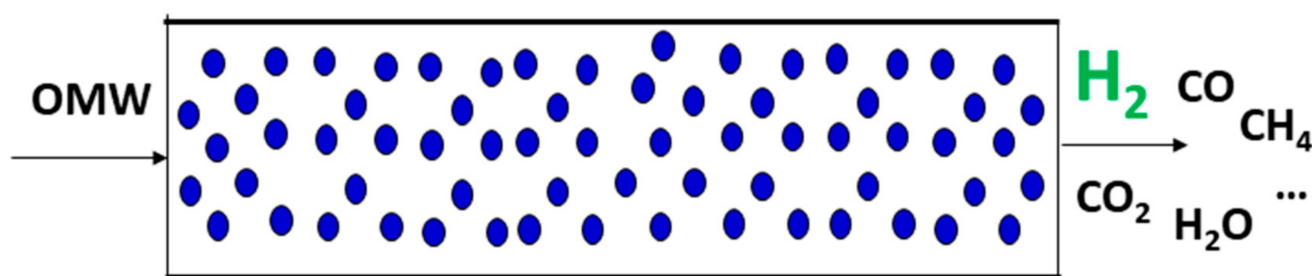


Figure 7. Scheme of the operation of the TR.

With the aim of resolving these difficulties, new catalyst formulations must be developed. Furthermore, new reactor configurations merging the OMWSR catalytic process and H₂ and/or CO₂ selective removal should be addressed, due to their potential to solve the restrictions mentioned above (namely shifting in the desired direction the reversible reactions, like the WGS). In this work, some of the important progress regarding the OMWSR process (developed catalysts) and its combination with a H₂ perm-selective membrane (in a membrane reactor—MR), in the perspective of process intensification, are reviewed; still, the potential of the utilization of the sorption-enhanced reactor (SER with a CO₂-selective sorbent) and the sorption-enhanced membrane reactor (SEMR—combining in the same device the separation of H₂ and capture of CO₂) are also addressed.

2. OMWSR Catalysts

Heterogeneous catalysis applied to the OMWSR is not very developed until now. The catalysts investigated so far have been Ni-, Pd-, Pt-, and Ru-based. However, several catalysts were extensively studied for the steam reforming of individual components that are similar to the components present in the OMWSR (like acetic acid, or similar molecules). Currently, the key goal is to prepare catalysts with high catalytic activity and high stability.

2.1. Catalysts Used for Steam Reforming of OMW

Firstly, this reaction was studied by Tosti et al. [1,6,89] and by Llorca et al. [28]. Recently, Alique et al. [89] also studied the steam reforming of the OMW in an MR, using a catalyst developed and tested in a previous work of Tosti et al. [89].

In the first study, Tosti et al. [6] used a commercial Pt-based catalyst (1 wt.% Pt on Al₂O₃—BASF SP-01 T) in an MR (150 µm thick Pd-Ag dense tubes). The experimental tests were carried out at 450 °C and in the range of 1–5 bar, at different space velocities (Weight Hourly Space Velocity—WHSV = 2.78×10^{-3} – 8.33×10^{-3} mol·h⁻¹·g_{cat}⁻¹). The gas chromatographic analysis of the retentate side revealed the existence of H₂, CO₂, and CH₄, thus showing the presence of side reactions such as the hydrogenolysis and cracking of high weight molecules. Additionally, catalyst deactivation due to coke formation was detected. Then, this research group prepared a new noble metals-based catalyst [89] and compared it with the commercial Pt-based catalyst used in the previous work under similar operation conditions (using the same reactor configuration—MR). The new catalyst consists of Al₂O₃ pellets coated with a CeO₂-ZrO₂ layer. The active species (Pd, Rh, and Pt) loading was lower than 3 wt.%. CeO₂-ZrO₂ presents several benefits in the steam reforming reactions: oxidation reactions and WGS reaction are enhanced by the high oxygen mobility, which is also related to the decrease of the coke formation and sintering inhibition. Moreover, when these supports are employed, Rh can exhibit high catalytic stability during the reaction, low Pt loadings (<1 %) are enough for limiting deactivation phenomena and Pd can show good stability even at very low steam-to-carbon feed ratios (SCFRs). This catalyst exhibited no substantial loss of activity after 6–8 h of operation, in contrast with the commercial Pt-based catalyst whose activity reduced after 1–2 h of experimental test. When compared to the commercial material, the new catalyst exhibited higher selectivity, allowing it to significantly reduce the production of CH₄ and coke; in this way, it is obtained a higher H₂ production and higher durability and stability. This new catalyst was also used in the recent work of Alique et al. [90], who reported that, in a MR, higher pressures increased the permeation of H₂, prevailing the membrane shift effect against the negative effect on thermodynamics of the reactions involved in the steam reforming process. In this way, an increase in H₂ production was obtained as the pressure increased.

Llorca and co-workers are another research group that studied this reaction [28] in the last few years in a TR. Several catalytic honeycombs loaded with Ni or noble metals (Ru, Pt, Rh, or Pd) over La-stabilized CeO₂ were prepared. The experiments were carried out at 1 bar and in the range of 600–750 °C, at different space velocities (Gas Hourly Space Velocity—GHSV = 4500–16,000 h⁻¹). Their catalytic performance in terms of production of H₂, stability and selectivity towards reforming products followed this trend: Pt/CeLa > Rh/CeLa > Ru/CeLa >> Ni/CeLa. The trend of coke formation on the surface of these catalysts was: Ru/CeLa > Rh/CeLa > Pt/CeLa, which is contrary to that of the catalytic performance, strongly suggesting that coke deposition was the cause of catalyst deactivation during OMWSR—see Figure 8. Besides, it was found that the selectivity for secondary reactions increases with time, for all the catalysts, and the catalyst with higher selectivity for H₂ formation was Rh/CeLa. In addition, Ca deposition was also observed after the stability tests in all samples; seemingly, calcium is present in the OMW and its possible influence on the long-term catalytic activity must be further studied. The 1 wt.% Pt/CeLa catalyst showed a very stable distribution of products in long term runs. An increase of the Pt load up to 2 wt.% had a positive effect on the product distribution, particularly on the suppression of CH₄.

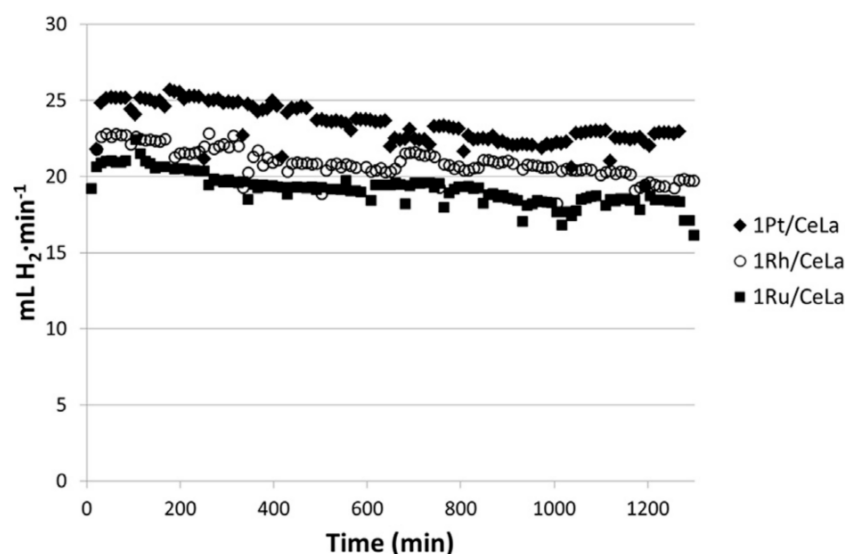


Figure 8. H₂ production at 700 °C over time on stream, $F_{\text{OMW}} = 0.6 \text{ mL} \cdot \text{min}^{-1}$, $\text{GHSV} = 9000 \text{ h}^{-1}$. Reprinted with permission from Ref. [28]. Copyright 2021 Elsevier.

Finally, Rocha et al. [85,91] tested several commercial and prepared catalysts (Cu-Zn-, Ni-, and noble metal-based) for the OMWSR process (using a synthetic OMW effluent—a complex mixture of model oxygenates, representative of a real effluent) to compare their catalytic performances. A catalytic screening study with all the materials was performed (@ 1 bar and 350/400 °C), and stability tests (@ 1 bar and 400 °C) were conducted with the most promising samples. Although there are a few materials with good catalytic performance, the commercial Rh-based catalyst stood out, exhibiting high performance (catalytic activity and stability): the H₂ yield (over 9 mol_{H₂} · mol⁻¹_{OMW}) and total TOC conversion (>98%) were high during the long-term experiment (24 h of the stability test)—see Figure 9.

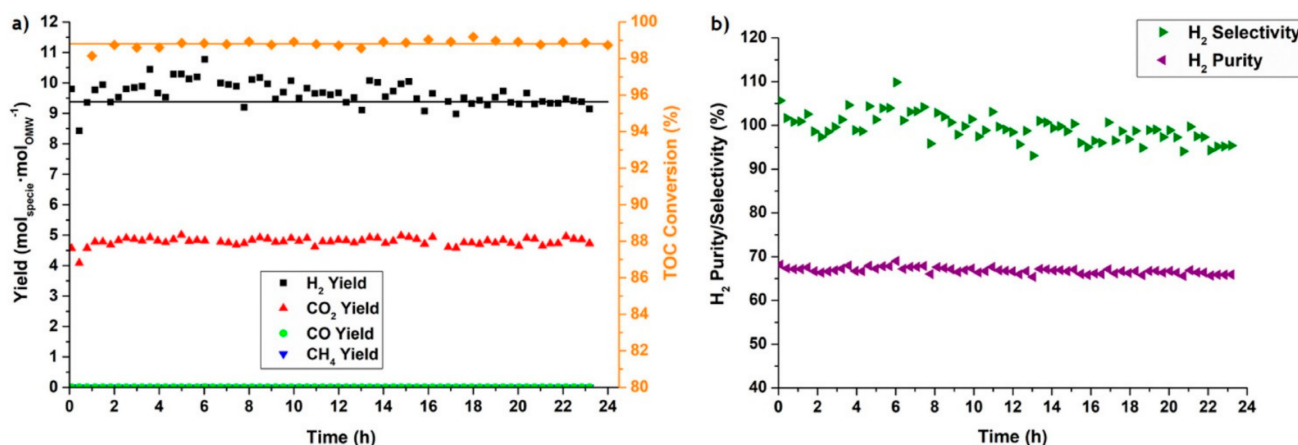


Figure 9. (a) Gaseous species yield and TOC conversion during a stability test using a Rh-based catalyst. (b) H₂ purity and H₂ selectivity obtained using a Rh catalyst. For interpretation of the references to color in this figure legend, the reader is referred to the Web version of this article. Reprinted with permission from Ref. [85]. Copyright 2021 Elsevier.

Besides that, several studies regarding the steam reforming of guaiacol (component typically present in the composition of the OMW) using Ni-based catalysts were also reported [92,93]. Finally, it is important to emphasize that several works have already studied the steam reforming of effluents (e.g., bio-oil and palm oil mill) with compositions very similar to OMW (oxygenated species), using Ni and Co-based catalysts [94–103].

A summary of some results obtained with the more relevant catalysts reviewed in this section is presented in Table 3.

Table 3. Summary of the catalytic performance and operating conditions of several catalysts on OMWSR.

Catalyst	Temperature (°C)	Pressure (Bar)	Feed Flow Rate	FOMW (g·h ⁻¹)	Conversion (%)	H ₂ Yield (%)	H ₂ Purity (%)	Ref.
1 wt.% Pt/Al ₂ O ₃ (commercial)	450	3	WHSV ^(a) = 5.56 × 10 ⁻³ mol·h ⁻¹ ·g _{cat} ⁻¹	10	n.d. ^(b)	40 ^(c)	38 ^(d)	[6]
1 wt.% Pt/Al ₂ O ₃ (commercial)	450	5	WHSV ^(a) = 1.74 × 10 ⁻² mol·h ⁻¹ ·g _{cat} ⁻¹	15	≈60 ^(e)	29 ^(c)	25 ^(d)	[89]
<3 wt.% Pt-Rh-Pd/CeZr ₂ -Al ₂ O ₃	450	5	WHSV ^(a) = 1.74 × 10 ⁻² mol·h ⁻¹ ·g _{cat} ⁻¹	15	>90 ^(e)	35 ^(c)	35 ^(d)	[89]
1 wt.% Pt/CeLa	700	1	GHSV ^(f) = 13,500 h ⁻¹	54	90–96 ^(g)	58 ⁽ⁱ⁾	72 ^(h)	[28]
1 wt.% Ru/CeLa	700	1	GHSV ^(f) = 13,500 h ⁻¹	54	90–96 ^(g)	52 ⁽ⁱ⁾	72 ^(h)	[28]
1 wt.% Rh/CeLa	700	1	GHSV ^(f) = 13,500 h ⁻¹	54	90–96 ^(g)	44 ⁽ⁱ⁾	73 ^(h)	[28]
10 wt.% Ni/CeLa	700	1	GHSV ^(f) = 13,500 h ⁻¹	54	90–96 ^(g)	42 ⁽ⁱ⁾	65 ^(h)	[28]
2 wt.% Rh/M-Al ₂ O ₃	400	1	WHSV ^(a) = 1.75 mol·h ⁻¹ ·g _{cat} ⁻¹	30 ^(j)	≈90 ^(g)	10 ^(k)	≈70 ^(h)	[85]

(a) WHSV: weight hourly space velocity. (b) Not defined. (c) Yield (%) = $\frac{H_{2perm}}{TOC_{feed}} \times 100$, in an MR with a H₂ recovery of 80%. Recovery (%) = $\frac{H_{2perm}}{H_{2perm} + H_{2ret}} \times 100$. (d) H₂ purity (%) = $\frac{H_2}{H_2 + CH_4 + CO_2 + CO} \times 100$, in an MR, on the retentate side, with a H₂ recovery of 80%. Recovery (%) = $\frac{H_{2perm}}{H_{2perm} + H_{2ret}} \times 100$. (e) Conversion of phenols. (f) GHSV: Gas Hourly Space Velocity. (g) Conversion of organic carbon. (h) H₂ purity (%) = $\frac{H_2}{H_2 + CH_4 + CO_2 + CO} \times 100$, in a TR. (i) Yield (%) = $\frac{H_{2prod}}{TOC_{feed}} \times 100$, in a TR. (j) Volumetric flow rate of OMW in mL·h⁻¹. (k) Yield (%) = $\frac{H_{2prod}}{F_{OS}}$, where F_{OS} is the molar flow rate of organic species present in the OMW fed to the reactor.

New catalysts must be developed for future catalytic screening and improvement. These catalysts will need to maximize the reaction conversion, decrease the coke formation, and increase the H₂ selectivity under milder operating conditions.

2.2. Catalysts Used for Steam Reforming of Model Molecules of OMW

Among the materials above-mentioned, numerous catalysts (Ni-, Pt-, Ru-, Co-, and Rh-based) have been extensively studied for the steam reforming of individual components similar to the species present in OMW. Thus, in this work, three different molecules were defined as OMW model compounds: acetic acid, phenol, and toluene. The catalytic performances of the catalysts used for the steam reforming of these species are affected by the active phase, support, and promoter agents. These topics are discussed in the following sections.

2.2.1. Effect of the Active Phase

The active phase is the metal element of the catalyst that catalyzes the reaction. Numerous catalysts (Ni-, Pt-, Ru-, Co-, and Rh-based) have been extensively studied for the steam reforming of oxygenates.

The Ni-based catalysts are the most used in the steam reforming processes because of their effectiveness (they have the potential to be highly active and stable), being commercially available and relatively cheap [104–108]. Nevertheless, the Ni loading, support, promoter(s), and synthesis method used in the catalyst preparation have a crucial impact on both catalytic activity and price [109]. In the study of Zhang et al. [110], it was concluded that the increase of Ni loading from 10 wt.% did not significantly increase the activity of the catalysts, but enhanced the stability, and especially the resistivity towards coking in the steam reforming of acetic acid (@ 1 bar, Liquid Hourly Space Velocity—LHSV = 4.2 h⁻¹, SCFR = 5 and 300–600 °C). The coke formed over the catalyst with the lower Ni loading was more amorphous and the coke formed over higher Ni loading was more fibrous [110]. It was verified by Borges et al. [111] that the higher the Ni loading is, the lower the temperature and the time necessary for the catalyst reduction. The catalyst with a molar ratio of Ni/Co = 3 exhibited the highest activity and the best carbon deposition resistance due to the high density of basic sites for the steam reforming of phenol. In a study by Yu et al. [112], the effect of the type of anion in the Ni precursors in the catalytic behavior of Ni/Al₂O₃ catalysts in steam reforming of acetic acid was studied. It was found that the NO₃⁻ and CH₃COO⁻ as the anions of the Ni precursors did not cause negative effects on the catalytic performance of the catalyst.

Güell et al. [113] reported that the Pt catalyst was active for the steam reforming of oxygenates compounds, as shown in the study of de Castro et al. [114]. Pant et al. [115] reported that Ni-Co, Ni-Co/CeO₂-ZrO₂, and Ni/La₂O₃-Al₂O₃ catalysts can catalyze the steam reforming reaction of acetic acid. Among the three catalysts investigated, the Ni-Co catalyst was found to be more effective for this reaction. Several authors [116–118] found that Rh-based catalysts have a high performance in the steam reforming of oxygenates and several of these materials exhibit superior performance when compared to a commercial Ni-based sample. A series of Ni-Cu bimetallic catalysts supported on sepiolite (Ni_x-Cu_y/SEP) were prepared by Liang et al. [119] for the steam reforming of phenol. The results show that the Ni-Cu alloys were successfully produced in bimetallic catalysts, and the addition of Cu decreased the size of the Ni particles, and improved the redox ability and metal dispersion of bimetallic materials (in this case, Cu can also be considered as a promoter of the catalyst).

The Fe₂O₃/SiO₂-Al₂O₃ catalyst was used by Adnan et al. [120] for the steam reforming of toluene. The results indicate that Fe₂O₃/SiO₂-Al₂O₃ is a promising catalyst (in terms of activity and stability, @ 500 °C, 3.8 bar and SCFR = 0.14) since it has a large quantity of acidic active sites. However, the study of Wang et al. [121] (steam reforming of acetic acid) reported that, in the Co-Fe catalysts, the more active component is Co rather than Fe.

Furthermore, several authors [122–124] show that multi-metallic catalysts show high activity and improve the H₂ yield due to synergistic effects of the multiple components of the active phase.

Finally, mixed oxides such as hydrotalcite-type oxides have been reported as promising catalyst precursors for the steam reforming of these types of oxygenates [111,125].

2.2.2. Effect of the Support

In several studies, it was verified that the support has a significant effect on the performance of the catalysts. Different catalyst supports significantly influenced the reforming reaction.

A series of Ni core-shell catalysts with various shell species (SiO₂, Al₂O₃, CeO₂, and TiO₂) were prepared by Pu et al. [126]. By comparing the catalytic activities of the catalysts with various shell materials, it was concluded that the Ni/Al₂O₃ catalyst was the most suitable material for the steam reforming of acetic acid, showing much higher catalytic activity than the other catalysts. It was also observed in the work of Li et al. [127] that Al₂O₃ support has a high specific area that can enhance the catalytic activity, but the acidity of Al₂O₃ promotes the carbon deposition, reducing the stability of the materials.

The nature of the support was also studied by Zhang et al. [128], using attapulgite (ATTP) and Al₂O₃ as support of Ni-based catalysts. It was verified that ATTP has a lower specific surface area and lower thermal stability than Al₂O₃. The stability of the Ni/Al₂O₃ catalyst was higher than that of the Ni/ATTP catalyst, not only due to the higher surface area of Al₂O₃, but also due to the type of coke formed on the surface of the Ni/Al₂O₃ catalysts (fibrous) instead of the amorphous coke formed on Ni/ATTP catalyst.

Chen et al. [129] studied the effect of biochar as support in Ni-based catalysts for the steam reforming of acetic acid. The results of the catalyst characterization showed that the porosity of biochar was increased significantly after activation, increasing the surface area of the materials and the dispersion of the Ni particles on the catalyst's surface. Besides that, in the work of Wang et al. [130]—study of the steam reforming of acetic acid—it was found that the treatment of biochar support with HNO₃ enhanced the quantity and the strength of the acidic active sites as well as the catalytic activity of the Ni/biochar catalysts.

Additionally, Yang et al. [131] using a NiO/MgO catalyst have concluded that the interaction between the support and active phase can prevent the material from sintering.

Finally, silicate structured mesoporous materials were reported to be less vulnerable to deactivation due to carbon formation than the traditional microporous catalyst supports. They also cause less resistance to the diffusion of reactants to the active sites [88].

2.2.3. Effect of Promoters

In several studies of the steam reforming of oxygenates, the catalysts were doped with promoters. It was reported that Cr inhibited the formation of Ni₃C and can modify the metal sites forming alloys with Ni [132,133], La₂O₃ led to a decrease in coke formation [105,132–136], K and MgO improved the stability [105,117,132,133,136–139], and TiO₂ decreased the conversion [132]. It was also observed that the addition of CeO₂ improved the activity and stability of the catalyst [106,108,114,135,140–142].

The work of Li et al. [143] reported that the presence of CeO₂ in the catalyst increased the support–metal interaction, restricting the growth of metal particles. Besides that, it was found that the oxygen vacancies of the CeO₂ are responsible for the activation of the water to generate OH[−] groups, which can react with intermediate products to produce CO₂ and H₂. In the study of Liada et al. [118], Ru/SrCO₃-Al₂O₃ catalysts with a low Ru loading exhibited higher catalytic activity for steam reforming of toluene compared to a commercial Ru/Al₂O₃ catalyst (@ 600 °C and SCFR = 2). In this way, it was possible to see that the SrCO₃ increases the performance of the catalyst. Additionally, in the study of Zhang et al. [144], it was found that the addition of KOH to Ni/Al₂O₃ with the lowest Ni loading significantly enhances the catalytic activity and promotes gasification of the reactive intermediates such as methyl group, carbonyl group, etc.

Choi et al. [145] studied the steam reforming of acetic acid by using catalysts modified by MgO, LaO₃, Cu, and KOH. Ni/Al₂O₃ modified with Mg showed the best performance at low temperatures. It was possible to verify that a catalyst with a large quantity of weak basic sites and few middle/strong basic sites is necessary to improve the catalytic performance and minimize the coke formation. Finally, it was observed that the toluene conversion and H₂ yields increased with the addition of alkaline-earth metals [146]. In a general way, the addition of basic oxides (e.g., MgO, CeO₂, La₂O₃, etc.) enhanced the coking resistance, thus improving the catalytic performance. These oxides aim to enhance the redox properties of the catalyst [143,147–150], which increases the oxidation of carbon deposits. For instance, Kumar et al. [151] reported that the coke formation was also significantly suppressed by the γ -Al₂O₃-La₂O₃-CeO₂ support.

Finally, Yu et al. [152] reported that the addition of Mn enhanced the specific area of the catalyst, by the formation of more pores and the addition of Fe, Mn, La, and Ce could enhance the dispersion of Ni particles in the support. Besides that, Co, K, La, Na, or Ce enhance the activity of Ni-based catalysts and K or Na addition enhanced the reduction of Ni oxides.

However, Galdamez et al. [153] concluded, in the steam reforming of bio-oil, that the addition of La₂O₃ in the Ni catalyst does not increase the H₂ yield. It was also found that ZrO₂ had a negligible effect on the performance of the catalyst [138].

A summary of the more relevant catalysts reviewed in this section for the steam reforming of individual components (or similar) of the OMW and their best catalytic performances are presented in Table 4. It is possible to verify that Ni-based catalysts are effective for these reactions (they exhibit similar catalytic performance compared to noble metal-based catalysts) and are relatively cheaper. Therefore, more detailed information about the catalytic stability and preparation method of these catalysts is reported in Table 5. It is possible to see that several Ni-based catalysts present no deactivation until the end of the experimental test, even though noble metal-based catalysts are less susceptible to coke formation [94,154,155]. Furthermore, the most used preparation method of these catalysts is the impregnation of the Ni on the support; however, there are only a few studies about the effect of the preparation method in the catalytic behavior of the materials for the steam reforming of long-chain oxygenates.

2.3. Summary

Until now, only a few catalysts have been developed for the OMWSR process: Ni-, Pd-, Pt-, Rh-, and Ru-based. However, several catalysts were studied for the steam reforming of components that are similar to species present in the OMW.

It is possible to conclude that Ni-based catalysts are promising for the steam reforming of oxygenated species. However, almost all these catalysts showed conversions close to 100% and high H₂ yields and selectivities, making it difficult to choose the best one. These results show how attractive Ni-based catalysts are for the OMWSR process, in comparison with the noble metal-based catalysts, due to their lower costs.

Almost all Ni-based catalysts were prepared by impregnation, appearing to be the best method for the preparation of these materials. It is still necessary to study the effect of the preparation method on the catalytic behavior of the materials.

A bi-metallic catalyst with Ni and one noble metal (e.g., Ru) as active phases, supported in an adequate material (e.g., Al₂O₃ or SiO₂) and doped with a promotor (e.g., CeO₂) is a potential catalyst to achieve high catalytic performance (H₂ yield and OMW conversion) for OMWSR during long reaction times.

In future studies, it is necessary to rigorously assess the costs associated with the preparation of the different catalysts (with different preparation methods, reagents, active phases, etc.), to better benchmark the numerous catalytic formulations available, i.e., make a selection (for industrial applications) based on both techno and economic criteria.

Table 4. Summary of the catalytic performance and operating conditions of catalysts on steam reforming reactions of oxygenated compounds.

Catalyst	Temperature (°C)	Pressure (Bar)	Feed Flow Rate	SCFR ^(a)	Conversion (%)	H ₂ Yield ^(b) (%)	H ₂ Selectivity ^(c) / Purity ^(d) (%)	Ref.
3.5 wt.% Ni/5 wt.% La ₂ O ₃ -ZrO ₂ ¹	700	1	GHSV ^(e) = 240,000 h ⁻¹	5	100	87	89/64	[105]
(2.5 + 2.5) wt.% Ni-Cu/Al ₂ O ₃ ¹	750	1	WHSV ^(f) = 28 h ⁻¹	1.25	100	67	68/57	[156]
15 wt.% Ni/α-Al ₂ O ₃ ¹	600	1	WHSV ^(f) = 20 h ⁻¹	1	≈100	90	90/66	[107]
(15 + 2) wt.% Ni-Ru/10 wt.% CeO ₂ -Al ₂ O ₃ ¹	700	1	WHSV ^(f) = 21 h ⁻¹	3.2	91	67	79/61	[140]
10 wt.% Ni/La ₂ O ₃ -Al ₂ O ₃ ¹ (La ₂ O ₃ /Al ₂ O ₃ = 1:3, weight ratio)	700	1	LHSV ^(g) = 10 h ⁻¹	1	100	72	71/59	[134]
15 wt.% Ni/Al ₂ O ₃ ¹	700	1	F _{Acetic Acid} = 10 g·h ⁻¹	1	100	57	58/54	[157]
3.2 wt.% Ni/CeO ₂ -ZrO ₂ ¹	700	1	WHSV ^(f) = 25 h ⁻¹	14	≈84	68	88/64	[106]
0.5 wt.% Pt/CeO ₂ ¹	700	n.s. ^(h)	GHSV ^(e) = 80,000 h ⁻¹	5	98	94	≈100/67	[113]
28 wt.% Co/7 wt.% K-Al ₂ O ₃ ¹	600	1	LHSV ^(g) = 10 h ⁻¹	7.5	100	86	87/64	[138]
(6.6 + 10) wt.% Ni-Fe/(CeO ₂) _{0.4} -PG _{0.6} ¹	600	1	LHSV ^(g) = 14,427 h ⁻¹	3	≈97	88	84/63	[141]
(35 wt.% NiO) Ni/Hydrotalcite ¹	600	1	n.s. ^(h)	1.5	≈100	47	67/56	[111]
Ni/BC4 ¹	700	1	LHSV ^(g) = 10 h ⁻¹	2.5	91.2	71	79/61	[129]
10 wt.% Ni/ATTP ¹	600	1	LHSV ^(g) = 7.2 h ⁻¹	5	≈100	72	91/65	[128]
25 wt.% Ni/Atta ¹	700	1	LHSV ^(g) = 10.4 h ⁻¹	5	96	89	90/64	[93]
15 wt.% Ni/Al ₂ O ₃ -La ₂ O ₃ -CeO ₂ ¹	650	1	Q _T = 2.5 mL·h ⁻¹	6.5	≈100	88	90/64	[151]
Co (unsupported)	600	1	LHSV ^(g) = 4 h ⁻¹	9.2	100	≈100	99/66	[121]
3 wt.% Ni/(0.4 + 5) wt.% K-LaO ₂ -ZrO ₂ ²	700	1	GHSV ^(e) = 950,000 h ⁻¹	20	≈81	83	98/70	[136]
0.1 wt.% Rh/(50 + 25) wt.% MgO-CeO ₂ -ZrO ₂ ²	700	1	GHSV ^(e) = 80,000 h ⁻¹	13	97	90	86/67	[116]
Ni-Fe/olivine ²	850	1	W/F ⁽ⁱ⁾ = 10.28 kg _{cat} ·h·m ⁻³	1	≈100	n.d. ^(h)	81/63	[158]
1.5 wt.% Pt/CeO ₂ -Al ₂ O ₃ ³	700	1	Q _T = 300 mL·min ⁻¹	6	≈95	n.d. ^(h)	81/66	[114]
16.4 wt.% Ni/Al ₂ O ₃ ³	800	1	GHSV ^(e) = 61,200 h ⁻¹	3	>94	91	75/66	[159]

(a) Steam to carbon feed ratio. (b) Yield (%) = $\frac{H_2}{H_{2,Max}}$ × 100. (c) Selectivity (%) = $\frac{H_2}{RR \times (CO_2 + CH_4 + CO)}$ × 100. RR is H₂/CO₂ reforming ratio. (d) Purity (%) = $\frac{H_2}{(H_2 + CO_2 + CH_4 + CO)}$ × 100. (e) GHSV: gas hourly space velocity. (f) WHSV: weight hourly space velocity. (g) LHSV: liquid hourly space velocity. (h) Not determined/specified. (i) W_{cat}/F_{phenol}. ¹ Steam reforming of acetic acid. ² Steam reforming of phenol. ³ Steam reforming of toluene.

Table 5. Stability and preparation methods for Ni-based catalysts used on steam reforming reactions of oxygenated species.

Catalyst	Mass of Catalyst (g)	Stability	Preparation Method	Ref.
3.5 wt.% Ni/5 wt.% La ₂ O ₃ -ZrO ₂ ¹	0.050	Lost 7% H ₂ yield in 20 h	Impregnation	[105]
(2.5 + 2.5) wt.% Ni-Cu/Al ₂ O ₃ ¹	0.1	Result of 7.5 h (no deactivation)	Impregnation over support prepared by following evaporation induced self-assembly	[156]
15 wt.% Ni/ α -Al ₂ O ₃ ¹	1.5	n.d. (a)	Impregnation	[107]
10 wt.% Ni/La ₂ O ₃ -Al ₂ O ₃ ¹ (La ₂ O ₃ /Al ₂ O ₃ = 1:3, weight ratio)	0.2	Result of 30 h (no deactivation)	Co-precipitation	[134]
15 wt.% Ni/Al ₂ O ₃ ¹	0.2	n.d. (a)	Incipient wetness impregnation	[157]
6.6 wt.% Ni-10 wt.% Fe/(CeO ₂) _{0.4} -PG _{0.6} ¹	n.s. (a)	Result of 20 h (no deactivation)	Co-precipitation	[141]
Ni/BC4 ¹	0.15	n.d. (a)	Impregnation	[129]
10 wt.% Ni/ATTP ¹	0.5	n.d. (a)	Impregnation	[128]
16.4 wt.% Ni/Al ₂ O ₃ ²	n.s. (a)	Result of 5 h (no deactivation)	Impregnation	[159]

(a) Not determined/specified. ¹ Steam reforming of acetic acid. ² Steam reforming of toluene.

3. Multifunctional Reactors

In the last few years, different reactor configurations for improving the catalytic steam reforming processes have been investigated and debated, since this process involves reversible reactions, and thus equilibrium limitations. Thus, the utilization of multifunctional reactors in the OMWSR process can become a very promising approach [160]. Even so, and despite the significant number of studies addressing such devices for other applications, in future works more attention should be paid to detailed techno-economic analyses to assess the economic feasibility of this process, as well as the difference, in financial terms, resulting from the application of different reactor configurations (traditional vs. multifunctional reactors). To the authors' knowledge, this type of study has not yet been developed for the OMWSR process.

3.1. Sorption-Enhanced Reactor

One of those alternatives for the process intensification of the OMWSR is the utilization of a SER (see Figure 10), which consists of combining the TR and CO₂ sorption in the same reactor. This innovative configuration allows shifting the thermodynamic equilibrium of the steam reforming reaction by removing one of the products (in this case CO₂) from the reaction medium—Le Chatelier principle [160,161]. This reactor configuration was already used in multiple applications [109,162–193] in the last decade. The SER can shift the equilibrium of the reversible reactions to higher conversions of the reagents. In this way, this reactor configuration will enhance the production of H₂, since the removal of CO₂ shifts the WGS reaction (Equation (3)) to the forward direction and inhibits CH₄ and coke production (Equations (5) and (12)).

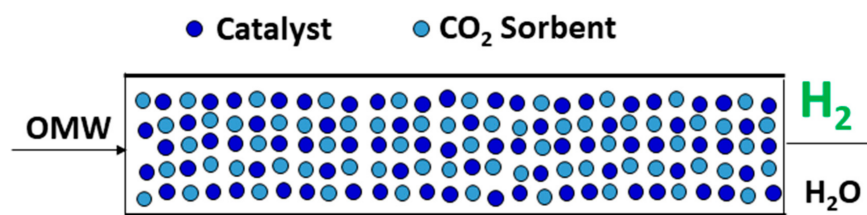


Figure 10. Scheme of the operation of the SER.

However, the drawback of this technology is that after some time the sorbent gets saturated with CO₂ and then regeneration is required. To make it possible to run continuously, the system must have at least two parallel devices, so that while one of the reactors is utilized as SER (reaction stage), the other is being regenerated. It is possible to distinguish three regimes along time: pre-breakthrough, breakthrough, and post-breakthrough. In the pre-breakthrough region, the CO₂ is being removed, thus enhancing H₂ production. In the breakthrough region, the H₂ concentration at the reactor outlet begins decreasing. In the post-breakthrough region, the sorbent is already saturated and so the improvement of the H₂ production due to CO₂ capture disappears—Figure 11.

The effect of the capture of CO₂ from the reaction medium was already discussed for the OMWSR from the thermodynamic point of view [194], though this effect has already been analyzed for other similar reactions [84,195,196]. In a previous work of Rocha et al. [197], a comparison of the performance between a SER and a TR was already performed for this process. This reactor configuration intensifies the performance of the process by combining the reaction and CO₂ capture in a single device. In this way, a SER allows the production of more high-purity products at the outlet (in this case, pure H₂ before the breakthrough time).

In this reactor configuration, the decrease of the CO₂ emissions also presents a very interesting environmental advantage. Since the industrial revolution, the global CO₂ concentration increased from about 280 ppm to 415 ppm in 150 years. The higher concentration of pollutants in the atmosphere increases the greenhouse effect with a huge environmental impact. To avoid irreversible changes to the global climate, the United Nations in the COP26 have agreed to establish goals to reduce the CO₂ emissions to limit its concentration in the atmosphere [198]. Therefore, this reactor configuration is also in line with this premise, in order to decrease the environmental impact of CO₂.

3.1.1. CO₂ Sorbents

Sorption-enhanced technologies require the mixture of a catalyst, that is stable and with high catalytic activity in the temperature range considered (in this case 300–500 °C, or even higher), and a solid sorbent, in this case with high CO₂ sorption capacity and with adequate sorption–desorption kinetics.

Several materials—such as CaO-based materials [199–208], hydrotalcites (HTCs) [209–224], lithium silicates [225–238], lithium cuprate [239] and lithium zirconates [240–242], among others—have been reported in the literature as high-temperature CO₂ sorbents. It is expected from a good CO₂ sorbent for the application envisaged herein to present high CO₂ capture capacity at moderate temperatures (300–500 °C), fast sorption–desorption kinetics [243], good mechanical and hydrothermal stability, and low price. A solid with high CO₂ sorption capacity with slow kinetics is not suitable since it requires a lot of time for the gas to get into the particle and long times are needed to reach saturation [244], as well as for sorbent regeneration.

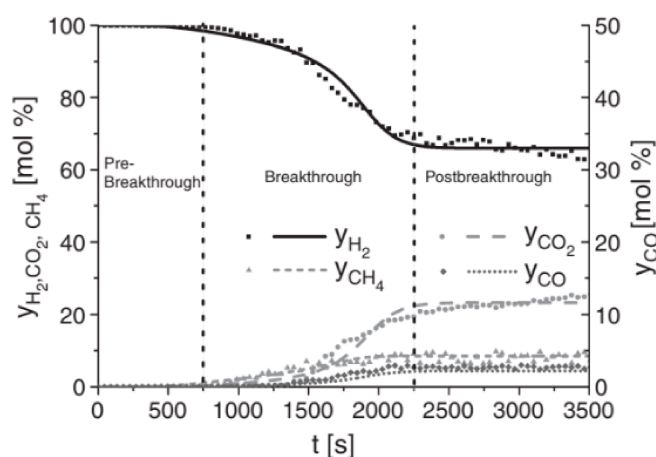


Figure 11. Example of product distribution as a function of time in the outlet of an SER (steam reforming of ethanol for hydrogen production). Reprinted with permission from Ref. [162]. Copyright 2021 Elsevier.

Although metal oxides (e.g., CaO) have a higher sorption capacity at high temperatures and can be stabilized when used as a mixture of oxides, they lose their properties very rapidly throughout the sorption–desorption cycles, an issue that is more marked when the adsorbent is in the presence of steam. Besides that, the sorption capacity of these materials decreases because of sintering phenomena [109]. Conversely, HTC has practically constant capacity over the cycles, increase their capacity in a wet environment, and have great thermal and mechanical stability. Moreover, compared to other possible sorbents such as CaO and lithium zirconates, HTCs show the best adsorption–desorption kinetics and the energy involved in their regeneration is considerably lower [244].

Nevertheless, some research was performed with other sorbents to compete with the HTCs, which is shortly described herein below.

Akgsornpeak et al. [245] avoided the sintering phenomena by preparing CaO materials through the sol–gel synthesis with cetyltrimethyl ammonium bromide. Besides that, the incorporation of Y_2O_3 has been lately stated to significantly enhance the carbonation (sorption) rate and adsorption capacity of CaO-based materials [206]. The addition of optimized quantities of K to Li_2ZrO_3 sorbents was reported to enhance their CO_2 sorption capacity, sorption rate, and stability in sorption–desorption cycles [226]. Seggiani et al. [226] examined the performance of several doped- Li_4SO_4 samples, having noticed that the K-doped and Na-doped sorbents presented the highest sorption capacities and sorption rates. In terms of stability, only the K-doped sorbent was capable of maintaining its properties after 25 sorption/desorption cyclic runs. However, Iwand et al. [240] concluded that the traditional preparation method of K-doped materials results in sorbents with slow regeneration step.

The CO_2 sorption capacities and the sorption and regeneration temperatures of several materials are summarized in Table 6.

HTC is a layered double hydroxide. This natural or synthetic lamellar hydroxide has two kinds of metallic cations (divalent and trivalent) in the main layers and interlayer space containing anionic species (compensating/interlayer anions)—Figure 12 [248,249]. These materials are used in a wide range of applications as catalysts, precursors, and sorbents [214]. Several thousands of tons of HTCs are produced annually by different chemical companies—such as BASF, SASOL, Clariant, Kisuma Chemicals, and Sakai Chemical [250]. The general formula is $[M_{1-x}^{2+}M_x^{3+}(OH)_2]^{x+} [A_{x/n}^{n-} \cdot yH_2O]^{x-}$, where M^{2+} is a divalent metal cation and M^{3+} is a trivalent metal cation. A^{n-} is a charge balancing anion (usually CO_3^{2-}) located in the interlayer volume and x is generally between 0.2 and 0.4, while y is the number of moles of water located in the interlayer space [209,210]. Similar layered structures of HTCs could be produced with several interlayer anions [222,224,246,247,250–257].

Table 6. Sorption capacities and sorption/regeneration temperatures of several CO₂ sorbents.

Sorbent	Sorption Capacity ^(a) (mmol·g ⁻¹)	Temperature (°C)	Regeneration Temperature (°C)	<i>p</i> _{CO₂} (Bar)	<i>p</i> _{H₂O} (Bar)	Ref.
CaO-Y ₂ O ₃ (20 wt.% Y ₂ O ₃)	12.95	850	850	n.s. ^(b)	-	[206]
CaO	17.30	600	700	0.30	-	[207]
CuO/CaO/Ca ₁₂ Al ₁₄ O ₃₃ (19/43/38 wt.%)	3.14	650	870	0.15	0.25	[202]
Na ₂ CO ₃ -CaO	14.7	800	800	1.00	-	[208]
CaO-Mg	10.22	600	700	0.50	-	[205]
Li ₂ ZrO ₃	5.00	500	n.s. ^(b)	n.s. ^(b)	n.s. ^(b)	[242]
Li ₄ SiO ₄	7.29	600	750	1.00	-	[236]
Li ₄ SiO ₄	6.24	550	700	0.15	-	[229]
K-Li ₄ SiO ₄ (30 wt.% K ₂ CO ₃)	5.23	580	700	0.04	-	[226]
K-Li ₄ SiO ₄	5.00	575	700	1.00	-	[241]
Li ₄ SiO ₄	5.00	550	700	0.15	-	[229]
CaNd75	10.9	650	n.s. ^(b)	0.15	-	[203]
cHTC (Mg/Al = 2)	0.81	300	n.s. ^(b)	1.03	-	[209]
HTC (Mg/Al = 2)	0.54	300	n.s. ^(b)	0.14	-	[210]
K-HTC	0.79	400	n.s. ^(b)	1.00	-	[243]
K-HTC (20 wt.% K ₂ CO ₂ , Mg/Al = 0.6)	0.28	400	400	0.50	-	[219]
K-HTC (22 wt.% K ₂ CO ₂ , Mg/Al ≈ 2)	0.58	400	400	0.47	-	[220]
HTC-20K (20 wt.% K, Mg/Al = 2)	2.14	300	n.s. ^(b)	1.10	-	[210]
cK-HTC (20 wt.% K, Mg/Al = 2)	1.42	300	n.s. ^(b)	1.02	-	[209]
MG30-K ^N (20 wt.% K, Mg/Al ≈ 0.5)	1.08	335	435	0.50	0.5	[221]
K-HTC (20 wt.% K ₂ CO ₂ and Mg/Al = 2)	9.40	300	600	0.34	4.5	[215]
K-HTC MW (20 wt.% K ₂ CO ₂ , Mg/Al = 2)	1.46	300	n.s. ^(b)	1.00	-	[223]

Table 6. Cont.

Sorbent	Sorption Capacity ^(a) (mmol·g ⁻¹)	Temperature (°C)	Regeneration Temperature (°C)	p _{CO2} (Bar)	p _{H2O} (Bar)	Ref.
cK-HTC MW (20 wt.% K, Mg/Al = 2)	1.51	300	n.s. ^(b)	1.00	-	[209]
HTC-10Ga(10 wt.% Ga, Mg/Al = 2)	0.58	300	n.s. ^(b)	1.12	-	[210]
HTC-10Ga-20K (10 wt.% Ga, 20 wt.% K, Mg/Al = 2)	1.82	300	300	1.08	-	[210]
cK-HTCGa MW (20 wt.% K, Mg/(Al+Ga) = 2, Al/Ga = 9)	1.70	300	n.s. ^(b)	1.05	-	[209]
Li/Na/K-MgAl-C ₁₆ (55 wt.% Li-Na-K, Mg/Al = 20)	3.21	200	400	1.00	-	[246]
Mg ₃ Al ₁ -CO ₃	0.53	200	n.s. ^(b)	1.00	-	[222]
Mg ₃ Al ₁ -NO ₃	0.21	200	n.s. ^(b)	1.00	-	[222]
Mg ₃ Al ₁ -HNO ₃	0.18	200	n.s. ^(b)	1.00	-	[222]
Mg ₃ Al ₁ -SO ₄	0.10	200	n.s. ^(b)	1.00	-	[222]
Mg ₃ Al ₁ -Cl	0.18	200	n.s. ^(b)	1.00	-	[222]
(Mg,Al)(Cl) (Mg/Al = 3)	0.44	330	n.s. ^(b)	1.00	-	[224]
(Mg,Al)(ClO ₄) (Mg/Al = 3)	3.55	330	n.s. ^(b)	1.00	-	[224]
(Mg,Al)(Fe(CN) ₆) (Mg/Al = 3)	0.75	330	n.s. ^(b)	1.00	-	[224]
MgAl-C ₁₆ (Mg/Al = 3)	0.91	200	400	1.00	-	[246]
Mg ₃ Al-stearate	1.25	300	n.s. ^(b)	1.00	-	[247]

^(a) Sorption capacity of the fresh sorbent. ^(b) Not specified (or regeneration step not performed).

3.1.2. Hydrotalcites

Co-precipitation is the most used method for the preparation of this type of material. It is based on the slow addition of a mixed solution of divalent and trivalent metals salts in adequate proportions into a reactor. An alkaline solution (e.g., NaOH) is added to the reactor in order to maintain the pH at a selected value, leading to the co-precipitation of the two metallic salts [248]. Therefore, there is often competition between some anionic species, and the tuning of the synthesis experimental conditions can lead to the selective intercalation of one of them as the primary interlamellar anion. Secondary interlamellar anions can replace them with further treatments such as an anionic exchange. In addition, it is not clear that a pure HTC phase is always obtained: for instance, although the overall composition of a certain precipitate corresponds to the estimated value, secondary phases such as hydroxides or basic salts of the divalent or trivalent metal can be present in the material [248]. HTCs can, however, be synthesized by various techniques depending on the specific requirement and properties of the compounds. Other methods include combustion, recrystallization, urea hydrolysis, ion exchange, reverse-microemulsion, sol-gel, and hydrothermal [209,258–262].

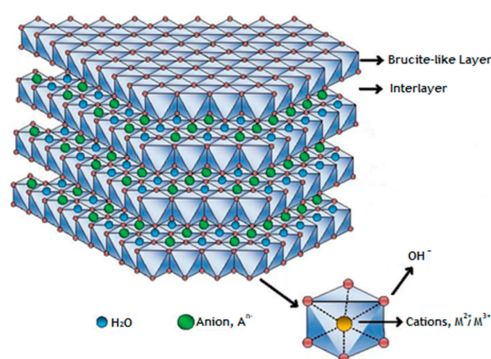


Figure 12. Schematic representation of the hydrotalcite structure. Adapted from Tronto et al. [249].

The morphology and the thermal stability of the synthesized HTCs affect CO₂ sorption performance. The physicochemical properties of HTCs can be modified by combining adequate cations and anions [222,224,246,247,250–257,263,264], by varying the molar ratio of M²⁺/M³⁺ [211,212,246], by changing the preparation conditions such as pH [222] (pH values between 8–10 can be used to synthesize HTCs [258]), calcination temperature [246,265,266], or aging process (e.g., microwave, ultrasonication, etc.) [209,223,267] among other parameters. On the other hand, the basicity of the sorbents can be improved by promotion with alkaline species [268], this way increasing their CO₂ sorption capacity.

Fresh HTCs as such are not excellent CO₂ sorbents due to poor basic properties and the presence of species that hinder CO₂ adsorption. Therefore, they are subjected to thermal treatment (calcination) to obtain a nearly amorphous mixed solid solution—with a poorly defined 3D network—with more favorable and stable properties for CO₂ sorption [248]. HTCs undergo different stages of transition during the calcination. These transitions depend on many aspects such as the nature and relative quantities of cations, type of anions, method of synthesis, and crystallinity. Several authors have methodically investigated the thermal decomposition process [214,261,263,265,269]. The optimum temperature of calcination is usually 400 °C, since it allows the decomposition of the interlayer anions (and then, the active sites can be occupied by the CO₂) and the formation of the amorphous phase (mixed oxides) with sorption properties, without the complete and irreversible destruction of the structure. Apparently, such optimum temperature results from the balance between surface area and the number of basic active sites [214,263]. In the calcination program, the first weight loss is detected between 70 °C and 190 °C, attributed to the loss of interlayer water; then, in the temperature range of 190 °C to 280 °C, the OH⁻ group bonded with Al³⁺ disappears [270]. The OH⁻ group bonded with Mg²⁺ disappears from the structure of the material in the temperature range 280 °C to 405 °C and the interlayer anions are usually

released between 405 °C and 580 °C [270]; in this way, the material becomes an amorphous mixed oxide solution, which is reversible if the calcination temperature is not higher than 550–600 °C [270,271]—see Figure 13. The use of very high calcination temperatures leads to the development of spinel phases (e.g., MgAl_2O_4), which should be prevented in order to conserve the platelet morphology of HTC and an acceptable basicity [244,246]. The original structures of the calcined samples can be recovered again by exposure to steam and atmospheric CO_2 (or through anion intercalation)—“memory effect” [264,272–274].

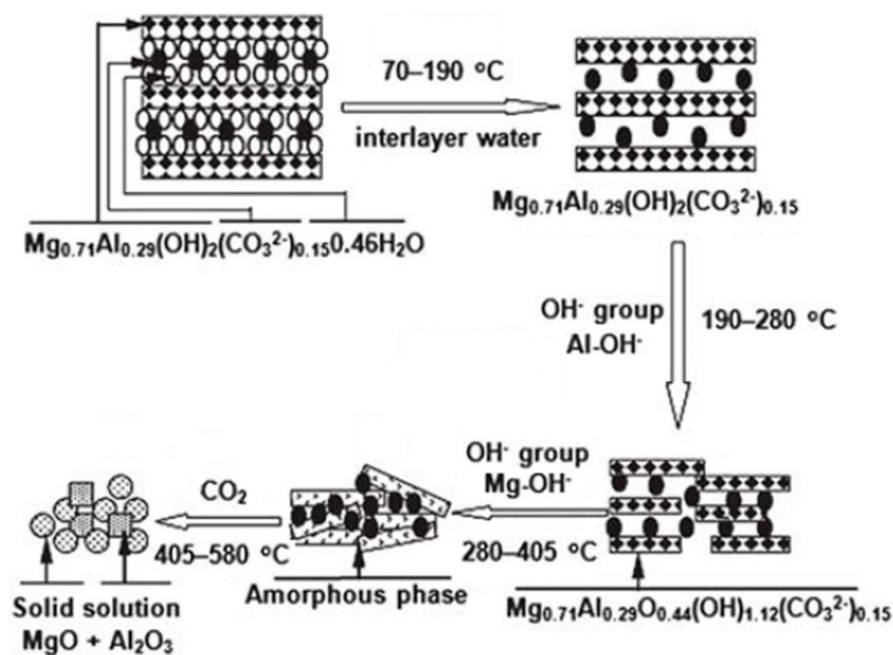


Figure 13. The structural evolution of a typical HTC as a function of calcination temperature. Adapted with permission from Ref. [275]. Copyright 2021 Royal Society of Chemistry.

Different optimum $\text{Mg}^{2+}/\text{Al}^{3+}$ ratios have been reported in the literature, which varies from 1:1 to 3:1—the optimum ratio depends on the type of interlayer anion used, preparation method, etc. [212,276,277]. Although high Mg^{2+} content allows the formation of a higher number of basic active sites in the material, at higher $\text{Mg}^{2+}/\text{Al}^{3+}$ ratios MgCO_3 may also form at high partial pressures of water (steam) and CO_2 , which can lead to mechanical stability problems [278,279]. In the work of Yong et al. [212], the authors studied the effect of different $\text{Mg}^{2+}/\text{Al}^{3+}$ ratios (0.5, 1.3, and 3.0) on the sorption capacity of three commercial HTCs from SASOL. It was verified that the HTC with $\text{Mg}^{2+}/\text{Al}^{3+}$ ratio of 1.3 had the highest performance. However, there is a lowest limit of the $\text{Mg}^{2+}/\text{Al}^{3+}$ ratio (≈ 2.0) to obtain a crystallographically pure HTC, since this ratio influences the electrostatic repulsion between neighboring trivalent metals in the layers [248,280]. The optimum $\text{Mg}^{2+}/\text{Al}^{3+}$ molar ratio reported in several studies is often equal to 2 [209,210,212,255] for the sorbents impregnated with potassium.

As previously mentioned in this section, the CO_2 sorption capacity of the HTCs can be enhanced by impregnating with an alkali metal such as Na, K, or Cs [281,282]. It was verified by several works that HTCs modified with alkali promoters like K_2CO_3 (or Na/ KNO_3) showed best CO_2 sorption performance than the base HTCs [209,210,218,243,281–286]—see, for instance, Figure 14. Besides that, several authors [209,210,218,287] have also shown that the simultaneous impregnation with K and substitution of Al^{3+} with Ga^{3+} markedly improved the sorption capacity of HTCs, the first modification acting as a chemical promoter and the latter providing a superstructure, robust and stable at elevated temperatures. For K_2CO_3 -modified HTCs with high $\text{Mg}^{2+}/\text{Al}^{3+}$ ratios, the doping is mostly concentrated in the bulk phase and behaves as a reactant to form high stable K-Mg double carbonates after sorbed CO_2 . With the increase of the Al^{3+} content, surface modifications occur and

become the dominant improvement mechanism via the interaction between the K^+ ions and unsaturated oxygen sites [283].

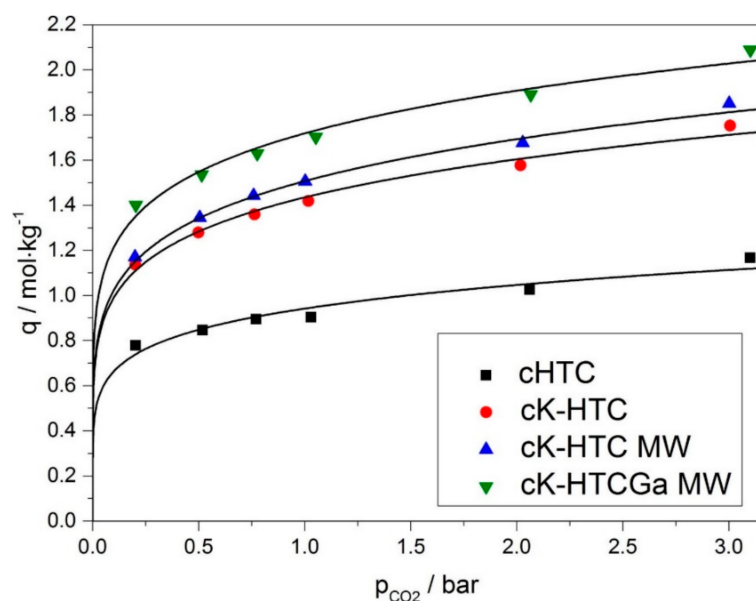


Figure 14. CO_2 sorption equilibrium isotherms at 300 °C on the calcined HTCs. The lines correspond to the fitting using the Freundlich equation (cHTC—calcined HTC; cK-HTC—calcined K-promoted HTC; cK-HTC MW—calcined K-promoted HTC aged under microwave irradiation; cK-HTCGa MW—calcined K-promoted Ga-substituted HTC aged under microwave irradiation). Reprinted with permission from Ref. [209]. Copyright 2021 Elsevier.

It has also been found that the physicochemical properties of HTCs are highly influenced by the interlayer anions used. The anion influences the crystallinity and layer spacing in HTCs. In this way, materials with different interlayer anions present different morphologies and chemical surfaces, influencing the sorption performance of the HTCs-derived mixed oxides. For instance, Yong and Rodrigues [288] reported that the sorption capacity of HTC containing $Fe(CN)_6^{4-}$ was higher ($1.3 \text{ mmol}\cdot\text{g}^{-1}$) than the one containing NO_3^- ($0.3 \text{ mmol}\cdot\text{g}^{-1}$) at 25 °C and 1 bar of CO_2 . However, Wang et al. [222] analyzed numerous charge interlayer anions (SO_4^{2-} , Cl^- , CO_3^{2-} , HCO_3^- , and NO_3^-) having noticed that when using CO_3^{2-} , a spheroidal “sand rose” type of HTC with a very high surface area was produced. On the other hand, the other compensating anions led to the formation of “stone” type HTCs with very low surface areas. For this reason, the HTC with CO_3^{2-} as interlayer anion presented the highest CO_2 capture capacity. However, larger size anions tend to increase the interlayer spacing; this space can help the K ions to disperse into the HTC interlayer and, thus, create more Al(Mg)–O–K bonds to enhance the performance of the sorbent [247].

Several works have shown that the existence of steam in the feed gas increases the CO_2 sorption capacity of potassium doped-HTCs by 10–17 wt.% and enhances the stability of these materials (in the temperature range of 200–400 °C and in the pressure range of 1–3.5 bar) [193,216,218,221,279,289–291]. It was observed that at least four different adsorption sites take part in the sorption/desorption of CO_2 and H_2O and the presence of steam activates some active sites for the CO_2 sorption. Two adsorption sites can be restored with N_2 (or other inert gas), whereas the other adsorption sites require the presence of H_2O to be activated/regenerated [279,289,290]. These features are particularly important for the application envisaged herein, once the OMWSR occurs in the presence of large excess of water.

The CO_2 sorption kinetics in dry conditions for these materials was studied by Miguel et al. [210] and Silva et al. [209] and it was noticed that the kinetics is dependent on

the morphology/composition of the material, with the physical sorption being faster than the chemical one.

The conclusion on which type of CO₂ sorbent is more suitable to be used in the SER strongly depends on the operating temperature at which it will be used. Since one of the main goals is to reduce the temperature of the steam reformer to reduce the operation costs, it is attractive to work at relatively low temperatures (300–500 °C). For such temperatures, HTCs have been reported to present higher CO₂ sorption capacities and faster sorption–desorption kinetics, as well as easier regeneration, and lower loss of sorption capacity along consecutive cycles. HTCs are also better than other sorbents due to nearly infinite selectivity for CO₂ sorption over gases like CH₄, CO, and N₂ [250]. Moreover, the fact that the CO₂ sorption capacity of HTCs is strongly improved under wet conditions (steam reforming process conditions) makes them an even better option for use in the OMWSR process using a SER (for instance, Lu et al. [207] reported that the sorption capacity of a CaO sorbent over the carbonation/decarbonation cycles decreased faster when steam was present in the system).

3.1.3. OMWSR in Sorption-Enhanced Reactors

As already mentioned, in a previous work of Rocha et al. [197], a comparison of the performance between different reactor configurations was performed for the OMWSR process. In a general way, it was verified that the conversion of the organic carbon (above 99%) remains almost complete along all the experimental tests when using a SER (@ 1 bar and 350/400 °C), and it was verified an improvement of the H₂ production during the pre-breakthrough of CO₂ as compared to the conventional reactor (TR)—see Figure 15.

In this work [197], the experimental tests with the SER configuration were separated into two different sets: a first set of experimental tests using a commercial sorbent, and a second set with a sorbent prepared in the laboratory. It was observed that, at both operating conditions and using the commercial sorbent (Figure 15), the H₂ yields obtained in the first cycle were higher than those reached for the first hour in the TR. Furthermore, it was noticed that the utilization of the commercial sorbent (that promotes the removal of CO₂ from the reaction medium) increased the stability of the catalyst in comparison with the performance of the TR—lower formation of coke.

3.1.4. Summary

The OMWSR through a SER consists of combining the reaction and CO₂ separation in the same device. This innovative reactor configuration requires, besides a catalyst, a solid sorbent with high CO₂ sorption capacity, which must be simple to regenerate and have good performance, particularly in the presence of steam. Several materials—such as CaO-based materials, lithium cuprate, lithium silicates, and lithium zirconates, among others—have been reported in the literature as high-temperature CO₂ sorbents. However, it is possible to conclude that HTCs have adequate properties to be used in a SER for OMWSR: practically constant and high CO₂ sorption capacity over the cycles at moderated temperatures, increased performance in a wet environment, adequate sorption–desorption kinetics, and great thermal and mechanical stability.

In this way, an HTC impregnated with potassium is a potential sorbent to be used to capture from the reaction medium the CO₂ produced in the OMWSR (sorption-enhanced process), increasing the purity of the H₂ and shifting the thermodynamic equilibrium to the production of more H₂ (increasing the H₂ yield).

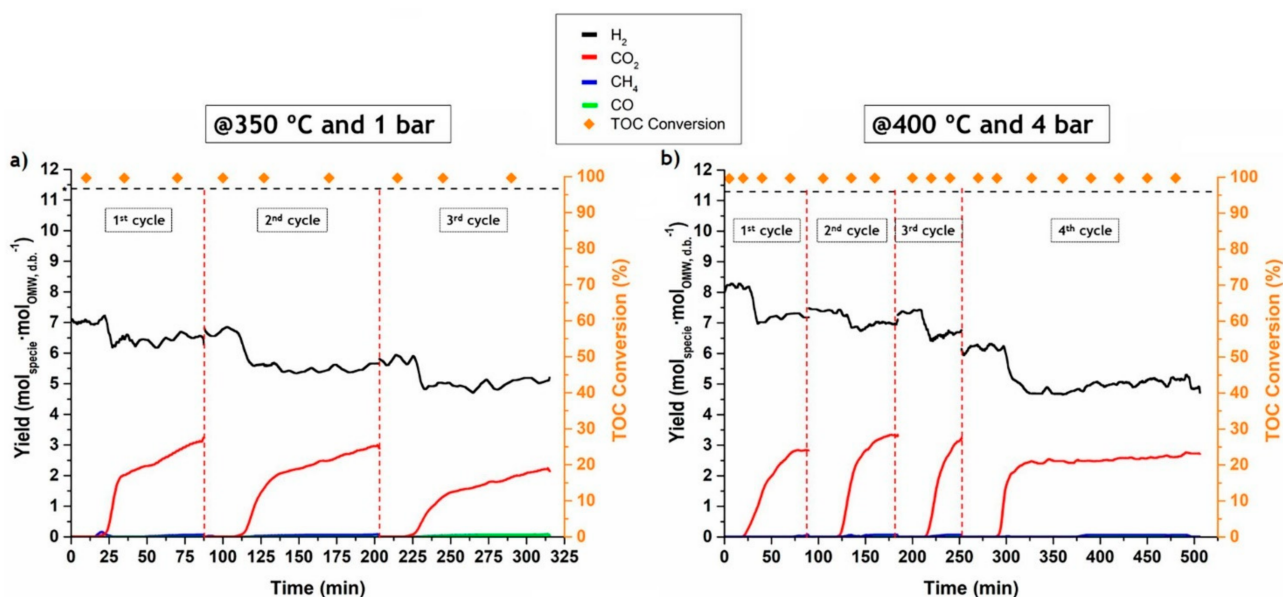


Figure 15. Gaseous species yield and TOC conversion using an SER at (a) 350 °C and 1 bar or (b) 400 °C and 4 bar. * Thermodynamic equilibrium for the H₂ yield in a TR at the operations conditions used in the respective experiments (dashed horizontal line). Dashed red vertical lines indicate instants of reactive regeneration. Reprinted with permission from Ref. [197]. Copyright 2021 Elsevier.

3.2. Membrane Reactor

Another alternative to enhance the OMWSR performance is the utilization of a MR (see Figure 16), which consists of combining the TR and H₂ separation in the same device. In such an MR, the membrane selectively removes one or more species, thus allowing to overcome the thermodynamic boundaries of equilibrium-limited reactions—Le Châtelier principle [160,163–292]—as is the case of the reversible WGS, which is, therefore, shifted forward. Regarding its advantages compared to TRs, they are the same as SERs, except for the reduction of the emissions of CO₂ in the pre-breakthrough zone, being that the capital costs reduction can be higher in the case of MRs since only one device is needed (instead of the parallel reactors required for the SER), as long as low-cost and long-lasting H₂ perm-selective membranes can be obtained.

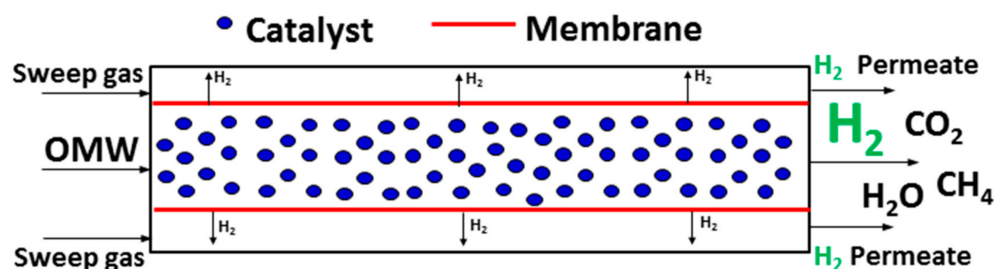


Figure 16. Scheme of the operation of the MR.

This reactor configuration was already used in other applications [173,293–304] and for the OMWSR [1,6,89,90,197] in the last decade.

One of the advantages of the MR for this particular application is that it is possible to produce ultra-pure H₂ streams if membranes with a nearly infinite H₂ perm-selectivity are used (e.g., dense Pd-based membrane). Thus, a MR is an important technology to increase the energy performance of the process by combining the reaction and recovery stages in a single device (avoiding the construction of two unit operations), leading to considerably smaller dimensions of plant layout, producing one stream with high-purity H₂ (in the permeate side—see a scheme of a MR in Figure 16). The effect of

the removal of H₂ from the reaction medium, from a thermodynamic point of view, was already studied for the OMWSR [194], though it was already analyzed for other applications [84,196,293,299,305–307].

In order to use a MR in the OMWSR process, it is fundamental to select a suitable H₂ perm-selective membrane. Consequently, the next sections comprise a short overview of H₂ perm-selective membranes described in the literature, as well as an evaluation of the experimental tests performed in MRs for OMWSR. The performance of a MR depends considerably on the flux of permeated H₂ obtained and on its purity. The stability of a membrane is here considered as the capability of a membrane to maintain a constant flux of H₂, as well as a constant perm-selectivity over time.

3.2.1. Hydrogen Perm-Selective Membranes

H₂ perm-selective membranes may be categorized as dense metallic membranes, proton-conducting dense ceramic membranes, dense polymeric membranes, microporous ceramic membranes, and porous carbon membranes [308,309]. The main benefit of dense metallic membranes is that typically they tolerate high temperatures (e.g., as compared to polymeric ones) and present high selectivity towards H₂, thus being possible to obtain high purity H₂-permeate streams [308]. Thus, and for the application envisaged herein, dense metallic membranes are preferable for ultra-pure H₂ production and will be the main target of focus. Nevertheless, dense ceramic membranes (proton conducting membranes) have also achieved high performance at high operation temperatures [310,311]. Although Pd-based membranes have been more used in the past for H₂ permeation, the advances in dense ceramic membranes in the last few years have been outstanding.

When selecting a membrane to be used in a MR, it is required to take into consideration the operating conditions under which the membrane will be applied. In the last years, there has been an incredible effort in order to develop appropriate membranes for MR applications. Pd-based membranes are presently the most promising for high purity H₂ production in MRs, especially Pd alloys (with transition metals—e.g., Pd-Ag, Pd-Ru, Pd-Cu, and Pd-Au), which are less sensitive than pure Pd to embrittlement (caused by the presence of H₂ at temperatures below 300 °C and H₂ pressures below 20 bar) and poisoning (caused by contact with CO, CO₂, or H₂S) [308,312–317]. The embrittlement phenomenon may produce pinholes/cracks on the membrane, which will negatively affect the H₂ perm-selectivity of the membrane. In addition, one of the biggest inhibitory factors for H₂ permeation across a Pd membrane is concentration polarization and it is necessary to avoid that (this topic will be more deeply discussed later in this section) [318]. However, and in spite of these negative aspects, the ability of Pd to dissociate H₂ to its atomic form makes this metal ideal for H₂ separation applications [319]. Pd-Ag membranes show good stability, relatively lower material costs, and better mechanical properties than pure Pd membranes. Besides, it has been shown that the addition of a third element to the Pd-Ag alloy (e.g., Au) improves the tolerance to poisoning with H₂S [320].

Several studies reported that the Pd alloys can obtain high permeances [321–325]. Moreover, their H₂ permeability increases with the percentage of Ag in the alloy up to a maximum, which occurs at around 23 wt.% Ag [326]. In previous studies, it was found that the maximum recommended operating temperature for long-term stable tests with Pd-Ag membranes was close to 500 °C [297,327–330]. Above this temperature, besides the existence of leakages through the sealings, it is observed the formation of surface defects (small pinholes) that leads to the decrease of the membrane performance [327]. Tosti et al. [331] demonstrated that self-supported dense 23 wt.% Pd-Ag tubular membranes with finger-type configuration are extremely durable and reliable since these membranes allow to attain complete H₂ selectivity and no malfunctions were observed after one year of hydrogenation and thermal cycles. These properties, together with high permeability, make such materials very promising for ultra-pure H₂ production in energetic and industrial applications [331]. Nevertheless, several works reported that the H₂ removal fraction never reaches a value higher than 0.80 [305,326,332] for low-to-medium pressures. Besides that, the application

of these dense membranes is still limited; for instance, self-supported Pd membranes are considered by several authors not being suitable in MR processes because of their large thickness required for reaching mechanical stability and corresponding low fluxes across the membrane and high costs. Due to these reasons, a strong effort has been put in the preparation of thinner Pd films over different supports and in the development of new membranes with less expensive metals. For instance, group V metals (such as V, Nb, and Ta) are promising alternative materials to Pd because of their lower costs and higher H₂ permeabilities. However, the main problem of these elements as membrane materials is their too high solubility to H₂, making the membranes susceptible to severe H₂ embrittlement, which can lead to the formation of cracks [333]. Still, direct use of these materials as a membrane is hindered due to the formation of oxide layers and the occurrence of surface reactions, which promote the reduction of the H₂ permeability through the membrane. Thus, the main criteria for membrane selection are high permeability, high selectivity, resistance to reactive gases—particularly CO, CO₂, CH₄ and H₂O—and resistance to coking [334].

Nowadays, many researchers are pursuing the possibility of using supported membranes with as thin as possible Pd-alloy layers [335], thus reducing costs and increasing hydrogen permeation fluxes. Concerning these supported membranes, it is important to emphasize that metallic supports are mechanically stronger and can be more easily assembled into metallic reactors than ceramics supports (lower probability of leakages). However, the metallic supports have low porosity, their pores are larger, the surface is rough and, at this moment, they are much more costly than ceramic supports [333]. Several works [329,336] reported that the materials (namely, the support) that contact with the membrane must be meticulously chosen. For instance, Okazaki et al. [329] stated that the decrease of the H₂ permeation observed in their work was related to the interaction between the Al₂O₃ support and the Pd layer of the membrane.

In terms of preparation methods of these H₂-selective membranes, namely supported ones, chemical vapor deposition (CVD) and electroless plating (EP) are the most used ones. The last method (EP) normally consists of the production of Pd particles through the reduction of a plating solution containing Pd-amine complexes. This method can provide high coating adhesion, requires low operation costs and allows simple operation. Though, the impurities present in the plating solution may lead to the presence of defects on the Pd layer. The CVD technique can very easily allow to deposit a metal film on a support with the utilization of several reactions with water [293].

Generally, the permeation of H₂ through a Pd-based membrane is described by a solution-diffusion mechanism composed by several steps, as shown in Figure 17.

The simplest model used to explain the mass transport of H₂ permeating through a dense membrane assumes that the H₂ diffuses through the membrane according to Fick's first law of diffusion for a pure component [338]. Still, in the permeation of H₂ through Pd-based membranes is commonly assumed that the diffusion coefficient is constant along the membrane and the mass transport kinetics is controlled by the diffusion step; this implies that the sorption and desorption process should be considered always to be at equilibrium (concentration of H₂ in the surface of the membrane in equilibrium with the gas phase—in the retentate and permeate sides); in the case of Pd-based membranes, the sorption isotherm is generally described by the Sieverts' law [339]. Taking into account all these considerations, the flux of H₂ that permeates through the membrane (J_{H_2}) can be determined by the integration of Fick's first law of diffusion along the thickness of the membrane (Equation (13)) [339–341].

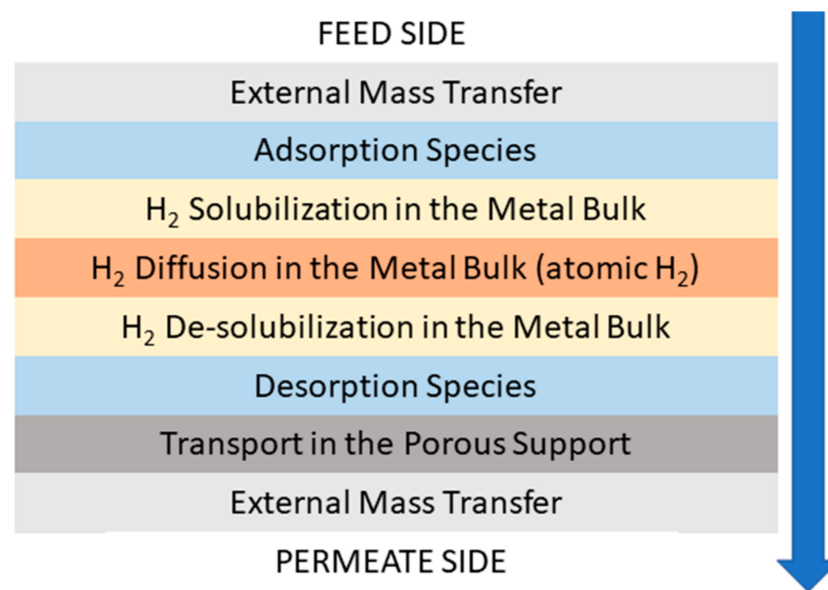


Figure 17. Solution-diffusion mechanism of the permeation of H₂ through a Pd-based membrane [337].

$$J_{\text{H}_2} = \frac{L_{\text{H}_2}}{\delta} \times \left(p_{\text{H}_2, \text{feed}}^{0.5} - p_{\text{H}_2, \text{permeate}}^{0.5} \right) \quad (13)$$

where L_{H_2} is the permeability of the membrane, δ is the membrane thickness, p_{H_2} is the partial pressures of H₂ in the retentate (inlet—feed side) or in the permeate (outlet) side. The ratio $\frac{L_{\text{H}_2}}{\delta}$ is normally called permeance.

The permeability is described by an Arrhenius-type dependency on the temperature (T)—Equation (14)

$$L_{\text{H}_2} = L_{\text{H}_2}^0 \times e^{\left(-\frac{E_a}{RT}\right)} \quad (14)$$

where $L_{\text{H}_2}^0$ is the pre-exponential factor, E_a is the activation energy of the membrane permeation process, and R is the universal gas constant.

Despite the extensive use of Equation (13), it is necessary to emphasize that this equation is valid only for certain operation conditions: for instance, the expression is only applicable to ideal H₂/metal mixtures and when the resistance in the diffusion of the H₂ along the thickness of the membrane is the rate-dominant process [323]. In general, the flux of H₂ can be influenced by several factors such as temperature, partial pressure difference, membrane thickness, membrane diffusivity, adsorption/desorption kinetics, and concentration polarization at the surface of the membrane. Ward and Dao [342] reported that for a clean Pd membrane, in the absence of external mass transfer resistance, the diffusion is the dominating step at moderately high temperatures, even for membrane thicknesses close to 1 μm .

However, as also reported by Ward and Dao [342] (and shown in Figure 17), beyond the H₂ diffusion through the membrane, other phenomena occur in the permeation process and the resistances to mass transport in the external gas phase may also be significant in some cases. The concentration polarization phenomenon is related to a decreased H₂ concentration in the feed side of the membrane in a multi-component system. In certain cases, due to the fluid dynamics inside the device, there is an accumulation of several species in the adjacent zone to the membrane surface, increasing the concentration of these species in the boundary film nearby to the membrane surface [343]. This causes a H₂ partial pressure gradient in the boundary layer and prevents the H₂ adsorption on the membrane surface (increase of the mass transport resistance). Thus, the H₂ concentration adjacent to the surface of the membrane is lower than that in the bulk gas and thus decreases the flux of H₂ permeated through the membrane [344–348]. The concentration polarization

is affected not only by the external hydrodynamic conditions of the module, but also by the mass transport process inside of the membrane layer [349]. While most of the existing permeation results for thick Pd membranes are consistent with the considerations for the diffusion-limited permeation, significant differences exist for membranes with less than 10 μm thickness, since the very high fluxes made possible with such thin membranes makes the external mass transfer resistances relevant [342].

In this manner, due to the several possible phenomena that occur in this separation process, it is typical to use the empirical Equation (15) to describe the permeating H_2 flux [340,341]. It was reported in the literature that the pressure exponent n , in a general way, can provide insight regarding which transport step(s) control the overall permeation process. Several works studied and evaluated the physical meaning of the exponent n [342,350,351] for H_2 permeation through Pd-based membranes.

$$J_{\text{H}_2} = \frac{L_{\text{H}_2}}{\delta} \times \left(p_{\text{H}_2, \text{feed}}^n - p_{\text{H}_2, \text{permeate}}^n \right) \quad (15)$$

As already mentioned, the parameter n obtained is near 0.5 for a situation of no external mass transfer resistance (and the diffusion through the membrane controls the permeation process) [342,351,352]. It was also observed that the required value of the exponent n usually varies between 0.5 and 1 in the presence of external mass transfer resistances (effects are particularly strong on the permeate side) [342]. Moreover, it was reported that, in the absence of external mass transfer resistances, the n value approaches zero when the H_2 permeation is desorption-limited and varies between 0 and 0.5 when the desorption and diffusion are both influencing the H_2 flux [342]. It was also stated that (again in the absence of external resistances) the value of the exponent n is equal to the unity if only the adsorption process in the feed side limits the H_2 flux, and varies between 0.5 and 1 when adsorption and diffusion in the metal bulk are both limiting the permeation [352]. In line with the aforementioned, the study of Caravella et al. [351] verified that, at low temperature and using a thin membrane, the value of the exponent n decreases toward values lower than 0.5—desorption-limited process. However, higher values (>1) for the pressure exponent have been determined in previous works [352,353]. Besides that, the H_2 diffusion coefficient may also exhibit a concentration dependence and the membrane may present defects on the membrane films which may lead, for instance, to Knudsen diffusion.

Tables 7 and 8 show a summary of different Pd-based membranes that have been described in the last few years with different parameters and performances.

3.2.2. OMWSR in Membrane Reactors

Just a few experimental works regarding the OMWSR in MRs are reported in the literature [1,6,89,90]; in such studies, the authors assessed the effects of pressure and gas/weight hourly space velocity (GHSV/WHSV) and will be summarized in this section.

In the first work of Tosti et al. [6], filtered and concentrated OMW was used for feeding a MR consisting of a dense Pd-Ag permeator tube packed with a Pt-based catalyst. Reforming tests were performed at 450 $^\circ\text{C}$ in the range of 1–5 bar total pressure. The experimental tests have shown the ability of the membrane device to selectively separate the H_2 produced and to provide a retentate stream rich in non-permeated H_2 , CO_2 , and CH_4 . A maximum H_2 yield equivalent to 2 kg of H_2 permeated per ton of OMW has been measured, when operating at 3 bar with a space velocity of $5.56 \times 10^3 \text{ mol}\cdot\text{h}^{-1}\cdot\text{g}^{-1}_{\text{cat}}$. The gas chromatographic analysis of the retentate stream showed the presence of H_2 , CO_2 , and CH_4 , thus proving evidence of the presence of side reactions such as the hydrogenolysis and cracking of alcohols. No detectable quantities of CO were determined due to the completion of the WGS promoted by the presence of the membrane. Additionally, a deactivation of the catalyst due to coke deposits was observed.

Table 7. Summary of Pd-based membranes' performances and respective characteristics (H_2 diffusion through the membrane controls the permeation process).

Membrane/Support	Temperature (°C)	δ (μm)	H_2 Permeance ($\text{mol}\cdot\text{m}^{-2}\cdot\text{s}^{-1}\cdot\text{Pa}^{-0.5}$) (a)	Selectivity (H_2/N_2)	Ref.
Pd-25 wt.% Ag/ Al_2O_3	300	50	1.15×10^{-4}	∞	[354]
Pd-23-25 wt.% Ag	350	84	2.26×10^{-4}	∞	[355]
Pd-5 wt.% Pt/YSZ	400	6.6	1.18×10^{-3}	994	[356]
Pd/ $\text{TiO}_2/\text{Ti-Al}$	500	14	1.07×10^{-3}	∞	[357]
Pd-23 wt.% Ag/stainless steel	400	150	1.27×10^{-4}	∞	[6]
Pd-15 wt.% Ag/ Al_2O_3	300	5	2.13×10^{-3}	528	[358]
Pd-23 wt.% Ag	400	61	1.46×10^{-4}	∞	[331]
Pd-20 wt.% Ag/ Al_2O_3	400	2.5	2.70×10^{-3}	∞	[323]
Pd-8 wt.% Ho	600	100	7.89×10^{-4}	n.d. (b)	[315]
Pd-Au/PSS	450	12	1.30×10^{-3}	∞	[359]
Pd-1.3 wt.% Ru/ Al_2O_3	500	1.8	4.12×10^{-3}	2611	[360]
Pd-20 wt.% Ag/ Al_2O_3	400	2.5	3.90×10^{-3}	$\geq 10,000$	[361]
Pd-23 wt.% Ag/PSS	400	2.8	3.25×10^{-3}	≥ 2900	[322]

(a) H_2 Permeance obtained by Equation (15). (b) Not determined.

Table 8. Summary of Pd-based thin membranes' performances and respective characteristics (H_2 diffusion through the membrane does not control the permeation process).

Membrane/Support	Temperature (°C)	δ (μm)	H_2 Permeance ($\text{mol}\cdot\text{m}^{-2}\cdot\text{s}^{-1}\cdot\text{Pa}^{-1}$) (a)	Selectivity (H_2/N_2)	Ref.
Pd-7 wt.% Ag/ Al_2O_3	400	0.78	1.14×10^{-5}	640	[362]
Pd-15 wt.% Ag/ Al_2O_3	400	4.0	4.2×10^{-6}	20,000	[363]
Pd-5 wt.% Ag/ Al_2O_3	400	1.0	4.6×10^{-6}	25,938	[294]
Pd-23 wt.% Ag/ ZrO_2	400	1.0	8.0×10^{-6}	500	[364]
Pd-Ag/ Al_2O_3	400	1.3	$9.0\text{--}9.4 \times 10^{-6}$	1900	[365]
Pd-7-8 wt.% Au/ Al_2O_3	500	2-3	6.2×10^{-6}	1400	[366]

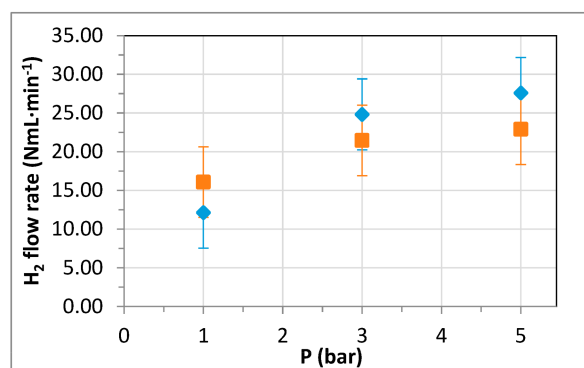
(a) Permeance values have been calculated for a H_2 partial pressure of 1 bar.

In the second work, Tosti et al. [89] conducted again the OMWSR process in a MR (using a Pd membrane) to investigate the capability to recuperate pure H_2 and H_2 -rich gas mixtures from OMW. Specifically, a Pt-Rh-Pd-based catalyst supported on rare earth oxides was used in order to validate the capability of this reactor configuration of maximizing the H_2 yield and decreasing side reactions. As a main result, this work permitted verifying the following capabilities of the studied membrane process: the production of H_2 from waste (up to 3.25 kg of H_2 per ton of OMW) and a reduction in the pollution potential of the OMW (phenols and total carbon concentrations are reduced by $\approx 90\%$). Compared to a commercial Pt-based material that was used in the previous work, the new catalyst demonstrated higher selectivity toward the steam reforming reaction, permitting a substantial decrease in the formation of CH_4 and coke and thus exhibiting a higher H_2 yield and higher stability of the catalyst. In fact, in all experiments, low CH_4 concentrations were found in the retentate stream, while no significant loss of catalyst activity was detected after 6–8 h of operation. The low selectivity of the noble metals-based catalyst toward CH_4 formation was related to its intrinsic high reforming activity.

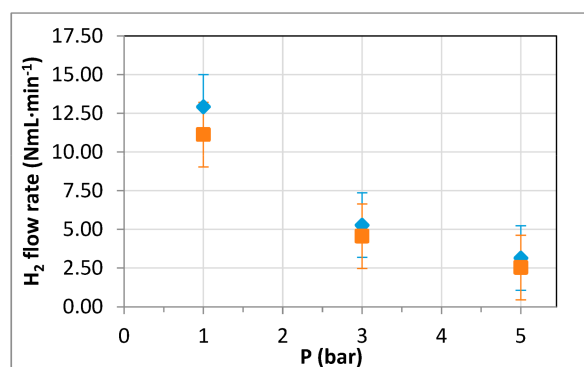
In the last work of the same research group [1], they tested the reforming of OMW and CH_4 in a Pd-membrane reformer and demonstrated that the steam reforming of

$\text{CH}_4 + \text{OMW}$ exhibits about the same H_2 yield of the reforming of the OMW alone. Besides that, the addition of CH_4 to OMW does not affect the ability of the steam reforming process to reduce pollution. Finally, it was possible to verify that the H_2 yield reached in the steam reforming of OMW together with CH_4 was higher than the H_2 yield obtained for the steam reforming of CH_4 alone.

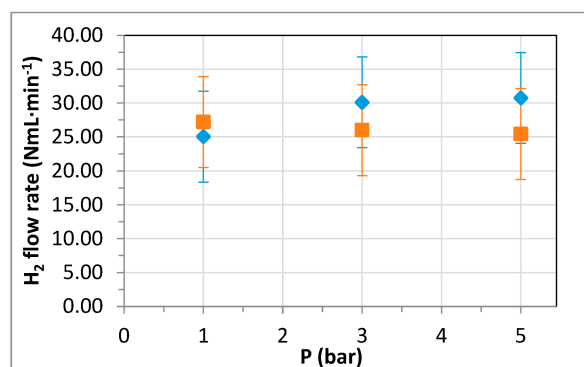
More recently, Alique et al. [90], using a catalytic material prepared by Tosti et al. in a previous study [89] reported that, in a MR, higher pressures were beneficial, dominating the membrane shift effect (with enhanced H_2 permeating fluxes) against the negative influence of thermodynamics on the steam reforming reactions—see Figure 18.



(a)



(b)



(c)

Figure 18. Effect of pressure in OMW–ethanol co-reforming experimental tests (@ 450 °C, ethanol concentration 7.5 vol.%, feed: 15 g·h⁻¹ mixture and 15 mL·min⁻¹ carrier gas): (a) permeate, (b) retentate, and (c) total produced H₂. Diamonds (◆) represent experiments with N₂, while squares (■) are obtained with air as the carrier gas. Reprinted from Alique et al. [90].

In addition, and as previously mentioned, in the work of Rocha et al. [197], several reactor configurations were tested for the OMWSR process—namely the SER and the SEMR (@ 1 bar and 350/400 °C). The difference between the H₂ yields obtained in the SER and SEMR is considerable, even after saturation of the sorbent (instant after which the system began to behave like a MR), showing that the impact of the membrane is very critical in this multifunctional system.

3.2.3. Summary

The OMWSR through a MR consists of combining the reaction and H₂ separation in the same device. This innovative reactor configuration requires a H₂ perm-selective membrane.

Pd-based membranes are currently promising for high purity H₂ production in MRs. Since the price of these dense membranes is still a restricting factor, a major effort has been put into the preparation of thinner Pd films over different supports, by several techniques. This decrease of the thickness of the membrane will allow the increase of the permeation flux, but the selectivity will be lower.

In this way, a thin supported Pd membrane is a potential membrane to separate from the reaction medium the H₂ produced in the OMWSR, in order to increase the H₂ yield (since it shifts the thermodynamic equilibrium to the production of more H₂) and produce an ultra-pure H₂ stream. However, it is necessary to further study the effect of the species present in the OMW on the membrane performance.

3.3. Sorption-Enhanced Membrane Reactor

Another technological alternative is the multifunctional hybrid reactor combining capture of CO₂ and H₂ separation: the SEMR (see Figure 19). This hybrid reactor configuration allows shifting the thermodynamic equilibrium of the steam reforming reaction by removing two of the reaction products from the reaction medium: hydrogen and carbon dioxide. This reactor configuration, intensifies the process even further by combining the reaction, H₂ separation, and CO₂ capture in a single device. This reactor configuration was not studied in detail until now for the OMWSR with the exception of a recent experimental work [197] and one (theoretical) thermodynamic study [194]. The SEMR combines the advantages of a SER and a MR; however, like in a SER, the CO₂ sorbent gets saturated at a certain point and then regeneration is needed (see details in Section 3.1). At this point, this reactor configuration is similar to a MR, since the CO₂ is not captured, but the H₂ is continuously separated from the reaction medium to the permeate side.

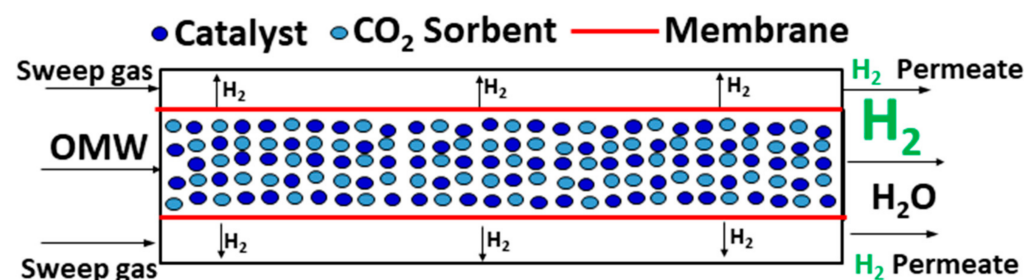


Figure 19. Scheme of the operation of the SEMR.

OMWSR in Sorption-Enhanced Membrane Reactors

As already stated, in the study of Rocha et al. [197], a comparison of the performance between different reactor configurations was performed for the OMWSR process (TR, SER, MR, and SEMR) @ 1 bar and 350/400 °C.

It was observed that the removal of H₂ and capture of CO₂ could provide higher H₂ yields in the SEMR during the pre-breakthrough region in comparison with the other hybrid multifunctional reactors. This reactor configuration allows the simultaneous production of highly pure H₂ in both the retentate and permeate sides. An H₂ yield improvement of

about 44% was seen compared to the TR, approximately 39% regarding the SER and about 16% compared to the MR.

The H₂ yield observed in the SEMR at 350 °C and 1 bar was permanently between 8.0 and 6.0 mol_{H₂}·mol_{OMW}⁻¹, and always between 11.5 and 9.0 mol_{H₂}·mol_{OMW}⁻¹ at 400 °C and 4 bar. This way, during the pre-breakthrough region, the H₂ yield reached practically the maximum theoretical yield (11.84 mol_{H₂}·mol_{OMW}⁻¹) in all cycles at 400 °C and 4 bar—see Figure 20. In the first cycle, the H₂ yield inclusively goes over the thermodynamic equilibrium yield calculated for the TR in these operating conditions (cf. Figure 20). Besides that, CH₄, CO, and CO₂ are not detected in the pre-breakthrough region, thus preventing the poisoning of the membrane and minimizing the coke deposits formation (particularly via CH₄ cracking).

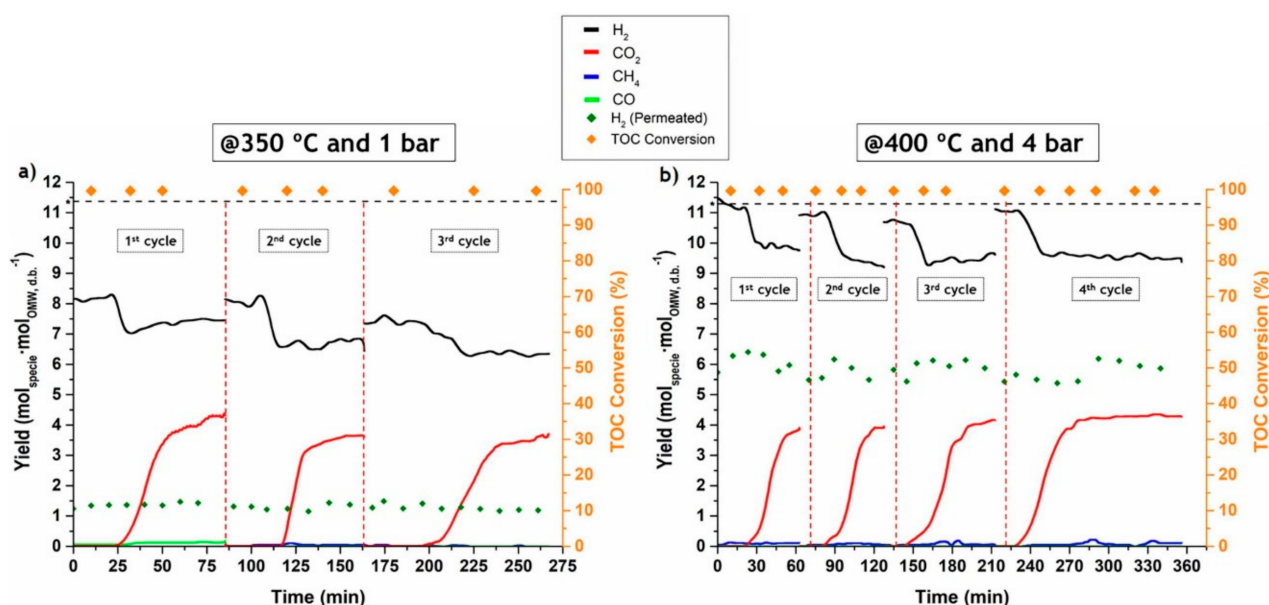


Figure 20. Gaseous species yield and TOC conversion using a SEMR operation at (a) 350 °C and 1 bar and at (b) 400 °C and 4 bar. Sweep gas = 100 mL_{N₂}·min⁻¹ and P_{permeate side} = 1 bar. * Thermodynamic equilibrium for the H₂ yield in a TR at the operations conditions used in the respective catalytic test (dashed horizontal line). Dashed red vertical lines indicate instants of reactive regeneration. Reprinted with permission from Ref. [197]. Copyright 2021 Elsevier.

Finally, with these experimental tests, it was observed that the OMWSR, when carried in a SEMR, can competently treat real OMW effluents, with high productions of H₂, with complete decrease of the pollutant load.

4. Conclusions

OMW is a polluting stream derived from the olive oil industry and is an important source of environmental pollution, particularly in the Mediterranean countries. This stream is typically constituted by polyphenols, sugars, fatty acids, and water. Nowadays, and in order to reduce the pollutant load, several treatment/valorization techniques are applied, but these technologies have large cost and efficiency problems. Thus, OMWSR presents as a good alternative, since this process decreases the pollutant load of the OMW and simultaneously the waste is valorized with the production of green H₂.

Currently, the OMWSR is an innovative treatment with high potential; however, alternatives for improving the process have been studied, since this process involves reversible reactions. In this way, it is expected that several reactor configurations (SER, MR, and SEMR) could work at lower temperatures than the conventional steam reformers and attain similar or even better performances than TRs operating at higher temperatures. Nevertheless, for the successful implementation of these reactor configurations, CO₂ sorbents

with high sorption capacity, easy regeneration, and high stability—as well as H₂ perm-selective membranes with high H₂ permeance and selectivity—have to be used. Nowadays, HTCs and Pd-based membranes are seen as promising systems for use in the SEMR at temperatures in the range of 300–400 °C.

Author Contributions: Conceptualization, M.A.S. and L.M.M.; investigation, C.R.; resources, L.M.M.; writing—original draft preparation, C.R.; writing—review and editing, M.A.S. and L.M.M.; supervision, M.A.S. and L.M.M.; funding acquisition, M.A.S. and L.M.M. All authors have read and agreed to the published version of the manuscript.

Funding: This work was financially supported by the Base Funding—UIDB/00511/2020—of the Laboratory for Process Engineering, Environment, Biotechnology and Energy (LEPABE) funded by national funds through the FCT/MCTES (PIDDAC), and by the Project NORTE-01-0247-FEDER-39789, funded by European Regional Development Fund (ERDF) through the Programa Operacional Regional do Norte (NORTE 2020). This work was also financially supported by: Base Funding—UIDB/50020/2020—of the Associate Laboratory LSRE-LCM, funded by national funds through FCT/MCTES (PIDDAC); and project HyGreen&LowEmissions, with reference NORTE-01-0145-FEDER-000077, through the Programa Operacional Regional do Norte (NORTE 2020), under the PORTUGAL 2020 Partnership Agreement, funded by the European Regional Development Fund (ERDF). M.A. Soria thanks the Portuguese Foundation for Science and Technology (FCT) for the financial support of his work contract through the Scientific Employment Support Program (Norma Transitória DL 57/2017).

Conflicts of Interest: The authors declare no conflict of interest.

Notation and Glossary

List of Variables

E_a	Activation energy (kJ·mol ⁻¹)
J_{H_2}	Flux of H ₂ (mol·m ⁻² ·s ⁻¹)
L_{H_2}	Permeability (mol·m ⁻¹ ·s ⁻¹ ·Pa ^{-0.5})
$L_{H_2}^0$	Pre-exponential factor (mol·m ⁻¹ ·s ⁻¹ ·Pa ^{-0.5})
n	Pressure exponent
$p_{H_2}^x$	Partial pressures of H ₂ (Pa)
R	Universal gas constant
T	Temperature (°C or K)
$\Delta H_r^{0\text{ }^\circ\text{C}}$	Enthalpy of reaction at standard conditions (kJ·mol ⁻¹)
δ	Membrane thickness (m)

List of Acronyms

BOD	Biochemical oxygen demand
COD	Carbon oxygen demand
CVD	Chemical vapor deposition
EP	Electroless plating
HTC	Hydrotalcite
LHSV	Liquid hourly space velocity
MR	Membrane reactor
OMW	Olive oil mill wastewater
OMWSR	Olive oil mill wastewater steam reforming
SCFR	Steam-to-carbon feed ratio
SEMR	Sorption-enhanced membrane reactor
SER	Sorption-enhanced reactor
TOC	Total organic carbon
TPOMW	Two-phase olive mill waste
TR	Traditional reactor
WGS	Water–gas shift

References

1. Tosti, S.; Fabbriano, M.; Pontoni, L.; Palma, V.; Ruocco, C. Catalytic reforming of olive mill wastewater and methane in a Pd-membrane reactor. *Int. J. Hydrogen Energy* **2016**, *41*, 5465–5474. [CrossRef]
2. Council, I.O. Prices & Balances. 2021. Available online: <https://www.internationaloliveoil.org/wp-content/uploads/2021/12/IOC-Olive-Oil-Dashboard-1.html> (accessed on 18 October 2021).
3. Roig, A.; Cayuela, M.L.; Sánchez-Monedero, M.A. An overview on olive mill wastes and their valorisation methods. *Waste Manag.* **2006**, *26*, 960–969. [CrossRef]
4. Rozzi, A.; Malpei, F. Treatment and disposal of olive mill effluents. *Int. Biodeterior. Biodegrad.* **1996**, *38*, 135–144. [CrossRef]
5. Dawson, D. Global Olive Oil Production to Dip in 2018/2019. 2018. Available online: <https://www.oliveoiltimes.com/olive-oil-business/global-olive-oil-production-to-dip-in-2018-19/66039> (accessed on 25 October 2021).
6. Tosti, S.; Accetta, C.; Fabbriano, M.; Sansovini, M.; Pontoni, L. Reforming of olive mill wastewater through a Pd-membrane reactor. *Int. J. Hydrogen Energy* **2013**, *38*, 10252–10259. [CrossRef]
7. Dermeche, S.; Nadour, M.; Larroche, C.; Moulti-Mati, F.; Michaud, P. Olive mill wastes: Biochemical characterizations and valorization strategies. *Process Biochem.* **2013**, *48*, 1532–1552. [CrossRef]
8. Alburquerque, J.A.; González, J.; García, D.; Cegarra, J. Agrochemical characterisation of “alperujo”, a solid by-product of the two-phase centrifugation method for olive oil extraction. *Bioresour. Technol.* **2004**, *91*, 195–200. [CrossRef]
9. Di Giovacchino, L.; Sestili, S.; di Vincenzo, D. Influence of olive processing on virgin olive oil quality. *Eur. J. Lipid Sci. Technol.* **2002**, *104*, 587–601. [CrossRef]
10. Niaounakis, M.; Halvadakis, C.P. Characterization of olive processing waste. *Olive Process. Waste Manag. Lit. Rev. Pat. Surv.* **2006**, *5*, 23–64.
11. Sanchez Moral, P.; Méndez, M.R. Production of pomace olive oil. *Grasas Y Aceites* **2006**, *57*, 47–55. [CrossRef]
12. Aktas, E.S.; Imre, S.; Ersoy, L. Characterization and lime treatment of olive mill wastewater. *Water Res.* **2001**, *35*, 2336–2340. [CrossRef]
13. Kapellakis, I.E.; Tsagarakis, K.P.; Crowther, J.C. Olive oil history, production and by-product management. *Rev. Environ. Sci. Bio/Technol.* **2008**, *7*, 1–26. [CrossRef]
14. Caputo, A.C.; Scacchia, F.; Pelagagge, P.M. Disposal of by-products in olive oil industry: Waste-to-energy solutions. *Appl. Therm. Eng.* **2003**, *23*, 197–214. [CrossRef]
15. Paredes, M.J.; Moreno, E.; Ramos-Cormenzana, A.; Martínez, J. Characteristics of soil after pollution with wastewaters from olive oil extraction plants. *Chemosphere* **1987**, *16*, 1557–1564. [CrossRef]
16. DellaGreca, M.; Monaco, P.; Pinto, G.; Pollio, A.; Previtera, L.; Temussi, F. Phytotoxicity of low-molecular-weight phenols from olive mill wastewaters. *Bull. Environ. Contam. Toxicol.* **2001**, *67*, 352–359. [CrossRef]
17. Rana, G.; Rinaldi, M.; Introna, M. Volatilisation of substances alter spreading olive oil waste water on the soil in a Mediterranean environment. *Agric. Ecosyst. Environ.* **2003**, *96*, 49–58. [CrossRef]
18. Anzelmo, B.; Wilcox, J.; Liguori, S. Hydrogen production via natural gas steam reforming in a Pd-Au membrane reactor. Investigation of reaction temperature and GHSV effects and long-term stability. *J. Membr. Sci.* **2018**, *565*, 25–32. [CrossRef]
19. Tsagaraki, E.; Lazarides, H.N.; Petrotos, K.B. Olive Mill Wastewater Treatment. In *Utilization of By-Products and Treatment of Waste in the Food Industry*; Springer: Boston, MA, USA, 2007; pp. 133–157.
20. Jaouad, Y.; Villain-Gambier, M.; Mandi, L.; Marrot, B.; Ouazzani, N. Comparison of aerobic processes for olive mill wastewater treatment. *Water Sci. Technol.* **2020**, *81*, 1914–1926. [CrossRef]
21. Aggoun, M.; Arhab, R.; Cornu, A.; Portelli, J.; Barkat, M.; Graulet, B. Olive mill wastewater microconstituents composition according to olive variety and extraction process. *Food Chem.* **2016**, *209*, 72–80. [CrossRef]
22. El-Abbassi, A.; Kiai, H.; Hafidi, A. Phenolic profile and antioxidant activities of olive mill wastewater. *Food Chem.* **2012**, *132*, 406–412. [CrossRef]
23. Zbakh, H.; el Abbassi, A. Potential use of olive mill wastewater in the preparation of functional beverages: A review. *J. Funct. Foods* **2012**, *4*, 53–65. [CrossRef]
24. Nasr, B.; Ahmed, B.; Abdellatif, G. Fenton treatment of olive oil mill wastewater-applicability of the method and parameters effects on the degradation process. *J. Environ. Sci.* **2004**, *16*, 942–944.
25. Katsoyannos, E.; Hatzikioseyan, A.; Remoundaki, E.; Tsezos, M. Photocatalytic treatment of olive mill wastewaters (OMW) in pilot scale. In Proceedings of the 13th International Symposium on Pollution and its Impact on Life in Mediterranean Region, Thessaloniki, Greece, 8–12 October 2005; National Technical University of Athens Greece: Athens, Greece, 2005.
26. Gebreyohannes, A.Y.; Mazzei, R.; Giorno, L. Trends and current practices of olive mill wastewater treatment: Application of integrated membrane process and its future perspective. *Sep. Purif. Technol.* **2016**, *162*, 45–60. [CrossRef]
27. Montero, C.; Oar-Arteta, L.; Remiro, A.; Arandia, A.; Bilbao, J.; Gayubo, A.G. Thermodynamic comparison between bio-oil and ethanol steam reforming. *Int. J. Hydrogen Energy* **2015**, *40*, 15963–15971. [CrossRef]
28. Casanovas, A.; Galvis, A.; Llorca, J. Catalytic steam reforming of olive mill wastewater for hydrogen production. *Int. J. Hydrogen Energy* **2015**, *40*, 7539–7545. [CrossRef]
29. Daassi, D.; Lozano-Sánchez, J.; Borrás-Linares, I.; Belbahri, L.; Woodward, S.; Zouari-Mechichi, H.; Mechichi, T.; Nasri, M.; Segura-Carretero, A. Olive oil mill wastewaters: Phenolic content characterization during degradation by *Corioliopsis gallica*. *Chemosphere* **2014**, *113*, 62–70. [CrossRef] [PubMed]

30. Fki, I.; Allouche, N.; Sayadi, S. The use of polyphenolic extract, purified hydroxytyrosol and 3,4-dihydroxyphenyl acetic acid from olive mill wastewater for the stabilization of refined oils: A potential alternative to synthetic antioxidants. *Food Chem.* **2005**, *93*, 197–204. [[CrossRef](#)]
31. Kyriacou, A.; Lasaridi, K.E.; Kotsou, M.; Balis, C.; Pilidis, G. Combined bioremediation and advanced oxidation of green table olive processing wastewater. *Process Biochem.* **2005**, *40*, 1401–1408. [[CrossRef](#)]
32. Araújo, M.; Pimentel, F.B.; Alves, R.C.; Oliveira, M.B.P.P. Phenolic compounds from olive mill wastes: Health effects, analytical approach and application as food antioxidants. *Trends Food Sci. Technol.* **2015**, *45*, 200–211. [[CrossRef](#)]
33. Kaleh, Z.; Geißen, S.U. Selective isolation of valuable biophenols from olive mill wastewater. *J. Environ. Chem. Eng.* **2016**, *4*, 373–384. [[CrossRef](#)]
34. Vlyssides, A.G.; Loizides, M.; Karlis, P.K. Integrated strategic approach for reusing olive oil extraction by-products. *J. Clean. Prod.* **2004**, *12*, 603–611. [[CrossRef](#)]
35. Paredes, C.; Cegarra, J.; Roig, A.; Sánchez-Monedero, M.A.; Bernal, M.P. Characterization of olive mill wastewater (alpechin) and its sludge for agricultural purposes. *Bioresour. Technol.* **1999**, *67*, 111–115. [[CrossRef](#)]
36. Feki, M.; Allouche, N.; Bouaziz, M.; Gargoubi, A.; Sayadi, S. Effect of storage of olive mill wastewaters on hydroxytyrosol concentration. *Eur. J. Lipid Sci. Technol.* **2006**, *108*, 1021–1027. [[CrossRef](#)]
37. Hamden, K.; Allouche, N.; Damak, M.; Elfeki, A. Hypoglycemic and antioxidant effects of phenolic extracts and purified hydroxytyrosol from olive mill waste in vitro and in rats. *Chem. Biol. Interact.* **2009**, *180*, 421–432. [[CrossRef](#)] [[PubMed](#)]
38. Justino, C.I.; Duarte, K.; Loureiro, F.; Pereira, R.; Antunes, S.C.; Marques, S.M.; Gonçalves, F.; Rocha-Santos, T.A.P.; Freitas, A.C. Toxicity and organic content characterization of olive oil mill wastewater undergoing a sequential treatment with fungi and photo-Fenton oxidation. *J. Hazard. Mater.* **2009**, *172*, 1560–1572. [[CrossRef](#)]
39. Zghari, B.; Pierre, D.; Abderrahmane, R.; Boukir, A. GC-MS, FTIR and ¹H,¹³C NMR Structural Analysis and Identification of Phenolic Compounds in Olive Mill Wastewater Extracted from Oued Oussefrou Effluent (Beni Mellal-Morocco). *J. Mater. Environ. Sci.* **2017**, *8*, 4496–4509. [[CrossRef](#)]
40. El-Abbassi, A.; Khayet, M.; Kiai, H.; Hafidi, A.; García-Payo, M.C. Treatment of crude olive mill wastewaters by osmotic distillation and osmotic membrane distillation. *Sep. Purif. Technol.* **2013**, *104* (Suppl. C), 327–332. [[CrossRef](#)]
41. El-Abbassi, A.; Kiai, H.; Hafidi, A.; García-Payo, M.C.; Khayet, M. Treatment of olive mill wastewater by membrane distillation using polytetrafluoroethylene membranes. *Sep. Purif. Technol.* **2012**, *98* (Suppl. C), 55–61. [[CrossRef](#)]
42. Allaoui, S.; Bennani, M.N.; Ziyat, H.; Qabaqous, O.; Tijani, N.; Ittobane, N. Removing polyphenols contained in olive mill wastewater by membrane based on natural clay and Hydrotalcite Mg-Al. *Moroc. J. Chem.* **2020**, *8*, 318–325. [[CrossRef](#)]
43. Ochando-Pulido, J.M.; Pimentel-Moral, S.; Verardo, V.; Martínez-Ferez, A. A focus on advanced physico-chemical processes for olive mill wastewater treatment. *Sep. Purif. Technol.* **2017**, *179*, 161–174. [[CrossRef](#)]
44. Un, U.T.; Altay, U.; Koparal, A.S.; Ogutveren, U.B. Complete treatment of olive mill wastewaters by electrooxidation. *Chem. Eng. J.* **2008**, *139*, 445–452. [[CrossRef](#)]
45. Rioja-Cabanillas, A.; Valdesueiro, D.; Fernández-Ibáñez, P.; Byrne, J.A. Hydrogen from wastewater by photocatalytic and photoelectrochemical treatment. *J. Phys. Energy* **2020**, *3*, 012006. [[CrossRef](#)]
46. Cañizares, P.; Paz, R.; Sáez, C.; Rodrigo, M.A. Costs of the electrochemical oxidation of wastewaters: A comparison with ozonation and Fenton oxidation processes. *J. Environ. Manag.* **2009**, *90*, 410–420. [[CrossRef](#)] [[PubMed](#)]
47. Lafi, W.K.; Shannak, B.; Al-Shannag, M.; Al-Anber, Z.; Al-Hasan, M. Treatment of olive mill wastewater by combined advanced oxidation and biodegradation. *Sep. Purif. Technol.* **2009**, *70*, 141–146. [[CrossRef](#)]
48. Frascari, D.; Rubertelli, G.; Arous, F.; Ragini, A.; Bresciani, L.; Arzu, A.; Pinelli, D. Valorisation of olive mill wastewater by phenolic compounds adsorption: Development and application of a procedure for adsorbent selection. *Chem. Eng. J.* **2019**, *360*, 124–138. [[CrossRef](#)]
49. Al Bsoul, A.; Hailat, M.; Abdelhay, A.; Tawalbeh, M.; Jum'ah, I.; Bani-Melhem, K. Treatment of olive mill effluent by adsorption on titanium oxide nanoparticles. *Sci. Total Environ.* **2019**, *688*, 1327–1334. [[CrossRef](#)] [[PubMed](#)]
50. Vavouraki, A.I.; Dareioti, M.A.; Kornaros, M. Olive Mill Wastewater (OMW) Polyphenols Adsorption onto Polymeric Resins: Part I—Batch Anaerobic Digestion of OMW. *Waste Biomass Valorization* **2020**, *12*, 2271–2281. [[CrossRef](#)]
51. Ochando-Pulido, J.M.; Vellido-Pérez, J.A.; González-Hernández, R.; Martínez-Férez, A. Optimization and modeling of two-phase olive-oil washing wastewater integral treatment and phenolic compounds recovery by novel weak-base ion exchange resins. *Sep. Purif. Technol.* **2020**, *249*, 117084. [[CrossRef](#)]
52. Ochando-Pulido, J.M.; González-Hernández, R.; Martínez-Ferez, A. On the Effect of the Operating Parameters for Two-Phase Olive-Oil Washing Wastewater Combined Phenolic Compounds Recovery and Reclamation by Novel Ion Exchange Resins. *Sep. Purif. Technol.* **2018**, *195*, 50–59. [[CrossRef](#)]
53. Sarika, R.; Kalogerakis, N.; Mantzavinos, D. Treatment of olive mill effluents: Part II. Complete removal of solids by direct flocculation with poly-electrolytes. *Environ. Int.* **2005**, *31*, 297–304. [[CrossRef](#)]
54. Alver, A.; Baştürk, E.; Kılıç, A.; Karataş, M. Use of advance oxidation process to improve the biodegradability of olive oil mill effluents. *Process Saf. Environ. Prot.* **2015**, *98*, 319–324. [[CrossRef](#)]
55. Uğurlu, M.; Kula, İ. Decolourization and removal of some organic compounds from olive mill wastewater by advanced oxidation processes and lime treatment. *Environ. Sci. Pollut. Res. Int.* **2007**, *14*, 319–325. [[CrossRef](#)] [[PubMed](#)]

56. Chatzisyneon, E.; Xekoukoulotakis, N.P.; Mantzavinos, D. Determination of key operating conditions for the photocatalytic treatment of olive mill wastewaters. *Catal. Today* **2009**, *144*, 143–148. [[CrossRef](#)]
57. Maduna, K.; Kumar, N.; Aho, A.; Wärnå, J.; Zrnčević, S.; Murzin, D.Y. Kinetics of Catalytic Wet Peroxide Oxidation of Phenolics in Olive Oil Mill Wastewaters over Copper Catalysts. *ACS Omega* **2018**, *3*, 7247–7260. [[CrossRef](#)] [[PubMed](#)]
58. Najjar, W.; Azabou, S.; Sayadi, S.; Ghorbel, A. Screening of Fe-BEA catalysts for wet hydrogen peroxide oxidation of crude olive mill wastewater under mild conditions. *Appl. Catal. B: Environ.* **2009**, *88*, 299–304. [[CrossRef](#)]
59. Azabou, S.; Najjar, W.; Bouaziz, M.; Ghorbel, A.; Sayadi, S. A compact process for the treatment of olive mill wastewater by combining wet hydrogen peroxide catalytic oxidation and biological techniques. *J. Hazard. Mater.* **2010**, *183*, 62–69. [[CrossRef](#)]
60. Kallel, M.; Belaid, C.; Boussahel, R.; Ksibi, M.; Montiel, A.; Elleuch, B. Olive mill wastewater degradation by Fenton oxidation with zero-valent iron and hydrogen peroxide. *J. Hazard. Mater.* **2009**, *163*, 550–554. [[CrossRef](#)]
61. Maamir, W.; Ouahabi, Y.; Poncin, S.; Li, H.-Z.; Bensadok, K. Effect of Fenton pretreatment on anaerobic digestion of olive mill wastewater and olive mill solid waste in mesophilic conditions. *Int. J. Green Energy* **2017**, *14*, 555–560. [[CrossRef](#)]
62. Esteves, B.M.; Rodrigues, C.S.D.; Madeira, L.M. Synthetic olive mill wastewater treatment by Fenton's process in batch and continuous reactors operation. *Environ. Sci. Pollut. Res.* **2018**, *25*, 34826–34838. [[CrossRef](#)]
63. Hodaifa, G.; Ochando-Pulido, J.M.; Rodriguez-Vives, S.; Martinez-Ferez, A. Optimization of continuous reactor at pilot scale for olive-oil mill wastewater treatment by Fenton-like process. *Chem. Eng. J.* **2013**, *220*, 117–124. [[CrossRef](#)]
64. Nieto, L.M.; Hodaifa, G.; Rodríguez, S.; Giménez, J.A.; Ochando, J. Degradation of organic matter in olive-oil mill wastewater through homogeneous Fenton-like reaction. *Chem. Eng. J.* **2011**, *173*, 503–510. [[CrossRef](#)]
65. Hodaifa, G.; García, C.A.; Borja, R. Study of Catalysts' Influence on Photocatalysis/Photodegradation of Olive Oil Mill Wastewater. Determination of the Optimum Working Conditions. *Catalysts* **2020**, *10*, 554. [[CrossRef](#)]
66. Adhoum, N.; Monser, L. Decolourization and removal of phenolic compounds from olive mill wastewater by electrocoagulation. *Chem. Eng. Processing Process Intensif.* **2004**, *43*, 1281–1287. [[CrossRef](#)]
67. Elkacmi, R.; Boudouch, O.; Hasib, A.; Bouzaid, M.; Bennajah, M. Photovoltaic electrocoagulation treatment of olive mill wastewater using an external-loop airlift reactor. *Sustain. Chem. Pharm.* **2020**, *17*, 100274. [[CrossRef](#)]
68. D'Annibale, A.; Stazi, S.R.; Vinciguerra, V.; Sermanni, G.G. Oxirane-immobilized *Lentinula edodes* laccase: Stability and phenolics removal efficiency in olive mill wastewater. *J. Biotechnol.* **2000**, *77*, 265–273. [[CrossRef](#)]
69. Casademont, P.; García-Jarana, M.B.; Sánchez-Oneto, J.; Portela, J.R.; de la Ossa, E.J.M. Hydrogen production by catalytic conversion of olive mill wastewater in supercritical water. *J. Supercrit. Fluids* **2018**, *141*, 224–229. [[CrossRef](#)]
70. García-Gómez, A.; Roig, A.; Bernal, M.P. Composting of the solid fraction of olive mill wastewater with olive leaves: Organic matter degradation and biological activity. *Bioresour. Technol.* **2003**, *86*, 59–64. [[CrossRef](#)]
71. Fadil, K.; Chahlaoui, A.; Ouahbi, A.; Zaid, A.; Borja, R. Aerobic biodegradation and detoxification of wastewaters from the olive oil industry. *Int. Biodeterior. Biodegrad.* **2003**, *51*, 37–41. [[CrossRef](#)]
72. Beltran-Heredia, J.; Torregrosa, J.; Dominguez, J.R.; Garcia, J. Treatment of black-olive wastewaters by ozonation and aerobic biological degradation. *Water Res.* **2000**, *34*, 3515–3522. [[CrossRef](#)]
73. Hajjouji, H.E.; Bailly, J.R.; Winterton, P.; Merlina, G.; Revel, J.C.; Hafidi, M. Chemical and spectroscopic analysis of olive mill waste water during a biological treatment. *Bioresour. Technol.* **2008**, *99*, 4958–4965. [[CrossRef](#)]
74. Bertin, L.; Berselli, S.; Fava, F.; Petrangeli-Papini, M.; Marchetti, L. Anaerobic digestion of olive mill wastewaters in biofilm reactors packed with granular activated carbon and "Manville" silica beads. *Water Res.* **2004**, *38*, 3167–3178. [[CrossRef](#)]
75. Gonçalves, M.R.; Costa, J.C.; Pereira, M.A.; Abreu, A.A.; Alves, M.M. On the independence of hydrogen production from methanogenic suppressor in olive mill wastewater. *Int. J. Hydrogen Energy* **2014**, *39*, 6402–6406. [[CrossRef](#)]
76. Eroğlu, E.; Eroğlu, İ.; Gündüz, U.; Türker, L.; Yücel, M. Biological hydrogen production from olive mill wastewater with two-stage processes. *Int. J. Hydrogen Energy* **2006**, *31*, 1527–1535. [[CrossRef](#)]
77. Caporaso, N.; Formisano, D.; Genovese, A. Use of phenolic compounds from olive mill wastewater as valuable ingredients for functional foods. *Crit. Rev. Food Sci. Nutr.* **2018**, *58*, 2829–2841. [[CrossRef](#)] [[PubMed](#)]
78. Agalias, A.; Magiatis, P.; Skaltsounis, A.-L.; Mikros, E.; Tsarbopoulos, A.; Gikas, E.; Spanos, I.; Manios, T. A New Process for the Management of Olive Oil Mill Waste Water and Recovery of Natural Antioxidants. *J. Agric. Food Chem.* **2007**, *55*, 2671–2676. [[CrossRef](#)] [[PubMed](#)]
79. Gonçalves, C.; Lopes, M.; Ferreira, J.P.; Belo, I. Biological treatment of olive mill wastewater by non-conventional yeasts. *Bioresour. Technol.* **2009**, *100*, 3759–3763. [[CrossRef](#)] [[PubMed](#)]
80. Servili, M.; Esposto, S.; Veneziani, G.; Urbani, S.; Taticchi, A.; di Maio, I.; Selvaggini, R.; Sordini, B.; Montedoro, G. Improvement of bioactive phenol content in virgin olive oil with an olive-vegetation water concentrate produced by membrane treatment. *Food Chem.* **2011**, *124*, 1308–1315. [[CrossRef](#)]
81. Mazzei, R.; Drioli, E.; Giorno, L. Enzyme membrane reactor with heterogenized β -glucosidase to obtain phytotherapeutic compound: Optimization study. *J. Membr. Sci.* **2012**, *390–391* (Suppl. C), 121–129. [[CrossRef](#)]
82. Kestioğlu, K.; Yonar, T.; Azbar, N. Feasibility of physico-chemical treatment and Advanced Oxidation Processes (AOPs) as a means of pretreatment of olive mill effluent (OME). *Process Biochem.* **2005**, *40*, 2409–2416. [[CrossRef](#)]
83. Drouiche, M.; le Mignot, V.; Lounici, H.; Belhocine, D.; Grib, H.; Pauss, A.; Mameri, N. A compact process for the treatment of olive mill wastewater by combining OF and UV/H₂O₂ techniques. *Desalination* **2004**, *169*, 81–88. [[CrossRef](#)]

84. Leal, A.L.; Soria, M.A.; Madeira, L.M. Autothermal reforming of impure glycerol for H₂ production: Thermodynamic study including in situ CO₂ and/or H₂ separation. *Int. J. Hydrogen Energy* **2016**, *41*, 2607–2620. [CrossRef]
85. Rocha, C.; Soria, M.A.; Madeira, L.M. Screening of commercial catalysts for steam reforming of olive mill wastewater. *Renew. Energy* **2021**, *169*, 765–779. [CrossRef]
86. Agency, I.E. Hydrogen. 2021. Available online: <https://www.iea.org/reports/hydrogen> (accessed on 29 November 2021).
87. Agency, I.E. Global Hydrogen Demand by Sector in the Net Zero Scenario, 2020–2030. 2021. Available online: <https://www.iea.org/data-and-statistics/charts/global-hydrogen-demand-by-sector-in-the-net-zero-scenario-2020-2030> (accessed on 29 November 2021).
88. Cakiryilmaz, N.; Arbag, H.; Oktar, N.; Dogu, G.; Dogu, T. Effect of W incorporation on the product distribution in steam reforming of bio-oil derived acetic acid over Ni based Zr-SBA-15 catalyst. *Int. J. Hydrogen Energy* **2018**, *43*, 3629–3642. [CrossRef]
89. Tosti, S.; Cavezza, C.; Fabbriano, M.; Pontoni, L.; Palma, V.; Ruocco, C. Production of hydrogen in a Pd-membrane reactor via catalytic reforming of olive mill wastewater. *Chem. Eng. J.* **2015**, *275* (Suppl. C), 366–373. [CrossRef]
90. Alique, D.; Bruni, G.; Sanz, R.; Calles, J.A.; Tosti, S. Ultra-Pure Hydrogen via Co-Valorization of Olive Mill Wastewater and Bioethanol in Pd-Membrane Reactors. *Processes* **2020**, *8*, 219. [CrossRef]
91. Rocha, C.; Soria, M.A.; Madeira, L.M. Use of Ni-containing catalysts for synthetic olive mill wastewater steam reforming. *Renew. Energy* **2022**, *185*, 1329–1342. [CrossRef]
92. Zhang, Z.; Zhang, L.; Liu, F.; Sun, Y.; Shao, Y.; Sun, K.; Zhang, S.; Liu, Q.; Hu, G.; Hu, X. Tailoring the surface properties of Ni/SiO₂ catalyst with sulfuric acid for enhancing the catalytic efficiency for steam reforming of guaiacol. *Renew. Energy* **2020**, *156*, 423–439. [CrossRef]
93. Zhang, Z.; Sun, Y.; Wang, Y.; Sun, K.; Gao, Z.; Xu, Q.; Zhang, S.; Hu, G.; Xu, L.; Hu, X. Steam reforming of acetic acid and guaiacol over Ni/Attapulgite catalyst: Tailoring pore structure of the catalyst with KOH activation for enhancing the resistivity towards coking. *Mol. Catal.* **2020**, *493*, 111051. [CrossRef]
94. Trane, R.; Dahl, S.; Skjøth-Rasmussen, M.S.; Jensen, A.D. Catalytic steam reforming of bio-oil. *Int. J. Hydrogen Energy* **2012**, *37*, 6447–6472. [CrossRef]
95. Xie, H.; Yu, Q.; Wei, M.; Duan, W.; Yao, X.; Qin, Q.; Zuo, Z. Hydrogen production from steam reforming of simulated bio-oil over Ce-Ni/Co catalyst with in continuous CO₂ capture. *Int. J. Hydrogen Energy* **2015**, *40*, 1420–1428. [CrossRef]
96. Soria, M.A.; Barros, D.; Madeira, L.M. Hydrogen production through steam reforming of bio-oils derived from biomass pyrolysis: Thermodynamic analysis including in situ CO₂ and/or H₂ separation. *Fuel* **2019**, *244*, 184–195. [CrossRef]
97. Kechagiopoulos, P.N.; Voutetakis, S.S.; Lemonidou, A.A.; Vasalos, I.A. Hydrogen Production via Steam Reforming of the Aqueous Phase of Bio-Oil in a Fixed Bed Reactor. *Energy Fuels* **2006**, *20*, 2155–2163. [CrossRef]
98. Remiro, A.; Valle, B.; Aguayo, A.T.; Bilbao, J.; Gayubo, A.G. Operating conditions for attenuating Ni/La₂O₃-αAl₂O₃ catalyst deactivation in the steam reforming of bio-oil aqueous fraction. *Fuel Processing Technol.* **2013**, *115*, 222–232. [CrossRef]
99. Remiro, A.; Arandia, A.; Oar-Arteta, L.; Bilbao, J.; Gayubo, A.G. Regeneration of NiAl₂O₄ spinel type catalysts used in the reforming of raw bio-oil. *Appl. Catal. B: Environ.* **2018**, *237*, 353–365. [CrossRef]
100. Valle, B.; Aramburu, B.; Olazar, M.; Bilbao, J.; Gayubo, A.G. Steam reforming of raw bio-oil over Ni/La₂O₃-αAl₂O₃: Influence of temperature on product yields and catalyst deactivation. *Fuel* **2018**, *216*, 463–474. [CrossRef]
101. Yu, N.; Rahman, M.M.; Chen, J.; Sun, J.; Engelhard, M.; Hernandez, X.I.P.; Wang, Y. Steam reforming of simulated bio-oil on K-Ni-Cu-Mg-Ce-O/Al₂O₃: The effect of K. *Catal. Today* **2019**, *323*, 183–190. [CrossRef]
102. Cheng, Y.W.; Khan, M.R.; Ng, K.H.; Wongsakulphasatch, S.; Cheng, C.K. Harnessing renewable hydrogen-rich syngas from valorization of palm oil mill effluent (POME) using steam reforming technique. *Renew. Energy* **2019**, *138*, 1114–1126. [CrossRef]
103. Cheng, Y.W.; Chong, C.C.; Lee, S.P.; Lim, J.W.; Wu, T.Y.; Cheng, C.K. Syngas from palm oil mill effluent (POME) steam reforming over lanthanum cobaltite: Effects of net-basicity. *Renew. Energy* **2019**, *148*, 349–362. [CrossRef]
104. Medrano, J.A.; Oliva, M.; Ruiz, J.; Garcia, L.; Arauzo, J. Catalytic steam reforming of acetic acid in a fluidized bed reactor with oxygen addition. *Int. J. Hydrogen Energy* **2008**, *33*, 4387–4396. [CrossRef]
105. Matas Güell, B.; ISilva, M.T.d.; Seshan, K.; Lefferts, L. Sustainable route to hydrogen—Design of stable catalysts for the steam gasification of biomass related oxygenates. *Appl. Catal. B: Environ.* **2009**, *88*, 59–65. [CrossRef]
106. Hoang, T.M.C.; Geerdink, B.; Sturm, J.M.; Lefferts, L.; Seshan, K. Steam reforming of acetic acid—A major component in the volatiles formed during gasification of humin. *Appl. Catal. B Environ.* **2015**, *163* (Suppl. C), 74–82. [CrossRef]
107. Chen, G.; Tao, J.; Liu, C.; Yan, B.; Li, W.; Li, X. Steam reforming of acetic acid using Ni/Al₂O₃ catalyst: Influence of crystalline phase of Al₂O₃ support. *Int. J. Hydrogen Energy* **2017**, *42*, 20729–20738. [CrossRef]
108. Savuto, E.; Navarro, R.M.; Mota, N.; di Carlo, A.; Bocci, E.; Carlini, M.; Fierro, J.L.G. Steam reforming of tar model compounds over Ni/Mayenite catalysts: Effect of Ce addition. *Fuel* **2018**, *224*, 676–686. [CrossRef]
109. Silva, J.M.; Soria, M.A.; Madeira, L.M. Challenges and strategies for optimization of glycerol steam reforming process. *Renew. Sustain. Energy Rev.* **2015**, *42*, 1187–1213. [CrossRef]
110. Zhang, Z.; Hu, X.; Li, J.; Gao, G.; Dong, D.; Westerhof, R.; Hu, S.; Xiang, J.; Wang, Y. Steam reforming of acetic acid over Ni/Al₂O₃ catalysts: Correlation of nickel loading with properties and catalytic behaviors of the catalysts. *Fuel* **2018**, *217*, 389–403. [CrossRef]
111. Borges, R.P.; Ferreira, R.A.R.; Rabelo-Neto, R.C.; Noronha, F.B.; Hori, C.E. Hydrogen production by steam reforming of acetic acid using hydrotalcite type precursors. *Int. J. Hydrogen Energy* **2018**, *43*, 7881–7892. [CrossRef]

112. Yu, Z.; Hu, X.; Jia, P.; Zhang, Z.; Dong, D.; Hu, G.; Hu, S.; Wang, Y.; Xiang, J. Steam reforming of acetic acid over nickel-based catalysts: The intrinsic effects of nickel precursors on behaviors of nickel catalysts. *Appl. Catal. B Environ.* **2018**, *237*, 538–553. [[CrossRef](#)]
113. Matas Güell, B.; Babich, I.; Nichols, K.P.; Gardeniers, J.G.E.; Lefferts, L.; Seshan, K. Design of a stable steam reforming catalyst—A promising route to sustainable hydrogen from biomass oxygenates. *Appl. Catal. B Environ.* **2009**, *90*, 38–44. [[CrossRef](#)]
114. de Castro, T.P.; Silveira, E.B.; Rabelo-Neto, R.C.; Borges, L.E.P.; Noronha, F.B. Study of the performance of Pt/Al₂O₃ and Pt/CeO₂/Al₂O₃ catalysts for steam reforming of toluene, methane and mixtures. *Catal. Today* **2018**, *299* (Suppl. C), 251–262. [[CrossRef](#)]
115. Pant, K.K.; Mohanty, P.; Agarwal, S.; Dalai, A.K. Steam reforming of acetic acid for hydrogen production over bifunctional Ni-Co catalysts. *Catal. Today* **2013**, *207* (Suppl. C), 36–43. [[CrossRef](#)]
116. Polychronopoulou, K.; Fierro, J.L.G.; Efstathiou, A.M. The phenol steam reforming reaction over MgO-based supported Rh catalysts. *J. Catal.* **2004**, *228*, 417–432. [[CrossRef](#)]
117. Constantinou, D.A.; Efstathiou, A.M. Low-temperature purification of gas streams from phenol by steam reforming over novel supported-Rh catalysts. *Appl. Catal. B Environ.* **2010**, *96*, 276–289. [[CrossRef](#)]
118. Iida, H.; Fujiyama, A.; Igarashi, A.; Okumura, K. Steam reforming of toluene over Ru/SrCO₃-Al₂O₃ catalysts. *Fuel Processing Technol.* **2017**, *168* (Suppl. C), 50–57. [[CrossRef](#)]
119. Liang, T.; Wang, Y.; Chen, M.; Yang, Z.; Liu, S.; Zhou, Z.; Li, X. Steam reforming of phenol-ethanol to produce hydrogen over bimetallic NiCu catalysts supported on sepiolite. *Int. J. Hydrogen Energy* **2017**, *42*, 28233–28246. [[CrossRef](#)]
120. Adnan, M.A.; Muraza, O.; Razzak, S.A.; Hossain, M.M.; de Lasa, H.I. Iron Oxide over Silica-Doped Alumina Catalyst for Catalytic Steam Reforming of Toluene as a Surrogate Tar Biomass Species. *Energy Fuels* **2017**, *31*, 7471–7481. [[CrossRef](#)]
121. Wang, S.; Li, X.; Guo, L.; Luo, Z. Experimental research on acetic acid steam reforming over Co-Fe catalysts and subsequent density functional theory studies. *Int. J. Hydrogen Energy* **2012**, *37*, 11122–11131. [[CrossRef](#)]
122. Furusawa, T.; Saito, K.; Kori, Y.; Miura, Y.; Sato, M.; Suzuki, N. Steam reforming of naphthalene/benzene with various types of Pt- and Ni-based catalysts for hydrogen production. *Fuel* **2013**, *103*, 111–121. [[CrossRef](#)]
123. Wang, S.; Zhang, F.; Cai, Q.; Zhu, L.; Luo, Z. Steam reforming of acetic acid over coal ash supported Fe and Ni catalysts. *Int. J. Hydrogen Energy* **2015**, *40*, 11406–11413. [[CrossRef](#)]
124. Nabgan, W.; Abdullah, T.A.T.; Mat, R.; Nabgan, B.; Gambo, Y.; Triwahyono, S. Influence of Ni to Co ratio supported on ZrO₂ catalysts in phenol steam reforming for hydrogen production. *Int. J. Hydrogen Energy* **2016**, *41*, 22922–22931. [[CrossRef](#)]
125. Silva, O.C.V.; Silveira, E.B.; Rabelo-Neto, R.C.; Borges, L.E.P.; Noronha, F.B. Hydrogen Production Through Steam Reforming of Toluene Over Ni Supported on MgAl Mixed Oxides Derived from Hydrotalcite-Like Compounds. *Catal. Lett.* **2018**, *148*, 1622–1633. [[CrossRef](#)]
126. Pu, J.; Nishikado, K.; Wang, N.; Nguyen, T.T.; Maki, T.; Qian, E.W. Core-shell nickel catalysts for the steam reforming of acetic acid. *Appl. Catal. B Environ.* **2018**, *224*, 69–79. [[CrossRef](#)]
127. Li, J.; Mei, X.; Zhang, L.; Yu, Z.; Liu, Q.; Wei, T.; Wu, W.; Dong, D.; Xu, L.; Hu, X. A comparative study of catalytic behaviors of Mn, Fe, Co, Ni, Cu and Zn-Based catalysts in steam reforming of methanol, acetic acid and acetone. *Int. J. Hydrogen Energy* **2020**, *45*, 3815–3832. [[CrossRef](#)]
128. Zhang, C.; Hu, X.; Yu, Z.; Zhang, Z.; Chen, G.; Li, C.; Liu, Q.; Xiang, J.; Wang, Y.; Hu, S. Steam reforming of acetic acid for hydrogen production over attapulgite and alumina supported Ni catalysts: Impacts of properties of supports on catalytic behaviors. *Int. J. Hydrogen Energy* **2019**, *44*, 5230–5244. [[CrossRef](#)]
129. Chen, J.; Wang, M.; Wang, S.; Li, X. Hydrogen production via steam reforming of acetic acid over biochar-supported nickel catalysts. *Int. J. Hydrogen Energy* **2018**, *43*, 18160–18168. [[CrossRef](#)]
130. Wang, Y.; Zhang, Z.; Zhang, S.; Wang, Y.; Hu, S.; Xiang, J.; Hu, X. Steam reforming of acetic acid over Ni/biochar catalyst treated with HNO₃: Impacts of the treatment on surface properties and catalytic behaviors. *Fuel* **2020**, *278*, 118341. [[CrossRef](#)]
131. Yang, X.; Wang, Y.; Li, M.; Sun, B.; Li, Y.; Wang, Y. Enhanced Hydrogen Production by Steam Reforming of Acetic Acid over a Ni Catalyst Supported on Mesoporous MgO. *Energy Fuels* **2016**, *30*, 2198–2203. [[CrossRef](#)]
132. Bangala, D.N.; Abatzoglou, N.; Chornet, E. Steam reforming of naphthalene on Ni-Cr/Al₂O₃ catalysts doped with MgO, TiO₂, and La₂O₃. *AIChE J.* **1998**, *44*, 927–936. [[CrossRef](#)]
133. Garcia, L.a.; French, R.; Czernik, S.; Chornet, E. Catalytic steam reforming of bio-oils for the production of hydrogen: Effects of catalyst composition. *Appl. Catal. A Gen.* **2000**, *201*, 225–239. [[CrossRef](#)]
134. Wang, M.; Zhang, F.; Wang, S. Effect of La₂O₃ replacement on γ -Al₂O₃ supported nickel catalysts for acetic acid steam reforming. *Int. J. Hydrogen Energy* **2017**, *42*, 20540–20548. [[CrossRef](#)]
135. Li, L.; Jiang, B.; Tang, D.; Zhang, Q.; Zheng, Z. Hydrogen generation by acetic acid steam reforming over Ni-based catalysts derived from La_{1-x}Ce_xNiO₃ perovskite. *Int. J. Hydrogen Energy* **2018**, *43*, 6795–6803. [[CrossRef](#)]
136. Matas Güell, B.; Babich, I.V.; Lefferts, L.; Seshan, K. Steam reforming of phenol over Ni-based catalysts—A comparative study. *Appl. Catal. B Environ.* **2011**, *106*, 280–286. [[CrossRef](#)]
137. Frusteri, F.; Freni, S.; Chiodo, V.; Spadaro, L.; di Blasi, O.; Bonura, G.; Cavallaro, S. Steam reforming of bio-ethanol on alkali-doped Ni/MgO catalysts: Hydrogen production for MC fuel cell. *Appl. Catal. A Gen.* **2004**, *270*, 1–7. [[CrossRef](#)]
138. Hu, X.; Dong, D.; Shao, X.; Zhang, L.; Lu, G. Steam reforming of acetic acid over cobalt catalysts: Effects of Zr, Mg and K addition. *Int. J. Hydrogen Energy* **2017**, *42*, 4793–4803. [[CrossRef](#)]

139. Ahmed, T.; Xiu, S.; Wang, L.; Shahbazi, A. Investigation of Ni/Fe/Mg zeolite-supported catalysts in steam reforming of tar using simulated-toluene as model compound. *Fuel* **2018**, *211* (Suppl. C), 566–571. [[CrossRef](#)]
140. Pu, J.; Ikegami, F.; Nishikado, K.; Qian, E.W. Effect of ceria addition on NiRu/CeO₂Al₂O₃ catalysts in steam reforming of acetic acid. *Int. J. Hydrogen Energy* **2017**, *42*, 19733–19743. [[CrossRef](#)]
141. Wang, Y.; Chen, M.; Yang, J.; Liu, S.; Yang, Z.; Wang, J.; Liang, T. Hydrogen Production from Steam Reforming of Acetic Acid over Ni-Fe/Palygorskite Modified with Cerium. *BioResources* **2017**, *12*, 4830–4853. [[CrossRef](#)]
142. Zhao, X.; Xue, Y.; Lu, Z.; Huang, Y.; Guo, C.; Yan, C. Encapsulating Ni/CeO₂-ZrO₂ with SiO₂ layer to improve its catalytic activity for steam reforming of toluene. *Catal. Commun.* **2017**, *101* (Suppl. C), 138–141. [[CrossRef](#)]
143. Li, L.; Tang, D.; Song, Y.; Jiang, B.; Zhang, Q. Hydrogen production from ethanol steam reforming on Ni-Ce/MMT catalysts. *Energy* **2018**, *149*, 937–943. [[CrossRef](#)]
144. Zhang, Z.; Hu, X.; Gao, G.; Wei, T.; Dong, D.; Wang, Y.; Hu, S.; Xiang, J.; Liu, Q.; Geng, D. Steam reforming of acetic acid over NiKOH/Al₂O₃ catalyst with low nickel loading: The remarkable promotional effects of KOH on activity. *Int. J. Hydrogen Energy* **2018**, *44*, 729–747. [[CrossRef](#)]
145. Choi, I.-H.; Hwang, K.-R.; Lee, K.-Y.; Lee, I.-G. Catalytic steam reforming of biomass-derived acetic acid over modified Ni/ γ -Al₂O₃ for sustainable hydrogen production. *Int. J. Hydrogen Energy* **2019**, *44*, 180–190. [[CrossRef](#)]
146. Higo, T.; Saito, H.; Ogo, S.; Sugiura, Y.; Sekine, Y. Promotive effect of Ba addition on the catalytic performance of Ni/LaAlO₃ catalysts for steam reforming of toluene. *Appl. Catal. A Gen.* **2017**, *530*, 125–131. [[CrossRef](#)]
147. Fally, F.; Perrichon, V.; Vidal, H.; Kaspar, J.; Blanco, G.; Pintado, J.M.; Bernal, S.; Colon, G.; Daturi, M.; Lavalley, J.C. Modification of the oxygen storage capacity of CeO₂-ZrO₂ mixed oxides after redox cycling aging. *Catal. Today* **2000**, *59*, 373–386. [[CrossRef](#)]
148. Vidal, H.; Kašpar, J.; Pijolat, M.; Colon, G.; Bernal, S.; Cordon, A.; Perrichon, V.; Fally, F. Redox behavior of CeO₂-ZrO₂ mixed oxides: II. Influence of redox treatments on low surface area catalysts. *Appl. Catal. B Environ.* **2001**, *30*, 75–85. [[CrossRef](#)]
149. Menendez, R.B.; Gracinsky, C.; Amadeo, N.E. Sorption-Enhanced Ethanol Steam Reforming Process in a Fixed-Bed Reactor. *Ind. Eng. Chem. Res.* **2018**, *57*, 11547–11553. [[CrossRef](#)]
150. Chen, M.; Wang, Y.; Yang, Z.; Liang, T.; Liu, S.; Zhou, Z.; Li, X. Effect of Mg-modified mesoporous Ni/Attapulgite catalysts on catalytic performance and resistance to carbon deposition for ethanol steam reforming. *Fuel* **2018**, *220*, 32–46. [[CrossRef](#)]
151. Kumar, A.; Sinha, A.S.K. Hydrogen production from acetic acid steam reforming over nickel-based catalyst synthesized via MOF process. *Int. J. Hydrogen Energy* **2020**, *45*, 24397–24411. [[CrossRef](#)]
152. Yu, Z.; Zhang, L.; Zhang, C.; Gao, G.; Ye, Z.; Zhang, S.; Liu, Q.; Hu, G.; Hu, X. Steam reforming of acetic acid over nickel catalysts: Impacts of fourteen additives on the catalytic behaviors. *J. Energy Inst.* **2020**, *93*, 1000–1019. [[CrossRef](#)]
153. Galdámez, J.R.; García, L.; Bilbao, R. Hydrogen Production by Steam Reforming of Bio-Oil Using Coprecipitated Ni–Al Catalysts. Acetic Acid as a Model Compound. *Energy Fuels* **2005**, *19*, 1133–1142. [[CrossRef](#)]
154. Rostrup-Nielsen, J.R.; Sehested, J.; Nørskov, J.K. Hydrogen and synthesis gas by steam- and CO₂ reforming. In *Advances in Catalysis*; Academic Press: Cambridge, MA, USA, 2002; Volume 47, pp. 65–139.
155. Bengaard, H.S.; Nørskov, J.K.; Sehested, J.; Clausen, B.S.; Nielsen, L.P.; Molenbroek, A.M.; Rostrup-Nielsen, J.R. Steam Reforming and Graphite Formation on Ni Catalysts. *J. Catal.* **2002**, *209*, 365–384. [[CrossRef](#)]
156. Pekmezci Karaman, B.; Cakiryilmaz, N.; Arbag, H.; Oktar, N.; Dogu, G.; Dogu, T. Performance comparison of mesoporous alumina supported Cu & Ni based catalysts in acetic acid reforming. *Int. J. Hydrogen Energy* **2017**, *42*, 26257–26269.
157. Goicoechea, S.; Kraveva, E.; Sokolov, S.; Schneider, M.; Pohl, M.-M.; Kockmann, N.; Ehrich, H. Support effect on structure and performance of Co and Ni catalysts for steam reforming of acetic acid. *Appl. Catal. A Gen.* **2016**, *514* (Suppl. C), 182–191. [[CrossRef](#)]
158. Meng, J.; Zhao, Z.; Wang, X.; Zheng, A.; Zhang, D.; Huang, Z.; Zhao, K.; Wei, G.; Li, H. Comparative study on phenol and naphthalene steam reforming over Ni-Fe alloy catalysts supported on olivine synthesized by different methods. *Energy Convers. Manag.* **2018**, *168*, 60–73. [[CrossRef](#)]
159. Zhu, H.L.; Pastor-Pérez, L.; Millan, M. Catalytic Steam Reforming of Toluene: Understanding the Influence of the Main Reaction Parameters over a Reference Catalyst. *Energies* **2020**, *13*, 813. [[CrossRef](#)]
160. Rodrigues, A.E.; Madeira, L.M.; Faria, R.; Wu, Y.J. *Sorption Enhanced Reaction Processes*; World Scientific Publishing Company Pte Limited: Singapore, 2017.
161. Ni, F.; Caram, H.S. Sorption enhanced reaction for high purity products in reversible reactions. *AIChE J.* **2017**, *63*, 5452–5461. [[CrossRef](#)]
162. Wu, Y.-J.; Li, P.; Yu, J.-G.; Cunha, A.F.; Rodrigues, A.E. Sorption-enhanced steam reforming of ethanol for continuous high-purity hydrogen production: 2D adsorptive reactor dynamics and process design. *Chem. Eng. Sci.* **2014**, *118*, 83–93. [[CrossRef](#)]
163. Soria, M.A.; Tosti, S.; Mendes, A.; Madeira, L.M. Enhancing the low temperature water-gas shift reaction through a hybrid sorption-enhanced membrane reactor for high-purity hydrogen production. *Fuel* **2015**, *159*, 854–863. [[CrossRef](#)]
164. Iliuta, I.; Radfarnia, H.R.; Iliuta, M.C. Hydrogen Production by Sorption-Enhanced Steam Glycerol Reforming: Sorption Kinetics and Reactor Simulation. *AIChE J.* **2013**, *59*, 2105–2118. [[CrossRef](#)]
165. Clough, P.T.; Boot-Handford, M.E.; Zheng, L.; Zhang, Z.; Fennell, P.S. Hydrogen Production by Sorption Enhanced Steam Reforming (SESR) of Biomass in a Fluidised-Bed Reactor Using Combined Multifunctional Particles. *Materials* **2018**, *11*, 859. [[CrossRef](#)]

166. Park, B.-G. A hybrid adsorbent-membrane reactor (HAMR) system for hydrogen production. *Korean J. Chem. Eng.* **2004**, *21*, 782–792. [[CrossRef](#)]
167. Wu, Y.J.; Alvarado, F.D.; Santos, J.C.; Gracia, F.; Cunha, A.F.; Rodrigues, A.E. Sorption-Enhanced Steam Reforming of Ethanol: Thermodynamic Comparison of CO₂ Sorbents. *Chem. Eng. Technol.* **2012**, *35*, 847–858. [[CrossRef](#)]
168. Dou, B.; Dupont, V.; Rickett, G.; Blakeman, N.; Williams, P.T.; Chen, H.; Ding, Y.; Ghadiri, M. Hydrogen production by sorption-enhanced steam reforming of glycerol. *Bioresour. Technol.* **2009**, *100*, 3540–3547. [[CrossRef](#)]
169. Martavaltzi, C.S.; Lemonidou, A.A. Hydrogen production via sorption enhanced reforming of methane: Development of a novel hybrid material—reforming catalyst and CO₂ sorbent. *Chem. Eng. Sci.* **2010**, *65*, 4134–4140. [[CrossRef](#)]
170. Aloisi, I.; Adi, G.; di Carlo, A.; Foscolo, P.U.; Courson, C.; Gallucci, K. Sorption enhanced catalytic Steam Methane Reforming: Experimental data and simulations describing the behaviour of bi-functional particles. *Chem. Eng. J.* **2017**, *314*, 570–582. [[CrossRef](#)]
171. Reijers, H.T.J.; Valster-Schiermeier, S.E.A.; Cobden, P.D.; van den Brink, R.W. Hydrotalcite as CO₂ Sorbent for Sorption-Enhanced Steam Reforming of Methane. *Ind. Eng. Chem. Res.* **2006**, *45*, 2522–2530. [[CrossRef](#)]
172. Kim, C.-H.; Han, J.-Y.; Lim, H.; Lee, K.-Y.; Ryi, S.-K. Hydrogen production by steam methane reforming in membrane reactor equipped with Pd membrane deposited on NiO/YSZ/NiO multilayer-treated porous stainless steel. *J. Membr. Sci.* **2018**, *563*, 75–82. [[CrossRef](#)]
173. Soria, M.A.; Mateos-Pedrero, C.; Rodríguez-Ramos, I.; Guerrero-Ruiz, A. Catalytic steam reforming of methane under conditions of applicability with Pd membranes over supported Ru catalysts. *Catal. Today* **2011**, *171*, 126–131. [[CrossRef](#)]
174. Adiya, Z.I.S.G.; Dupont, V.; Mahmud, T. Steam reforming of shale gas with nickel and calcium looping. *Fuel* **2019**, *237*, 142–151. [[CrossRef](#)]
175. Omoniyi, O.A.; Dupont, V. Optimised cycling stability of sorption enhanced chemical looping steam reforming of acetic acid in a packed bed reactor. *Appl. Catal. B Environ.* **2019**, *242*, 397–409. [[CrossRef](#)]
176. Diglio, G.; Bareschino, P.; Mancusi, E.; Pepe, F.; Montagnaro, F.; Hanak, D.P.; Manovic, V. Feasibility of CaO/CuO/NiO sorption-enhanced steam methane reforming integrated with solid-oxide fuel cell for near-zero-CO₂ emissions cogeneration system. *Appl. Energy* **2018**, *230*, 241–256. [[CrossRef](#)]
177. Xie, H.; Zhang, W.; Zhao, X.; Chen, H.; Yu, Q.; Qin, Q. Sorption-enhanced reforming of tar: Influence of the preparation method of CO₂ absorbent. *Korean J. Chem. Eng.* **2018**, *35*, 2191–2197. [[CrossRef](#)]
178. Di Felice, L.; Kazi, S.S.; Sørby, M.H.; Martinez, I.; Grasa, G.; Maury, D.; Meyer, J. Combined sorbent and catalyst material for sorption enhanced reforming of methane under cyclic regeneration in presence of H₂O and CO₂. *Fuel Processing Technol.* **2019**, *183*, 35–47. [[CrossRef](#)]
179. Di Giuliano, A.; Giancaterino, F.; Gallucci, K.; Foscolo, P.U.; Courson, C. Catalytic and sorbent materials based on mayenite for sorption enhanced steam methane reforming with different packed-bed configurations. *Int. J. Hydrogen Energy* **2018**, *43*, 21279–21289. [[CrossRef](#)]
180. Ghungrud, S.A.; Dewoolkar, K.D.; Vaidya, P.D. Cerium-promoted bi-functional hybrid materials made of Ni, Co and hydrotalcite for sorption-enhanced steam methane reforming (SESMR). *Int. J. Hydrogen Energy* **2018**, *44*, 694–706. [[CrossRef](#)]
181. Dang, C.; Wu, S.; Cao, Y.; Wang, H.; Peng, F.; Yu, H. Co-production of high quality hydrogen and synthesis gas via sorption-enhanced steam reforming of glycerol coupled with methane reforming of carbonates. *Chem. Eng. J.* **2019**, *360*, 47–53. [[CrossRef](#)]
182. Cherbański, R.; Molga, E. Sorption-enhanced steam methane reforming (SE-SMR)—A review: Reactor types, catalysts and sorbents characterization, process modelling. *Chem. Process Eng.* **2018**, *39*, 427–448.
183. Jang, H.M.; Lee, K.B.; Caram, H.S.; Sircar, S. High-purity hydrogen production through sorption enhanced water gas shift reaction using K₂CO₃-promoted hydrotalcite. *Chem. Eng. Sci.* **2012**, *73*, 431–438. [[CrossRef](#)]
184. Xie, H.; Yu, Q.; Lu, H.; Ji, L.; Chen, H.; Qin, Q. Selection and preparation of CO₂ sorbent for sorption-enhanced steam reforming process of raw coke oven gas. *Environ. Prog. Sustain. Energy* **2019**, *38*, 89–97. [[CrossRef](#)]
185. Soria, M.A.; Rocha, C.; Tosti, S.; Mendes, A.; Madeira, L.M. CO_x free hydrogen production through water-gas shift reaction in different hybrid multifunctional reactors. *Chem. Eng. J.* **2019**, *356*, 727–736. [[CrossRef](#)]
186. Vanga, G.; Gattia, D.M.; Stendardo, S.; Scaccia, S. Novel synthesis of combined CaO-Ca₁₂Al₁₄O₃₃-Ni sorbent-catalyst material for sorption enhanced steam reforming processes. *Ceram. Int.* **2019**, *45*, 7594–7605. [[CrossRef](#)]
187. Liu, L.; Hong, D.; Wang, N.; Guo, X. High purity H₂ production from sorption enhanced bio-ethanol reforming via sol-gel-derived Ni-CaO-Al₂O₃ bi-functional materials. *Int. J. Hydrogen Energy* **2020**, *45*, 34449–34460. [[CrossRef](#)]
188. Wang, X.; He, Y.; Xu, T.; Xiao, B.; Liu, S.; Hu, Z.; Li, J. CO₂ sorption-enhanced steam reforming of phenol using Ni-M/CaO-Ca₁₂Al₁₄O₃₃ (M = Cu, Co, and Ce) as catalytic sorbents. *Chem. Eng. J.* **2020**, *393*, 124769. [[CrossRef](#)]
189. Dang, C.; Wu, S.; Yang, G.; Cao, Y.; Wang, H.; Peng, F.; Wang, S.; Yu, H. Hydrogen Production from Sorption-Enhanced Steam Reforming of Phenol over a Ni-Ca-Al-O Bifunctional Catalyst. *ACS Sustain. Chem. Eng.* **2020**, *8*, 7111–7120. [[CrossRef](#)]
190. Nimmas, T.; Wongsakulphasatch, S.; Cheng, C.K.; Assabumrungrat, S. Bi-metallic CuO-NiO based multifunctional material for hydrogen production from sorption-enhanced chemical looping autothermal reforming of ethanol. *Chem. Eng. J.* **2020**, *398*, 125543. [[CrossRef](#)]
191. Li, H.; Tian, H.; Chen, S.; Sun, Z.; Liu, T.; Liu, R.; Assabumrungrat, S.; Saupsor, J.; Mu, R.; Gong, C.P.J. Sorption enhanced steam reforming of methanol for high-purity hydrogen production over Cu-MgO/Al₂O₃ bifunctional catalysts. *Appl. Catal. B Environ.* **2020**, *276*, 119052. [[CrossRef](#)]

192. Zhang, W.; Xie, H.; Yu, Z.; Wang, P.; Wang, Z.; Yu, Q. Steam reforming of tar from raw coke oven gas over bifunctional catalysts: Reforming performance for H₂ production. *Environ. Prog. Sustain. Energy* **2021**, *40*, e13501. [CrossRef]
193. Coenen, K.; Gallucci, F.; Cobden, P.; van Dijk, E.; Hensen, E.; Annaland, M.V. Influence of material composition on the CO₂ and H₂O adsorption capacities and kinetics of potassium-promoted sorbents. *Chem. Eng. J.* **2018**, *334*, 2115–2123. [CrossRef]
194. Rocha, C.; Soria, M.A.; Madeira, L.M. Steam reforming of olive oil mill wastewater with in situ hydrogen and carbon dioxide separation—Thermodynamic analysis. *Fuel* **2017**, *207*, 449–460. [CrossRef]
195. Lima da Silva, A.; Müller, I.L. Hydrogen production by sorption enhanced steam reforming of oxygenated hydrocarbons (ethanol, glycerol, n-butanol and methanol): Thermodynamic modelling. *Int. J. Hydrogen Energy* **2011**, *36*, 2057–2075. [CrossRef]
196. Silva, J.M.; Soria, M.A.; Madeira, L.M. Thermodynamic analysis of Glycerol Steam Reforming for hydrogen production with in situ hydrogen and carbon dioxide separation. *J. Power Sources* **2015**, *273*, 423–430. [CrossRef]
197. Rocha, C.; Soria, M.A.; Madeira, L.M. Olive mill wastewater valorization through steam reforming using hybrid multifunctional reactors for high-purity H₂ production. *Chem. Eng. J.* **2022**, *430*, 132651. [CrossRef]
198. Nations, U. COP26 Keeps 1.5C Alive and Finalises Paris Agreement. 2021. Available online: <https://ukcop26.org/cop26-keeps-1-5c-alive-and-finalises-paris-agreement/> (accessed on 30 November 2021).
199. Al-Mamoori, A.; Thakkar, H.; Li, X.; Rownaghi, A.A.; Rezaei, F. Development of Potassium- and Sodium-Promoted CaO Adsorbents for CO₂ Capture at High Temperatures. *Ind. Eng. Chem. Res.* **2017**, *56*, 8292–8300. [CrossRef]
200. Martavaltzi, C.S.; Lemonidou, A.A. Development of new CaO based sorbent materials for CO₂ removal at high temperature. *Microporous Mesoporous Mater.* **2008**, *110*, 119–127. [CrossRef]
201. Wang, S.; Shen, H.; Fan, S.; Zhao, Y.; Ma, X.; Gong, J. Enhanced CO₂ adsorption capacity and stability using CaO-based adsorbents treated by hydration. *AIChE J.* **2013**, *59*, 3586–3593. [CrossRef]
202. Westbye, A.; di Felice, L.; Aranda, A.; Dietzel, P.D.C. Efficient calcination of CaCO₃ by means of combined Ca-Cu materials for Sorption Enhanced Reforming. In Proceedings of the 25th International Conference on Chemical Reaction Engineering, Florence, Italy, 20–23 May 2018.
203. Zhang, Y.; Gong, X.; Chen, X.; Yin, L.; Zhang, J.; Liu, W. Performance of synthetic CaO-based sorbent pellets for CO₂ capture and kinetic analysis. *Fuel* **2018**, *232*, 205–214. [CrossRef]
204. Yoon, H.J.; Lee, K.B. Introduction of chemically bonded zirconium oxide in CaO-based high-temperature CO₂ sorbents for enhanced cyclic sorption. *Chem. Eng. J.* **2019**, *355*, 850–857. [CrossRef]
205. Guo, H.; Xu, Z.; Jiang, T.; Zhao, Y.; Ma, X.; Wang, S. The effect of incorporation Mg ions into the crystal lattice of CaO on the high temperature CO₂ capture. *J. CO₂ Util.* **2020**, *37*, 335–345. [CrossRef]
206. Zhang, X.; Li, Z.; Peng, Y.; Su, W.; Sun, X.; Li, J. Investigation on a novel CaO-Y₂O₃ sorbent for efficient CO₂ mitigation. *Chem. Eng. J.* **2014**, *243* (Suppl. C), 297–304. [CrossRef]
207. Lu, H.; Reddy, E.P.; Smirniotis, P.G. Calcium Oxide Based Sorbents for Capture of Carbon Dioxide at High Temperatures. *Ind. Eng. Chem. Res.* **2006**, *45*, 3944–3949. [CrossRef]
208. Di Giuliano, A.; Gallucci, K. Sorption enhanced steam methane reforming based on nickel and calcium looping: A review. *Chem. Eng. Processing Process Intensif.* **2018**, *130*, 240–252. [CrossRef]
209. Silva, J.M.; Trujillano, R.; Rives, V.; Soria, M.A.; Madeira, L.M. High temperature CO₂ sorption over modified hydrotalcites. *Chem. Eng. J.* **2017**, *325*, 25–34. [CrossRef]
210. Miguel, C.V.; Trujillano, R.; Rives, V.; Vicente, M.A.; Ferreira, A.F.P.; Rodrigues, A.E.; Mendes, A.; Madeira, L.M. High temperature CO₂ sorption with gallium-substituted and promoted hydrotalcites. *Sep. Purif. Technol.* **2014**, *127* (Suppl. C), 202–211. [CrossRef]
211. Kim, S.; Jeon, S.G.; Lee, K.B. High-Temperature CO₂ Sorption on Hydrotalcite Having a High Mg/Al Molar Ratio. *ACS Appl. Mater. Interfaces* **2016**, *8*, 5763–5767. [CrossRef] [PubMed]
212. Yong, Z.; Mata, V.; Rodrigues, A.E. Adsorption of Carbon Dioxide onto Hydrotalcite-like Compounds (HTLcs) at High Temperatures. *Ind. Eng. Chem. Res.* **2001**, *40*, 204–209. [CrossRef]
213. Wang, X.P.; Yu, J.J.; Cheng, J.; Hao, Z.P.; Xu, Z.P. High-Temperature Adsorption of Carbon Dioxide on Mixed Oxides Derived from Hydrotalcite-Like Compounds. *Environ. Sci. Technol.* **2008**, *42*, 614–618. [CrossRef] [PubMed]
214. Ram Reddy, M.K.; Xu, P.; Lu, G.Q.; da Costa, J.C.D. Layered Double Hydroxides for CO₂ Capture: Structure Evolution and Regeneration. *Ind. Eng. Chem. Res.* **2006**, *45*, 7504–7509. [CrossRef]
215. Maroño, M.; Torreiro, Y.; Gutierrez, L. Influence of steam partial pressures in the CO₂ capture capacity of K-doped hydrotalcite-based sorbents for their application to SEWGS processes. *Int. J. Greenh. Gas Control* **2013**, *14* (Suppl. C), 183–192. [CrossRef]
216. Coenen, K.; Gallucci, F.; Cobden, P.; van Dijk, E.; Hensen, E.; Annaland, M.v. Chemisorption working capacity and kinetics of CO₂ and H₂O of hydrotalcite-based adsorbents for sorption-enhanced water-gas-shift applications. *Chem. Eng. J.* **2016**, *293*, 9–23. [CrossRef]
217. Helwani, Z.; Wiheeb, A.D.; Kim, J.; Othman, M.R. Improved carbon dioxide capture using metal reinforced hydrotalcite under wet conditions. *Int. J. Greenh. Gas Control* **2012**, *7*, 127–136.
218. Silva, J.M.; Trujillano, R.; Rives, V.; Soria, M.A.; Madeira, L.M. Dynamic behaviour of a K-doped Ga substituted and microwave aged hydrotalcite-derived mixed oxide during CO₂ sorption experiments. *J. Ind. Eng. Chem.* **2019**, *72*, 491–503. [CrossRef]
219. Boon, J.; Cobden, P.D.; van Dijk, H.A.J.; Hoogland, C.; van Selow, E.R.; Annaland, M.v. Isotherm model for high-temperature, high-pressure adsorption of CO₂ and H₂O on K-promoted hydrotalcite. *Chem. Eng. J.* **2014**, *248*, 406–414. [CrossRef]

220. Halabi, M.H.; de Croon, M.H.J.M.; van der Schaaf, J.; Cobden, P.D.; Schouten, J.C. High capacity potassium-promoted hydrotalcite for CO₂ capture in H₂ production. *Int. J. Hydrogen Energy* **2012**, *37*, 4516–4525. [[CrossRef](#)]
221. Wu, Y.-J.; Li, P.; Yu, J.-G.; Cunha, A.F.; Rodrigues, A.E. K-Promoted Hydrotalcites for CO₂ Capture in Sorption Enhanced Reactions. *Chem. Eng. Technol.* **2013**, *36*, 567–574. [[CrossRef](#)]
222. Wang, Q.; Wu, Z.; Tay, H.H.; Chen, L.; Liu, Y.; Chang, J.; Zhong, Z.; Luo, J.; Borgna, A. High temperature adsorption of CO₂ on Mg-Al hydrotalcite: Effect of the charge compensating anions and the synthesis pH. *Catal. Today* **2011**, *164*, 198–203. [[CrossRef](#)]
223. Hanif, A.; Dasgupta, S.; Divekar, S.; Arya, A.; Garg, M.O.; Nanoti, A. A study on high temperature CO₂ capture by improved hydrotalcite sorbents. *Chem. Eng. J.* **2014**, *236* (Suppl. C), 91–99. [[CrossRef](#)]
224. Hutson, N.D.; Attwood, B.C. High temperature adsorption of CO₂ on various hydrotalcite-like compounds. *Adsorption* **2008**, *14*, 781–789. [[CrossRef](#)]
225. Sanna, A.; Thompson, S.; Whitty, K.J.; Maroto-Valer, M.M. Fly Ash Derived Lithium Silicate for in-situ Pre-combustion CO₂ Capture. *Energy Procedia* **2017**, *114* (Suppl. C), 2401–2404. [[CrossRef](#)]
226. Seggiani, M.; Puccini, M.; Vitolo, S. Alkali promoted lithium orthosilicate for CO₂ capture at high temperature and low concentration. *Int. J. Greenh. Gas Control* **2013**, *17* (Suppl. C), 25–31. [[CrossRef](#)]
227. Seggiani, M.; Stefanelli, E.; Puccini, M.; Vitolo, S. CO₂ sorption/desorption performance study on K₂CO₃-doped Li₄SiO₄-based pellets. *Chem. Eng. J.* **2018**, *339*, 51–60. [[CrossRef](#)]
228. Gao, N.; Ma, K.; Ding, T.; Cai, J.; Tian, Y.; Li, X. Enhanced carbon dioxide adsorption performance and kinetic study of K and Al co-doped Li₄SiO₄. *Chin. Chem. Lett.* **2018**, *29*, 482–484. [[CrossRef](#)]
229. Hu, Y.; Liu, W.; Zhou, Z.; Yang, Y. Preparation of Li₄SiO₄ Sorbents for Carbon Dioxide Capture via a Spray-Drying Technique. *Energy Fuels* **2018**, *32*, 4521–4527. [[CrossRef](#)]
230. Wang, H.; Zhang, J.; Wang, G.; Wang, Q.; Song, T. High-temperature capture of CO₂ by Li₄SiO₄ prepared with blast furnace slag and kinetic analysis. *J. Therm. Anal. Calorim.* **2018**, *133*, 981–989. [[CrossRef](#)]
231. Hu, Y.; Qu, M.; Li, H.; Yang, Y.; Yang, J.; Qu, W.; Liu, W. Porous extruded-spheronized Li₄SiO₄ pellets for cyclic CO₂ capture. *Fuel* **2019**, *236*, 1043–1049. [[CrossRef](#)]
232. Izquierdo, M.T.; Saleh, A.; Sánchez-Fernández, E.; Maroto-Valer, M.M.; García, S. High-Temperature CO₂ Capture by Li₄SiO₄ Sorbents: Effect of CO₂ Concentration and Cyclic Performance under Representative Conditions. *Ind. Eng. Chem. Res.* **2018**, *57*, 13802–13810. [[CrossRef](#)]
233. Hu, Y.; Liu, W.; Yang, Y.; Qu, M.; Li, H. CO₂ capture by Li₄SiO₄ sorbents and their applications: Current developments and new trends. *Chem. Eng. J.* **2019**, *359*, 604–625. [[CrossRef](#)]
234. Kwon, Y.M.; Chae, H.J.; Cho, M.S.; Park, Y.K.; Seo, H.M.; Lee, S.C.; Kim, J.C. Effect of a Li₂SiO₃ phase in lithium silicate-based sorbents for CO₂ capture at high temperatures. *Sep. Purif. Technol.* **2019**, *214*, 104–110. [[CrossRef](#)]
235. Zhang, T.; Li, M.; Ning, P.; Jia, Q.; Wang, Q.; Wang, J. K₂CO₃ promoted novel Li₄SiO₄-based sorbents from sepiolite with high CO₂ capture capacity under different CO₂ partial pressures. *Chem. Eng. J.* **2020**, *380*, 122515. [[CrossRef](#)]
236. Li, H.; Qu, M.; Hu, Y. Preparation of spherical Li₄SiO₄ pellets by novel agar method for high-temperature CO₂ capture. *Chem. Eng. J.* **2020**, *380*, 122538. [[CrossRef](#)]
237. Fang, Y.; Zou, R.; Chen, X. High-temperature CO₂ adsorption over Li₄SiO₄ sorbents derived from different lithium sources. *Can. J. Chem. Eng.* **2020**, *98*, 1495–1500. [[CrossRef](#)]
238. Kim, H.; Jang, H.D.; Choi, M. Facile synthesis of macroporous Li₄SiO₄ with remarkably enhanced CO₂ adsorption kinetics. *Chem. Eng. Process.* **2015**, *280*, 132–137. [[CrossRef](#)]
239. Palacios-Romero, L.M.; Pfeiffer, H. Lithium Cuprate (Li₂CuO₂): A New Possible Ceramic Material for CO₂ Chemisorption. *Chem. Lett.* **2008**, *37*, 862–863. [[CrossRef](#)]
240. Iwan, A.; Stephenson, H.; Ketchie, W.C.; Lapkin, A.A. High temperature sequestration of CO₂ using lithium zirconates. *Chem. Eng. J.* **2009**, *146*, 249–258. [[CrossRef](#)]
241. Peltzer, D.; Münner, J.; Cornaglia, L.; Strumendo, M. Characterization of potassium doped Li₂ZrO₃ based CO₂ sorbents: Stability properties and CO₂ desorption kinetics. *Chem. Eng. J.* **2018**, *336*, 1–11. [[CrossRef](#)]
242. Halabi, M.H.; de Croon, M.H.J.M.; van der Schaaf, J.; Cobden, P.D.; Schouten, J.C. Reactor modeling of sorption-enhanced autothermal reforming of methane. Part I: Performance study of hydrotalcite and lithium zirconate-based processes. *Chem. Eng. J.* **2011**, *168*, 872–882. [[CrossRef](#)]
243. Lee, K.B.; Verdooren, A.; Caram, H.S.; Sircar, S. Chemisorption of carbon dioxide on potassium-carbonate-promoted hydrotalcite. *J. Colloid Interface Sci.* **2007**, *308*, 30–39. [[CrossRef](#)] [[PubMed](#)]
244. Iruretagoyena Ferrer, D. Supported Layered Double Hydroxides as CO₂ Adsorbents for Sorption-Enhanced H₂ Production. Ph.D. Thesis, Chemical Engineering Department, Imperial College London, London, UK, 2014.
245. Akgornpeak, A.; Witoon, T.; Mungcharoen, T.; Limtrakul, J. Development of synthetic CaO sorbents via CTAB-assisted sol-gel method for CO₂ capture at high temperature. *Chem. Eng. J.* **2014**, *237* (Suppl. C), 189–198. [[CrossRef](#)]
246. Qin, Q.; Wang, J.; Zhou, T.; Zheng, Q.; Huang, L.; Zhang, Y.; Lu, P.; Umar, A.; Louis, B.; Wang, Q. Impact of organic interlayer anions on the CO₂ adsorption performance of Mg-Al layered double hydroxides derived mixed oxides. *J. Energy Chem.* **2017**, *26*, 346–353. [[CrossRef](#)]
247. Li, S.; Shi, Y.; Yang, Y.; Zheng, Y.; Cai, N. High-Performance CO₂ Adsorbent from Interlayer Potassium-Promoted Stearate-Pillared Hydrotalcite Precursors. *Energy Fuels* **2013**, *27*, 5352–5358. [[CrossRef](#)]

248. De Roy, A.; Forano, C.; Besse, J.P. Layered Double Hydroxides: Synthesis and post synthesis modification. In *Layered Double Hydroxides: Present and Future*; Nova Science Publishers: New York, NY, USA, 2001; pp. 1–39.
249. Tronto, J.; Bordonal, A.C.; Naal, Z.; Valim, J.B. Conducting Polymers/Layered Double Hydroxides Intercalated Nanocomposites. In *Materials Science—Advanced Topics*; Mastai, Y., Ed.; IntechOpen: London, UK, 2013.
250. Bhatta, L.K.G.; Subramanyam, S.; Chengala, M.D.; Olivera, S.; Venkatesh, K. Progress in hydrotalcite like compounds and metal-based oxides for CO₂ capture: A review. *J. Clean. Prod.* **2015**, *103* (Suppl. C), 171–196.
251. Khan, A.I.; O'Hare, D. Intercalation chemistry of layered double hydroxides: Recent developments and applications. *J. Mater. Chem.* **2002**, *12*, 3191–3198. [[CrossRef](#)]
252. Brindley, G.; Kikkawa, S. A crystal-chemical study of Mg, Al and Ni, N hydroxy-perchlorates and hydroxycarbonates. *Am. Mineral.* **1979**, *64*, 836–843.
253. Meyer, O.; Roessner, F.; Rakoczy, R.A.; Fischer, R.W. Impact of Organic Interlayer Anions in Hydrotalcite Precursor on the Catalytic Activity of Hydrotalcite-Derived Mixed Oxides. *ChemCatChem* **2010**, *2*, 314–321. [[CrossRef](#)]
254. Velu, S.; Ramjumar, V.; Narayana, A.; Swamy, C.S. Effect of interlayer anions on the physicochemical properties of zinc-aluminium hydrotalcite-like compounds. *J. Mater. Sci.* **1997**, *32*, 957–964. [[CrossRef](#)]
255. Yamamoto, T.; Kodama, T.; Hasegawa, N.; Tsuji, M.; Tamaura, Y. Synthesis of hydrotalcite with high layer charge for CO₂ adsorbent. *Energy Convers. Manag.* **1995**, *36*, 637–640. [[CrossRef](#)]
256. Tanaka, R.; Ogino, I.; Mukai, S.R. Synthesis of Mg-Al Mixed Oxides with Markedly High Surface Areas from Layered Double Hydroxides with Organic Sulfonates. *ACS Omega* **2018**, *3*, 16916–16923. [[CrossRef](#)] [[PubMed](#)]
257. Wang, Q.; Tay, H.H.; Zhong, Z.; Luo, J.; Borgna, A. Synthesis of high-temperature CO₂ adsorbents from organo-layered double hydroxides with markedly improved CO₂ capture capacity. *Energy Environ. Sci.* **2012**, *5*, 7526–7530. [[CrossRef](#)]
258. Othman, M.R.; Helwani, Z.; Martunus; Fernando, W.J.N. Synthetic hydrotalcites from different routes and their application as catalysts and gas adsorbents: A review. *Appl. Organomet. Chem.* **2009**, *23*, 335–346. [[CrossRef](#)]
259. Zeng, S.; Xu, X.; Wang, S.; Gong, Q.; Liu, R.; Yu, Y. Sand flower layered double hydroxides synthesized by co-precipitation for CO₂ capture: Morphology evolution mechanism, agitation effect and stability. *Mater. Chem. Phys.* **2013**, *140*, 159–167. [[CrossRef](#)]
260. Ezech, C.I.; Huang, X.; Yang, X.; Sun, C.-G.; Wang, J. Sonochemical surface functionalization of exfoliated LDH: Effect on textural properties, CO₂ adsorption, cyclic regeneration capacities and subsequent gas uptake for simultaneous methanol synthesis. *Ultrason. Sonochem.* **2017**, *39*, 330–343. [[CrossRef](#)]
261. León, M.; Díaz, E.; Bennici, S.; Vega, A.; Ordóñez, S.; Auroux, A. Adsorption of CO₂ on Hydrotalcite-Derived Mixed Oxides: Sorption Mechanisms and Consequences for Adsorption Irreversibility. *Ind. Eng. Chem. Res.* **2010**, *49*, 3663–3671. [[CrossRef](#)]
262. Yang, Z.-z.; Wei, J.-j.; Zeng, G.-m.; Zhang, H.-q.; Tan, X.-f.; Ma, C.; Li, X.-c.; Li, Z.-h.; Zhang, C. A review on strategies to LDH-based materials to improve adsorption capacity and photoreduction efficiency for CO₂. *Coord. Chem. Rev.* **2019**, *386*, 154–182.
263. Wang, Q.; Tay, H.H.; Ng, D.J.W.; Chen, L.; Liu, Y.; Chang, J.; Zhong, Z.; Luo, J.; Borgna, A. The Effect of Trivalent Cations on the Performance of Mg-M-CO₃ Layered Double Hydroxides for High-Temperature CO₂ Capture. *ChemSusChem* **2010**, *3*, 965–973. [[CrossRef](#)]
264. Goh, K.-H.; Lim, T.-T.; Dong, Z. Application of layered double hydroxides for removal of oxyanions: A review. *Water Res.* **2008**, *42*, 1343–1368. [[PubMed](#)]
265. Hutson, N.D.; Speakman, S.A.; Payzant, E.A. Structural Effects on the High Temperature Adsorption of CO₂ on a Synthetic Hydrotalcite. *Chem. Mater.* **2004**, *16*, 4135–4143. [[CrossRef](#)]
266. Othman, M.R.; Fernando, W.J. Elevated temperature carbon dioxide capture via reinforced metal hydrotalcite. *Microporous Mesoporous Mater.* **2011**, *138*, 110–117.
267. Tichit, D.; Rolland, A.; Prinetto, F.; Fetter, G.; Martinez-Ortiz, M.d.; Valenzuela, M.A.; Bosch, P. Comparison of the structural and acid-base properties of Ga- and Al-containing layered double hydroxides obtained by microwave irradiation and conventional ageing of synthesis gels. *J. Mater. Chem.* **2002**, *12*, 3832–3838. [[CrossRef](#)]
268. Walspurger, S.; Cobden, P.D.; Safonova, O.V.; Wu, Y.; Anthony, E.J. High CO₂ Storage Capacity in Alkali-Promoted Hydrotalcite-Based Material: In Situ Detection of Reversible Formation of Magnesium Carbonate. *Chem. A Eur. J.* **2010**, *16*, 12694–12700. [[CrossRef](#)]
269. Othman, M.R.; Rasid, N.M.; Fernando, W.J.N. Mg-Al hydrotalcite coating on zeolites for improved carbon dioxide adsorption. *Chem. Eng. Sci.* **2006**, *61*, 1555–1560. [[CrossRef](#)]
270. Yang, W.; Kim, Y.; Liu, P.K.T.; Sahimi, M.; Tsotsis, T.T. A study by in situ techniques of the thermal evolution of the structure of a Mg-Al-CO₃ layered double hydroxide. *Chem. Eng. Sci.* **2002**, *57*, 2945–2953. [[CrossRef](#)]
271. Reichle, W.T.; Kang, S.Y.; Everhardt, D.S. The nature of the thermal decomposition of a catalytically active anionic clay mineral. *J. Catal.* **1986**, *101*, 352–359. [[CrossRef](#)]
272. Mascolo, G.; Mascolo, M.C. On the synthesis of layered double hydroxides (LDHs) by reconstruction method based on the “memory effect”. *Microporous Mesoporous Mater.* **2015**, *214*, 246–248. [[CrossRef](#)]
273. Yuan, X.; Wang, Y.; Wang, J.; Zhou, C.; Tang, Q.; Rao, X. Calcined graphene/MgAl-layered double hydroxides for enhanced Cr(VI) removal. *Chem. Eng. J.* **2013**, *221*, 204–213. [[CrossRef](#)]
274. Guo, Y.; Zhu, Z.; Qiu, Y.; Zhao, J. Enhanced adsorption of acid brown 14 dye on calcined Mg/Fe layered double hydroxide with memory effect. *Chem. Eng. J.* **2013**, *219*, 69–77. [[CrossRef](#)]

275. Wang, Q.; Luo, J.; Zhong, Z.; Borgna, A. CO₂ capture by solid adsorbents and their applications: Current status and new trends. *Energy Environ. Sci.* **2011**, *4*, 42–55.
276. Yang, J.-I.; Kim, J.-N. Hydrotalcites for adsorption of CO₂ at high temperature. *Korean J. Chem. Eng.* **2006**, *23*, 77–80. [[CrossRef](#)]
277. Aschenbrenner, O.; McGuire, P.; Alsamaq, S.; Wang, J.; Supasitmongkol, S.; Al-Duri, B.; Styring, P.; Wood, J. Adsorption of carbon dioxide on hydrotalcite-like compounds of different compositions. *Chem. Eng. Res. Des.* **2011**, *89*, 1711–1721. [[CrossRef](#)]
278. van Selow, E.R.; Cobden, P.D.; Wright, A.D.; van den Brink, R.W.; Jansen, D. Improved sorbent for the sorption-enhanced water-gas shift process. *Energy Procedia* **2011**, *4*, 1090–1095. [[CrossRef](#)]
279. Coenen, K.; Gallucci, F.; Pio, G.; Cobden, P.; van Dijk, E.; Hensen, E.; Annaland, M.v. On the influence of steam on the CO₂ chemisorption capacity of a hydrotalcite-based adsorbent for SEWGS applications. *Chem. Eng. J.* **2017**, *314* (Suppl. C), 554–569. [[CrossRef](#)]
280. Drits, V.A.; Bookin, A.S. Crystal Structure and Xray Identification of Layered Double Hydroxides. In *Layered Double Hydroxides: Present and Future*; Nova Science Publishers: New York, NY, USA, 2001; pp. 41–100.
281. Oliveira, E.L.G.; Grande, C.A.; Rodrigues, A.E. CO₂ sorption on hydrotalcite and alkali-modified (K and Cs) hydrotalcites at high temperatures. *Sep. Purif. Technol.* **2008**, *62*, 137–147. [[CrossRef](#)]
282. Sun, L.; Yang, Y.; Ni, H.; Liu, D.; Sun, Z.; Li, P.; Yu, J. Enhancement of CO₂ Adsorption Performance on Hydrotalcites Impregnated with Alkali Metal Nitrate Salts and Carbonate Salts. *Ind. Eng. Chem. Res.* **2020**, *59*, 6043–6052. [[CrossRef](#)]
283. Zhu, X.; Chen, C.; Wang, Q.; Shi, Y.; O'Hare, D.; Cai, N. Roles for K₂CO₃ doping on elevated temperature CO₂ adsorption of potassium promoted layered double oxides. *Chem. Eng. J.* **2019**, *366*, 181–191. [[CrossRef](#)]
284. Zheng, Y.; Shi, Y.; Li, S.; Yang, Y.; Cai, N. Elevated temperature hydrogen/carbon dioxide separation process simulation by integrating elementary reaction model of hydrotalcite adsorbent. *Int. J. Hydrogen Energy* **2014**, *39*, 3771–3779. [[CrossRef](#)]
285. Ebner, A.D.; Reynolds, S.P.; Ritter, J.A. Nonequilibrium Kinetic Model That Describes the Reversible Adsorption and Desorption Behavior of CO₂ in a K-Promoted Hydrotalcite-like Compound. *Ind. Eng. Chem. Res.* **2007**, *46*, 1737–1744. [[CrossRef](#)]
286. Ding, Y.; Alpay, E. Equilibria and kinetics of CO₂ adsorption on hydrotalcite adsorbent. *Chem. Eng. Sci.* **2000**, *55*, 3461–3474. [[CrossRef](#)]
287. Yavuz, C.T.; Shinall, B.D.; Iretskii, A.V.; White, M.G.; Golden, T.; Atilhan, M.; Ford, P.C.; Stucky, G.D. Markedly Improved CO₂ Capture Efficiency and Stability of Gallium Substituted Hydrotalcites at Elevated Temperatures. *Chem. Mater.* **2009**, *21*, 3473–3475. [[CrossRef](#)]
288. Yong, Z.; Rodrigues, A.R.E. Hydrotalcite-like compounds as adsorbents for carbon dioxide. *Energy Convers. Manag.* **2002**, *43*, 1865–1876. [[CrossRef](#)]
289. Lee, C.H.; Choi, S.W.; Yoon, H.J.; Kwon, H.J.; Lee, H.C.; Jeon, S.G.; Lee, K.B. Na₂CO₃-doped CaO-based high-temperature CO₂ sorbent and its sorption kinetics. *Chem. Eng. J.* **2018**, *352*, 103–109. [[CrossRef](#)]
290. Coenen, K.; Gallucci, F.; Hensen, E.; Annaland, M.v. CO₂ and H₂O chemisorption mechanism on different potassium-promoted sorbents for SEWGS processes. *J. CO₂ Util.* **2018**, *25*, 180–193. [[CrossRef](#)]
291. Du, H.; Williams, C.T.; Ebner, A.D.; Ritter, J.A. In Situ FTIR Spectroscopic Analysis of Carbonate Transformations during Adsorption and Desorption of CO₂ in K-Promoted HTlc. *Chem. Mater.* **2010**, *22*, 3519–3526. [[CrossRef](#)]
292. Giorno, L. The Principle of Membrane Reactors. In *Encyclopedia of Membranes*; Drioli, E., Giorno, L., Eds.; Springer: Berlin/Heidelberg, Germany, 2015; pp. 1–3.
293. Mendes, D.; Mendes, A.; Madeira, L.M.; Iulianelli, A.; Sousa, J.M.; Basile, A. The water-gas shift reaction: From conventional catalytic systems to Pd-based membrane reactors—A review. *Asia-Pac. J. Chem. Eng.* **2010**, *5*, 111–137.
294. Arratibel, A.; Tanaka, A.P.; Laso, I.; Annaland, M.v.; Gallucci, F. Development of Pd-based double-skinned membranes for hydrogen production in fluidized bed membrane reactors. *J. Membr. Sci.* **2018**, *550*, 536–544. [[CrossRef](#)]
295. Rahimpour, M.R.; Samimi, F.; Babapoor, A.; Tohidian, T.; Mohebi, S. Palladium membranes applications in reaction systems for hydrogen separation and purification: A review. *Chem. Eng. Processing: Process Intensif.* **2017**, *121*, 24–49.
296. Fedotov, A.; Antonov, D.; Uvarov, V.; Tsodikov, M. Syngas and ultrapure hydrogen co-production from biomass products and synthetic fuel using hybrid membrane-catalytic reactor. In Proceedings of the 25th International Conference on Chemical Reaction Engineering, Florence, Italy, 20–23 May 2018.
297. Lin, K.-H.; Lin, W.-H.; Hsiao, C.-H.; Chang, H.-F.; Chang, A.C.C. Hydrogen production in steam reforming of glycerol by conventional and membrane reactors. *Int. J. Hydrogen Energy* **2012**, *37*, 13770–13776. [[CrossRef](#)]
298. Basile, A.; Gallucci, F.; Paturzo, L. Hydrogen production from methanol by oxidative steam reforming carried out in a membrane reactor. *Catal. Today* **2005**, *104*, 251–259. [[CrossRef](#)]
299. Mendes, D.; Sá, S.; Tosti, S.; Sousa, J.M.; Madeira, L.M.; Mendes, A. Experimental and modeling studies on the low-temperature water-gas shift reaction in a dense Pd-Ag packed-bed membrane reactor. *Chem. Eng. Sci.* **2011**, *66*, 2356–2367. [[CrossRef](#)]
300. Tong, J.; Su, L.; Kashima, Y.; Shirai, R.; Suda, H.; Matsumura, Y. Simultaneously Depositing Pd–Ag Thin Membrane on Asymmetric Porous Stainless Steel Tube and Application To Produce Hydrogen from Steam Reforming of Methane. *Ind. Eng. Chem. Res.* **2006**, *45*, 648–655. [[CrossRef](#)]
301. Chang, A.C.C.; Lin, W.-H.; Lin, K.-H.; Hsiao, C.-H.; Chen, H.-H.; Chang, H.-F. Reforming of glycerol for producing hydrogen in a Pd/Ag membrane reactor. *Int. J. Hydrogen Energy* **2012**, *37*, 13110–13117. [[CrossRef](#)]
302. Didenko, L.P.; Babak, V.N.; Sementsova, L.A.; Chizhov, P.E.; Dorofeeva, T.V. Effect of Pd-Ru alloy membrane thickness on H₂ flux from steam reforming products. *Pet. Chem.* **2017**, *57*, 935–946. [[CrossRef](#)]

303. Coenen, K.; Gallucci, F.; Mezari, B.; Hensen, E.; Annaland, M.v. An in-situ IR study on the adsorption of CO₂ and H₂O on hydrotalcites. *J. CO₂ Util.* **2018**, *24*, 228–239. [[CrossRef](#)]
304. Lytkina, A.A.; Orekhova, N.V.; Yaroslavtsev, A.B. Methanol Steam Reforming in Membrane Reactors. *Pet. Chem.* **2018**, *58*, 911–922. [[CrossRef](#)]
305. Gallucci, F.; Paturzo, L.; Basile, A. Hydrogen Recovery from Methanol Steam Reforming in a Dense Membrane Reactor: Simulation Study. *Ind. Eng. Chem. Res.* **2004**, *43*, 2420–2432. [[CrossRef](#)]
306. Macedo, M.S.; Soria, M.A.; Madeira, L.M. Glycerol steam reforming for hydrogen production: Traditional versus membrane reactor. *Int. J. Hydrogen Energy* **2019**, *44*, 24719–24732. [[CrossRef](#)]
307. Parente, M.; Soria, M.A.; Madeira, L.M. Hydrogen and/or syngas production through combined dry and steam reforming of biogas in a membrane reactor: A thermodynamic study. *Renew. Energy* **2020**, *157*, 1254–1264. [[CrossRef](#)]
308. Gallucci, F.; Fernandez, E.; Corengia, P.; Annaland, M.v. Recent advances on membranes and membrane reactors for hydrogen production. *Chem. Eng. Sci.* **2013**, *92* (Suppl. C), 40–66.
309. Adhikari, S.; Fernando, S. Hydrogen Membrane Separation Techniques. *Ind. Eng. Chem. Res.* **2006**, *45*, 875–881. [[CrossRef](#)]
310. Rebollo, E.; Mortalò, C.; Escolástico, S.; Boldrini, S.; Barison, S.; Serra, J.M.; Fabrizio, M. Exceptional hydrogen permeation of all-ceramic composite robust membranes based on BaCe_{0.65}Zr_{0.20}Y_{0.15}O_{3-δ} and Y- or Gd-doped ceria. *Energy Environ. Sci.* **2015**, *8*, 3675–3686. [[CrossRef](#)]
311. Montaleone, D.; Mercadelli, E.; Escolástico, S.; Gondolini, A.; Serra, J.M.; Sanson, A. All-ceramic asymmetric membranes with superior hydrogen permeation. *J. Mater. Chem. A* **2018**, *6*, 15718–15727. [[CrossRef](#)]
312. Miguel, C.V.; Mendes, A.; Tosti, S.; Madeira, L.M. Effect of CO and CO₂ on H₂ permeation through finger-like Pd-Ag membranes. *Int. J. Hydrogen Energy* **2012**, *37*, 12680–12687. [[CrossRef](#)]
313. O'Brien, C.P.; Lee, I.C. CO Poisoning and CO Hydrogenation on the Surface of Pd Hydrogen Separation Membranes. *J. Phys. Chem. C* **2017**, *121*, 16864–16871. [[CrossRef](#)]
314. Pérez, P.; Cornaglia, C.A.; Mendes, A.; Madeira, L.M.; Tosti, S. Surface effects and CO/CO₂ influence in the H₂ permeation through a Pd-Ag membrane: A comprehensive model. *Int. J. Hydrogen Energy* **2015**, *40*, 6566–6572. [[CrossRef](#)]
315. Shirasaki, Y.; Tsuneki, T.; Seki, T.; Yasuda, I.; Sato, T.; Itoh, N. Improvement in Hydrogen Permeability of Palladium Membrane by Alloying with Transition Metals. *J. Chem. Eng. Jpn.* **2018**, *51*, 123–125. [[CrossRef](#)]
316. Dalla Fontana, A.; Sirini, N.; Cornaglia, L.M.; Tarditi, A.M. Hydrogen permeation and surface properties of PdAu and PdAgAu membranes in the presence of CO, CO₂ and H₂S. *J. Membr. Sci.* **2018**, *563*, 351–359. [[CrossRef](#)]
317. Lewis, F.A. The palladium-hydrogen system: Structures near phase transition and critical points. *Int. J. Hydrogen Energy* **1995**, *20*, 587–592. [[CrossRef](#)]
318. Nakajima, T.; Kume, T.; Ikeda, Y.; Shiraki, M.; Kurokawa, H.; Iseki, T.; Kajitani, M.; Tanaka, H.; Hikosaka, H.; Ito, Y.T.M. Effect of concentration polarization on hydrogen production performance of ceramic-supported Pd membrane module. *Int. J. Hydrogen Energy* **2015**, *40*, 11451–11456. [[CrossRef](#)]
319. Al-Mufachi, N.A.; Rees, N.V.; Steinberger-Wilkens, R. Hydrogen selective membranes: A review of palladium-based dense metal membranes. *Renew. Sustain. Energy Rev.* **2015**, *47*, 540–551. [[CrossRef](#)]
320. Peters, T.A.; Kaleta, T.; Stange, M.; Bredesen, R. Development of ternary Pd-Ag-TM alloy membranes with improved sulphur tolerance. *J. Membr. Sci.* **2013**, *429*, 448–458. [[CrossRef](#)]
321. Mejdell, A.L.; Jøndahl, M.; Peters, T.A.; Bredesen, R.; Venvik, H.J. Experimental investigation of a microchannel membrane configuration with a 1.4 μm Pd/Ag23wt.% membrane—Effects of flow and pressure. *J. Membr. Sci.* **2009**, *327*, 6–10. [[CrossRef](#)]
322. Peters, T.A.; Stange, M.; Bredesen, R. On the high pressure performance of thin supported Pd-23%Ag membranes—Evidence of ultrahigh hydrogen flux after air treatment. *J. Membr. Sci.* **2011**, *378*, 28–34. [[CrossRef](#)]
323. Pizzi, D.; Worth, R.; Baschetti, M.G.; Sarti, G.C.; Noda, K.-i. Hydrogen permeability of 2.5 μm palladium-silver membranes deposited on ceramic supports. *J. Membr. Sci.* **2008**, *325*, 446–453. [[CrossRef](#)]
324. Maneerung, T.; Hidajat, K.; Kawi, S. Ultra-thin (<1 μm) internally-coated Pd-Ag alloy hollow fiber membrane with superior thermal stability and durability for high temperature H₂ separation. *J. Membr. Sci.* **2014**, *452* (Suppl. C), 127–142. [[CrossRef](#)]
325. Babak, V.N.; Didenko, L.P.; Kvurt, Y.P.; Sementsova, L.A. Studying the Operation of a Membrane Module Based on Palladium Foil at High Temperatures. *Theor. Found. Chem. Eng.* **2018**, *52*, 181–194. [[CrossRef](#)]
326. Mendes, D. Use of Pd-Ag Membrane Reactors in the Water-Gas Shift Reaction for Producing Ultra-Pure Hydrogen. Ph.D. Thesis, FEUP, Porto, Portugal, 2010.
327. Nooijer, N.d.; Plazaola, A.A.; Rey, J.M.; Fernandez, E.; Tanaka, D.A.P.; Annaland, M.v.S.; Gallucci, F. Long-Term Stability of Thin-Film Pd-Based Supported Membranes. *Processes* **2019**, *7*, 106. [[CrossRef](#)]
328. Gallucci, F.; Medrano, J.; Fernandez, E.; Melendez, J.; Annaland, M.v.; Pacheco, A. Advances on High Temperature Pd-Based Membranes and Membrane Reactors for Hydrogen Purification and Production. *J. Membr. Sci. Res.* **2017**, *3*, 142–156.
329. Okazaki, J.; Ikeda, T.; Tanaka, D.A.P.; Sato, K.; Suzuki, T.M.; Mizukami, F. An investigation of thermal stability of thin palladium-silver alloy membranes for high temperature hydrogen separation. *J. Membr. Sci.* **2011**, *366*, 212–219. [[CrossRef](#)]
330. Gallucci, F.; Gesalaga, E.F.; Jimenez, J.A.M.; Tanaka, D.A.P.; Annaland, M.v. Pd-based membranes for high temperature applications: Current status. *Austin Chem. Eng.* **2016**, *3*, 1025.
331. Tosti, S.; Basile, A.; Bettinali, L.; Borgognoni, F.; Chiaravalloti, F.; Gallucci, F. Long-term tests of Pd-Ag thin wall permeator tube. *J. Membr. Sci.* **2006**, *284*, 393–397. [[CrossRef](#)]

332. Jokar, S.; Rahimpour, M.; Shariati, A.; Iulianelli, A.; Bagnato, G.; Vita, A.; Dalena, F.; Basile, A. Pure Hydrogen Production in Membrane Reactor with Mixed Reforming Reaction by Utilizing Waste Gas: A Case Study. *Processes* **2016**, *4*, 33. [\[CrossRef\]](#)
333. Pacheco Tanaka, D.A.; Medrano, J.A.; Sole, J.L.V.; Gallucci, F. 1—Metallic membranes for hydrogen separation. In *Current Trends and Future Developments on (Bio-) Membranes*; Basile, A., Gallucci, F., Eds.; Elsevier: Amsterdam, The Netherlands, 2020; pp. 1–29.
334. Patil, C. Membrane Reactor Technology for Ultrapure Hydrogen Production. Ph.D. Thesis, University of Twente, Enschede, The Netherlands, 2005.
335. Brunetti, A.; Caravella, A.; Fernandez, E.; Tanaka, D.A.P.; Gallucci, F.; Drioli, E.; Curcio, E.; Viviente, J.L.; Barbieri, G. Syngas upgrading in a membrane reactor with thin Pd-alloy supported membrane. *Int. J. Hydrogen Energy* **2015**, *40*, 10883–10893. [\[CrossRef\]](#)
336. Fernandez, E.; Helmi, A.; Coenen, K.; Melendez, J.; Viviente, J.L.; Tanaka, D.A.P.; Annaland, M.v.; Gallucci, F. Development of thin Pd-Ag supported membranes for fluidized bed membrane reactors including WGS related gases. *Int. J. Hydrogen Energy* **2015**, *40*, 3506–3519. [\[CrossRef\]](#)
337. Li, H.; Caravella, A.; Xu, H.Y. Recent progress in Pd-based composite membranes. *J. Mater. Chem. A* **2016**, *4*, 14069–14094.
338. Shah, M.R.; Noble, R.D.; Clough, D.E. Analysis of transient permeation as a technique for determination of sorption and diffusion in supported membranes. *J. Membr. Sci.* **2006**, *280*, 452–460. [\[CrossRef\]](#)
339. Campo, M.; Tanaka, A.; Mendes, A.; Sousa, J.M. 3—Characterization of membranes for energy and environmental applications. In *Advanced Membrane Science and Technology for Sustainable Energy and Environmental Applications*; Basile, A., Nunes, S.P., Eds.; Woodhead Publishing: Sawston, UK, 2011; pp. 56–89.
340. Basile, A.; Gallucci, F.; Tosti, S. Synthesis Characterization, and Applications of Palladium Membranes. In *Membrane Science and Technology*; Elsevier: Amsterdam, The Netherlands, 2008; pp. 255–323.
341. Yun, S.; Ted Oyama, S. Correlations in palladium membranes for hydrogen separation: A review. *J. Membr. Sci.* **2011**, *375*, 28–45.
342. Ward, T.L.; Dao, T. Model of hydrogen permeation behavior in palladium membranes. *J. Membr. Sci.* **1999**, *153*, 211–231. [\[CrossRef\]](#)
343. Musket, R.G. Effects of contamination on the interaction of hydrogen gas with palladium: A review. *J. Less Common Met.* **1976**, *45*, 173–183. [\[CrossRef\]](#)
344. Zhang, X.-L. 7—Effect of poisoning on metallic membranes. In *Current Trends and Future Developments on (Bio) Membranes*; Basile, A., Gallucci, F., Eds.; Elsevier: Amsterdam, The Netherlands, 2020; pp. 169–187.
345. Hara, S.; Sakaki, K.; Itoh, N. Decline in Hydrogen Permeation Due to Concentration Polarization and CO Hindrance in a Palladium Membrane Reactor. *Ind. Eng. Chem. Res.* **1999**, *38*, 4913–4918. [\[CrossRef\]](#)
346. Hou, K.; Hughes, R. The effect of external mass transfer, competitive adsorption and coking on hydrogen permeation through thin Pd/Ag membranes. *J. Membr. Sci.* **2002**, *206*, 119–130. [\[CrossRef\]](#)
347. Zhang, J.; Liu, D.; He, M.; Xu, H.; Li, W. Experimental and simulation studies on concentration polarization in H₂ enrichment by highly permeable and selective Pd membranes. *J. Membr. Sci.* **2006**, *274*, 83–91. [\[CrossRef\]](#)
348. Mori, N.; Nakamura, T.; Noda, K.-i.; Sakai, O.; Takahashi, A.; Ogawa, N.; Sakai, H.; Iwamoto, Y.; Hattori, T. Reactor Configuration and Concentration Polarization in Methane Steam Reforming by a Membrane Reactor with a Highly Hydrogen-Permeable Membrane. *Ind. Eng. Chem. Res.* **2007**, *46*, 1952–1958. [\[CrossRef\]](#)
349. Nagy, E.; Kulcsár, E. The effect of the concentration polarization and the membrane layer mass transport on membrane separation. *Desalination Water Treat.* **2010**, *14*, 220–226. [\[CrossRef\]](#)
350. Caravella, A.; Hara, S.; Drioli, E.; Barbieri, G. Sieverts law pressure exponent for hydrogen permeation through Pd-based membranes: Coupled influence of non-ideal diffusion and multicomponent external mass transfer. *Int. J. Hydrogen Energy* **2013**, *38*, 16229–16244. [\[CrossRef\]](#)
351. Caravella, A.; Scura, F.; Barbieri, G.; Drioli, E. Sieverts Law Empirical Exponent for Pd-Based Membranes: Critical Analysis in Pure H₂ Permeation. *J. Phys. Chem. B* **2010**, *114*, 6033–6047. [\[CrossRef\]](#)
352. Gielens, F.C.; Tong, H.D.; van Rijn, C.J.M.; Vorstman, M.A.G.; Keurentjes, J.T.F. Microsystem technology for high-flux hydrogen separation membranes. *J. Membr. Sci.* **2004**, *243*, 203–213. [\[CrossRef\]](#)
353. Keurentjes, J.T.F.; Gielens, F.C.; Tong, H.D.; van Rijn, C.J.M.; Vorstman, M.A.G. High-Flux Palladium Membranes Based on Microsystem Technology. *Ind. Eng. Chem. Res.* **2004**, *43*, 4768–4772. [\[CrossRef\]](#)
354. Mendes, D.; Chibante, V.; Zheng, J.-M.; Tosti, S.; Borgognoni, F.; Mendes, A.; Madeira, L.M. Enhancing the production of hydrogen via water-gas shift reaction using Pd-based membrane reactors. *Int. J. Hydrogen Energy* **2010**, *35*, 12596–12608. [\[CrossRef\]](#)
355. Santucci, A.; Borgognoni, F.; Vadrucci, M.; Tosti, S. Testing of dense Pd-Ag tubes: Effect of pressure and membrane thickness on the hydrogen permeability. *J. Membr. Sci.* **2013**, *444* (Suppl. C), 378–383. [\[CrossRef\]](#)
356. Lewis, A.E.; Kershner, D.C.; Paglieri, S.N.; Slepicka, M.J.; Way, J.D. Pd-Pt/YSZ composite membranes for hydrogen separation from synthetic water-gas shift streams. *J. Membr. Sci.* **2013**, *437* (Suppl. C), 257–264. [\[CrossRef\]](#)
357. Zhang, D.; Zhou, S.; Fan, Y.; Xu, N.; He, Y. Preparation of dense Pd composite membranes on porous Ti-Al alloy supports by electroless plating. *J. Membr. Sci.* **2012**, *387–388* (Suppl. C), 24–29. [\[CrossRef\]](#)
358. Pacheco Tanaka, D.A.; Tanco, M.A.L.; Niwa, S.-i.; Wakui, Y.; Mizukami, F.; Namba, T.; Suzuki, T.M. Preparation of palladium and silver alloy membrane on a porous α -alumina tube via simultaneous electroless plating. *J. Membr. Sci.* **2005**, *247*, 21–27. [\[CrossRef\]](#)
359. Anzelmo, B.; Wilcox, J.; Liguori, S. Hydrogen production via natural gas steam reforming in a Pd-Au membrane reactor. Comparison between methane and natural gas steam reforming reactions. *J. Membr. Sci.* **2018**, *568*, 113–120. [\[CrossRef\]](#)

360. Liu, J.; Bellini, S.; de Nooijer, N.C.A.; Sun, Y.; Tanaka, D.A.P.; Tang, C.; Li, H.; Gallucci, F.; Caravella, A. Hydrogen permeation and stability in ultra-thin PdRu supported membranes. *Int. J. Hydrogen Energy* **2020**, *45*, 7455–7467. [[CrossRef](#)]
361. Catalano, J.; Baschetti, M.G.; Sarti, G.C. Influence of the gas phase resistance on hydrogen flux through thin palladium-silver membranes. *J. Membr. Sci.* **2009**, *339*, 57–67. [[CrossRef](#)]
362. Melendez, J.; Gesalaga, E.F.; Farimani, A.H.S.; Gallucci, F.; Arias, P.L.; Tanaka, D.A.P. Preparation and characterization of ultra-thin (<1 micron) Pd-Ag membranes on porous alumina support (100 nm pore size). In Proceedings of the 12th International Conference on Catalysis in Membrane Reactors (ICCMR12), Szczecin, Poland, 22–25 June 2015.
363. Helmi, A.; Fernandez, E.; Melendez, J.; Tanaka, D.A.P.; Gallucci, F.; Annaland, M.v. Fluidized Bed Membrane Reactors for Ultra Pure H₂ Production—A Step forward towards Commercialization. *Molecules* **2016**, *21*, 376. [[CrossRef](#)]
364. Fernandez, E.; Sanchez-Garcia, J.A.; Melendez, J.; Spallina, V.; Annaland, M.v.; Gallucci, F.; Tanaka, D.A.P.; Prema, R. Development of highly permeable ultra-thin Pd-based supported membranes. *Chem. Eng. J.* **2016**, *305*, 149–155. [[CrossRef](#)]
365. Fernandez, E.; Helmi, A.; Medrano, J.A.; Coenen, K.; Arratibel, A.; Melendez, J.; de Nooijer, N.C.A.; Spallina, V.; Viviente, J.L.; Zuñiga, J.; et al. Palladium based membranes and membrane reactors for hydrogen production and purification: An overview of research activities at Tecalia and TU/e. *Int. J. Hydrogen Energy* **2017**, *42*, 13763–13776. [[CrossRef](#)]
366. Shi, L.; Goldbach, A.; Xu, H. High-flux H₂ separation membranes from (Pd/Au)_n nanolayers. *Int. J. Hydrogen Energy* **2011**, *36*, 2281–2284. [[CrossRef](#)]